Galactic Center Clocks as Probes of Gravity

Dissertation

zur

Erlangung der naturwissenschaftlichen Doktorwürde
(Dr. sc. nat.)

vorgelegt der

Mathematisch-naturwissenschaftlichen Fakultät

der

Universität Zürich

von

Raymond Lloyd Angélil

aus Südafrika und von Küsnacht ZH

Promotionskomitee

Prof. Dr.	Uroš Seljak	(Vorsitz)
Dr.	Prasenjit Saha	(Leiter)
Prof. Dr.	Philippe Jetzer	
Dr.	Stefan Gillessen	
Prof. Dr.	Scott Tremaine	

Zürich 2012

Foreword

This dissertation is about testing gravity. The simplest gravitational theory we have which manages to successfully account for all gravitational phenomena we've encountered is general relativity, so this what tests of gravity through observation should be compared with. General relativity was conceived one hundred years ago. Since then, our grasp of the equations and their consequences have grown faster than we can test them in nature. While the weak-field consequences of gravity outside compact sources are well understood, tests for features beyond the leading-order remain imprecise or missing. The ultimate testing ground for gravity is the space-time in the vicinity of a remarkable entity predicted by general relativity - the event horizon of the Black Hole. Yet it's curious that even though the notion of a Black Hole has been part of collective gospel for decades, we're not yet close to imaging one, let alone had nature provide us with direct clues as to the principles which govern its nature. Now, telescopes like the VLT in Chile, and Keck in Hawaii take us to the outskirts of the space-time surrounding what is most likely a supermassive black hole in the centre of the Milky Way. This is a window into the strongest gravitational field ever observed, and so a fantastic playground in which to subject tests of the theory of general relativity. Whatever the truth may turn out to be, the work herein will play a small role in building the bridge between gravitational theory, and gravity in nature.

A large part of the first chapter to this dissertation makes up a paper which is under review. The subject matter turned out to be quite encompassing of my work as a whole, and so we felt it would make a sound introduction to the papers which follow. I have appended these papers not in chronological publishing order, but rather in the order in which they ought to be read.

Except for the next sentence, I have decided that you will find no acknowledgments anywhere. This because each of you around me over the last three years who have played a role in my life are aware of it, and to you I extend great appreciation.

These pages omit a textbook-styled introduction to general relativity. A few pages of such would be too many, and many pages too few. General relativity has been around long enough (and unchanged enough) for time to spawn multiple adequate introductory texts, to which I refer enthusiastic readers. Instead, I will delve straight into what relativity decrees for our particular testbed - the galactic center S star system. Also, this way it will be less boring.

Summary

Through the monitoring of stars and pulsars on orbits around Sgr A*, the metric in the vicinity of the black hole can be measured by way of stellar redshifts or pulsar timing. These orbits are ballistic trajectories which probe gravitational physics in the strongest field yet observed. I treat each orbit as a clock falling in the Kerr geometry, which emits ticks in equal intervals of proper time. These tick signals propagate on the same space-time until they reach the observer. The resulting observable is the pulse coordinate time-of-arrival, whose derivative with respect to the proper time of emission is simply the redshift of a spectral line. Using this consolidated approach to redshift and pulsar timing, I investigate Schwarzschild effects, as well as high-order Kerr signals, which include spin and spin-squared effects. I address remarks made in the literature linking such experiments to tests of the no-hair conjecture. If general relativity is correct, then geodesic tests of relativity in the Solar system and in binary pulsar systems probe the same metric as galactic center tests do. However, because the fields are far stronger yet the orbits longer, the relativistic observables expected from Sgr A* orbits are not simply scaled-up versions of the classic tests. Transient phenomena on the orbit, signal propagation delay, gravitational time dilation and higher-order effects are among those neither observable in solar system nor on binary pulsar systems. This dissertation highlights the properties of redshift and time-of-arrival curves that emerge due to general relativity in the strong field yet still, long-period regime that S stars and S pulsars inhabit. Along with each effect, I will give an idea as to the observational capabilities necessary to resolve these signals. Finally, I will briefly present a wavelet-based method which aims to detect relativistic signals when shrouded by perturbations due to an extended mass system.

Zusammenfassung

Durch die Beobachtung von Sternen und Pulsaren auf Umlaufbahnen um Sgr A* kann die Metrik in der Umgebung des schwarzen Loches über stellare Rotverschiebungen oder Messung der Ankunftszeiten von Pulsarsignalen gemessen werden. Die Umlaufbahnen dieser Objekte sind ballistische Trajektorien die Gravitationsphysik im bisher stärksten je beobachteten Feld prüfen. Im Rahmen dieser Doktorarbeit wird jede Laufbahn als eine in der Kerrgeometrie fallende Uhr behandelt, deren Ticksignale in gleichen Eigenzeitabständen ausgesendet werden. Diese Ticksignale propagieren auf derselben Raumzeit bis sie den Beobachter erreichen. Die sich daraus ergebende Beobachtungsgrösse ist die Pulsankunftszeit, deren Ableitung nach der Emmisionseigenzeit die Rotverschiebung einer Spektralinie ist. Mit diesem kombinierten Vorgehen werden Schwarzschild-Effekte sowie Kerr Signale höherer Ordnung , die Spin und Spinquadratterme einschliessen untersucht. Auch wird auf die in der Literatur zu findenden Behauptungen eingegangen, die das no-hair Theorem mit Spin-Experimenten zu testen versucht. Wenn die allgemeine Relativitätstheorie korrekt ist, wird durch geodetische Tests Relativität im Sonnensystem wie auch im galaktischem Zentrum dieselbe Metrik geprüft. Da die Felder im galaktischen Zentrum allerdings viel stärker sind, die Umlaufbahnen jedoch länger, sind die erwarteten Beobachtungsgrössen von Sgr A* Umlaufbahnen nicht einfach hochskalierte Versionen der klassischen Tests. Kurzzeitige Phänomene auf der Laufbahn, die verlangsamte Ausbreitung von Signalen, Gravitationszeitdilatation und Effekte höherer Ordnung sind weder im Sonnensystem noch in Binärpulsarsystemen beobachtbar. In dieser Doktorarbeit werden die Eigenschaften von Rotverschiebungs- und Ankunftszeitkurven untersucht, die von der allgemeinen Relativität im Regime starker Felder und langer Umlaufzeiten verursacht werden, in dem sich die S-Sterne und S-Pulsare befinden. Schliesslich wird eine Wavelet-Methode vorgestellt, mit der relativistische Signale ausfindig gemacht werden können wenn sie von Störungen durch eine erweiterte Massenverteilung überlagert werden.

Contents

1 Introduction

1.1 Clocks around Sgr A*

A clock is a recurrent natural physical process with an unchanging period. At least, so claims our intrepid experimentalist Bob, with clock in hand. To our observer Alice, watching from a different frame, the clock frequency may change. In the absence of gravity, the frequency depends on the relative motion of the clock and the observer, and is constant, unless Bob and his clock accelerate[1]. Enter gravity, and Bob, falling-freely with his clock, must accelerate. If the clock is far enough away from the source of the gravity field, and if the trajectory is bound, then the orbit will be elliptical. Each time Bob's clock ticks, he broadcasts the fact to Alice. Monitoring from afar, she takes a counter and her own clock, and records when she sees the signal flashes. She finds that the light flashes arrive at a sinusoidal rate, corresponding to Bob's orbital period. She soon realizes, that using some laws first written down a few centuries ago, she is able to estimate the mass of the gravitational source. If this was everything to be learned though, physicists like Alice and Bob could have packed their bags a century ago. Urging our tick-counting physicist to stay on, and modestly changing our example, things will begin to get interesting. For this to happen, either Alice needs a more accurate way of making measurements, or Bob and his clock must be on an orbit which take them closer to the source of the gravity. Then, our persistent physicist will begin to notice remarkable deviations from the sinusoidal rate. Were she unfamiliar with gravitational time dilation, she might be bewildered to notice that even after taking Bob's speed into account, the closer he is to Sgr A*, the longer she must wait between ticks. The surprises will continue. Further upping the capability of her timer, she will realize that her tick-curves don't quite fit with an elliptical orbit. She will conclude that for things to make sense, the orbit must be precessing. Additionally, she will notice curious transient perturbations to what she expects — Bob's clock speeds up and then slows down before and after pericenter passage. Things still don't fit however, until Alice grasps that not just the orbiting clock, but the very signals which carry the ticks from the clock to her, are subject to the whims of the gravitational field - as the tick-signals propagate past the gravitational source, their trajectories bend. This plays a role in further lowering the observed tick frequency. Figure 1.1 shows an example of what Alice might see. Ahead of her still lie many more remarkable findings. One of the most exciting of these discoveries is that if she observes a clock closer still to the gravitational source, she will probably realize that not just the mass, but the angular momentum of Sgr A* plays a role in setting the gravitational field. Armed with the particulars of gravitational physics in the vicinity of a black hole, Alice will find herself in good stead to test fundamental theories of gravity.

[1] This clock has some kind of rocket booster attached.

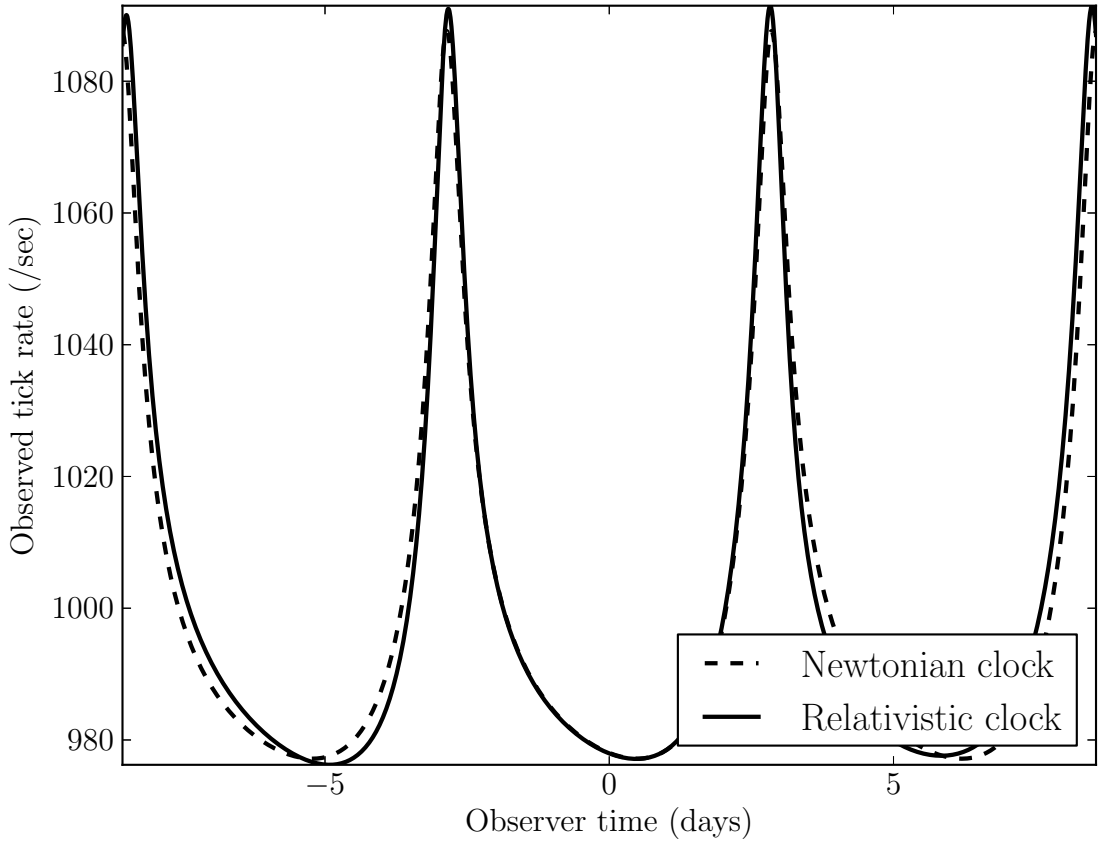

Figure 1.1: An observer watches a clock which, in its rest frame, ticks 1000 times every second. This clock is falling freely on an eccentric orbit around a source with nonzero spin. The trajectory has semi-major axis $\sim 1000 r_g$, and distance of closest approach $\sim 100 r_g$, where r_g is the gravitational radius of the source, in this case, a $\sim 4 \cdot 10^6 M_\odot$ black hole. The eccentricity is 0.6, and the orbit is inclined with respect to the line of sight by 45°. In this regime, the tick rate for the relativistic orbit is quite different from the newtonian tick rate. The orbits of both clocks are made to coincide at $\tau = 0$. Relativity changes both the clock's orbit, as well as the paths that the signals take to reach the observer.

The preceding paragraph is, needless to mention, a thought-experiment of the milliparsec region of the Galactic center, home to a compact mass of $\sim 4 \cdot 10^6 M_\odot$ at Sgr A*, and a population of stars which orbit it at speeds up to a few percent of light, as shown by astrometric and spectroscopic observations (Schödel et al., 2002; Gillessen et al., 2009b,a; Martins et al., 2008b; Eisenhauer et al., 2003; Eckart et al., 2005; Eckhart et al., 2005). Dozens of these 'S'-stars have been observed and it is expected that many more thousands of stars, as-yet undetected, orbit the central black hole. Stars carry excited atoms, whose electrons interact with the electric field. These transitions have a natural frequency which is equal to that of the electric and magnetic waves produced. Because stars

are home to a bath of atoms, each allowing potentially multiple transitions, each corresponding to a spectral line, a star is a freely-falling ticktock. The redshift of these lines for some of the S stars has been measured, and astrometric monitoring of these stars has also been done (Eisenhauer et al., 2003; Gillessen et al., 2009a). See figures 1.2 and 1.3. Spectroscopic accuracy of $\sim$ 10km/s has been reached for some of the S stars, and is expected to improve with the next generation of instruments. But still, due to the breadth of the spectral lines, and the power of modern spectroscopy, accurately measuring the position of these lines is limited in comparison to pulsar time-of-arrival measurements. The tick rate of a pulsar is its rotational frequency, and they boast an incredibly large moment of inertia. Pulsar-quakes and spin-slowdowns aside, pulsars are ideal clocks. Pulsars have not yet been discovered on short-period orbits around Sgr A*, but population models argue that there should be a small handful of observable pulsars with periods $<$ year. (Cordes and Lazio, 1997; Pfahl and Loeb, 2004; Macquart et al., 2010; Kramer et al., 2000)

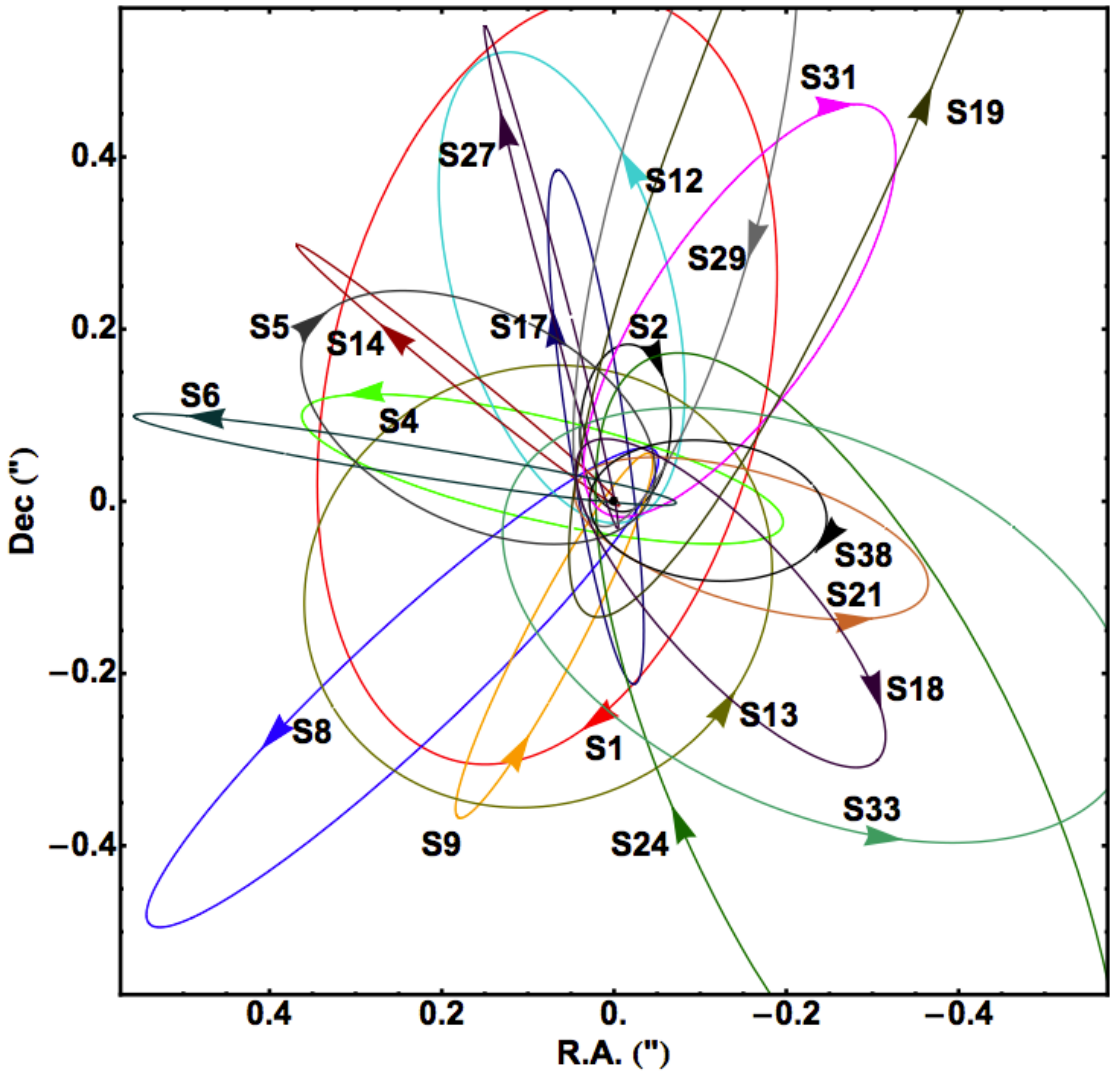

Figure 1.2: Best-fit orbits of the galactic center S stars from Gillessen et al. (2009b). S2 is the most relativistic orbit, reaching an angular pericenter distance from the black hole of $\sim 0.12''$, or 2800 gravitational radii. The observed S stars are extremely bright, and typically belong to the OB spectral class. Future observations are expected to further crowd this plot, as less luminous stars become visible to our telescopes.

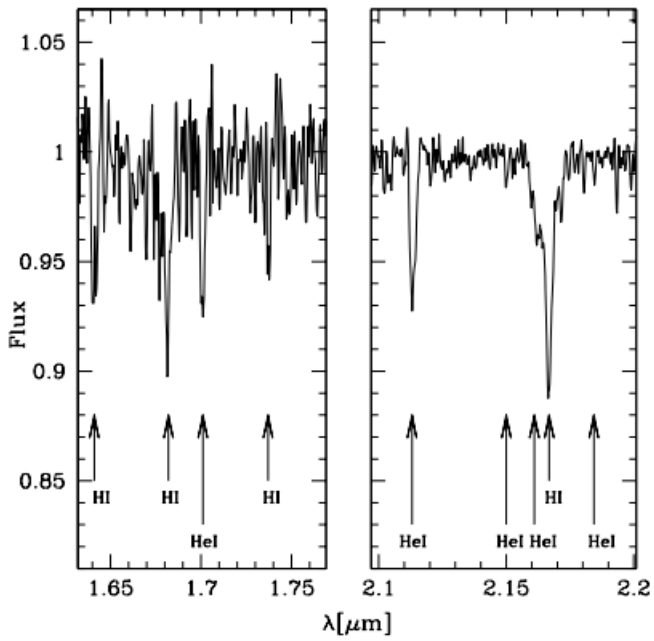

Figure 1.3: An example of an integrated observed spectrum of an S star from Martins et al. (2008a), in this case S2. This spectrum was measured with the Spectrograph for Integral Field Obervations in the Near Infrared (or SINFONI) of the European Southern Observatory's Very Large Telescope (VLT). The sharpest feature in this NIR K-band ($2.0-2.4\mu$m) spectrum contains the hydrogen Brackett-γ 2.16μm absorption line, present in early B-type stars.

Testing relativity in the Galactic center through monitoring the S Stars has been extensively discussed in the literature. The effect of gravitational time dilation on S Star redshifts has been addressed by Zucker et al. (2006), and Angélil and Saha (2011). General relativistic periastron precession has been discussed in Rubilar and Eckart (2001); Preto and Saha (2009), and Kannan and Saha (2009). Depending on the orbit size, perturbations due to the extended mass are expected to obscure relativistic signals, and is discussed in Rubilar and Eckart (2001); Sabha et al. (2012); Merritt et al. (2010) and Sadeghian and Will (2011). Relativistic effects on light paths has also been treated by Bozza and Mancini (2009) which calculates astrometric shifts due to lensing, and by Angélil and Saha (2010) and Angélil et al. (2010), which consider light path effects on S Star redshifts. Galactic center pulsars have been considered as probes of strong-field gravity. Liu et al. (2012) simulate pulsar timing on $\sim 0.3yr$ orbits, and attempt to include high-order spin effects, although include neither transient effects nor higher-order propagation delay. Angélil et al. (2010) includes both, although showcases relativistic redshift effects explicitly, as opposed to pulsar timing. In this thesis, I include all relativistic effects yet considered, and due to the elegant relationship between the two, apply them simultaneously to redshift measurements as well as pulsar timing. I will highlight transient relativistic orbit effects in particular, as well as higher-order spin effects on both orbits and signal propagation.

I take the 'clock'-approach to galactic center tests of general relativity. Clocks orbit Sgr A*, and we, observers at infinity, count the ticks. Each measurement of a 'tick' made on Earth at an arrival

time t_a, has an associated proper time of emission τ_e. For pulsar flashes, if I mark the local time at which each pulse comes in, the observable is $\tau_e(t_a)$. For the case of a star, the observable is the frequency of a spectral line, and is the derivative,

$$\ln \nu_{obs}(t_a) = K - \ln \frac{dt_a}{d\tau_e}(t_a), \tag{1.1}$$

where K is a constant which depends on the laboratory line frequency, plus the relative line-of-sight solar-Sgr A* velocity. Revisiting Fig. 1.1 in this light; the curves can be interpreted as the frequency of a 'line' with intrinsic frequency 1000Hz.

In this thesis, I am not interested in the clock position on the sky, although a complete analysis could include astrometric information if available. The primary purpose of this exercise is to highlight what can be expected from timing curves from pulsars, and redshift curves from stars, both on short-period orbits around Sgr A*, under the effects of relativity. The E-ELT and the SKA are among the next generation of telescopes expected to discover clocks closer in to the black hole. The closer they are, the more the relativistic effects are expected to prevail over perturbations due to the other masses. It is these such $< yr$-period orbits I we focus my attention on. By performing numerical calculations, I intend to give a straightforward idea of what effects can be expected from the zoo of weak-field Kerr relativistic metric terms.

The galactic center system is set apart from other relativistic testbeds by the comparatively long orbit periods. Tests of relativity carried out so far which involve a timelike trajectory, rely on the build-up of a perturbation over many orbits. There are effects associated with each metric component which are transient - in that they do not accumulate. For example, the presence of the metric term which precesses Mercury's orbit does more than just that; among other things, it induces a slight speed-up and then slow-down around pericenter from what Keplerian dynamics expects. Integrated, they cancel out. To measure a relativistic metric term on a relativistic binary pulsar, we wait for it to impart a cumulative perturbation which is allowed to build-up over many orbits. The before-and-after best-fit instantaneous Keplerian elements can then be differenced, which reveals something about the sought-after metric term. To measure the same metric term for an S star, a similar strategy would not only be impractical, but unnecessary. An experiment which provides sufficient accuracy can be sensitive to far more than just the cumulative perturbation on the orbit due to any particular metric term. In principle, the metric components as functions of r and t could be inferred, and not just a single integrated quantity. In the coming sections I will solve the equations and show the difference that the inclusion of transient effects makes.

In the next section, I will briefly review metric tests of gravity already performed. In Section 3, I will review the equations of motion of the trajectories in the weak-field Kerr geometry, and take a look at some of the relativistic effects that manifest on the orbit. Next, I will turn to the observable - the tick-rate curve, which can be calculated by broadcasting the signals from the clock's orbit to the distant observer. Each 'tick' and subsequent 'tock' of the clock happen in equal intervals of proper time. These signals propagate on the same metric as the clock itself, and by arriving at the observer, the time-of-arrival between successive ticks is known. When interested in the shift of a spectral line instead, I can simply take the derivative (1.1). Section 4 addresses remarks in the literature regarding what galactic center tests of relativity can tell us about multipole moments and the no-hair conjecture.

1.2 Geodesic tests of General Relativity

The starting point when solving a relativistic system typically involves a metric solution to the gravitational field equations. Because no geodesic experiments test physics in the vicinity of the event horizon yet, the field is weak, and so the metric components may be expanded about infinity. The leading-order terms give the newtonian features, and the higher-order ones relativistic perturbations whose coefficients are set by the theory of gravity. Tests of relativity try to determine the values these coefficients take. These experiments test gravitational physics insofar as they probe the metric - not the field equations. This is especially true in the weak-field. One can conceive of modifications, of say, to the Einstein Field Equations which drastically modify the geometry around a spinning source from the Kerr solution, yet still manage to keep the weak-field parameters identical to the Kerr ones up to a certain order[2]. By inferring the components of the metric by looking at their effects on the behavior of geodesics or the parallel transport of vectors, we implicitly test another central aspect of relativity: the essential notion that motivate them, the principle of equivalence.

The galactic center S star system is a laboratory in which relativity can be tested by measuring the paths that freely falling bodies make around an isolated source. Such are Solar system tests of relativity, albeit in far weaker fields. In this thesis, the values for the expanded coefficients take on the Einstein values.

- **Gravitational time dilation**

  One of the basic consequences of the equivalence principle is that a clock in a strong gravitational field ticks more slowly than one which isn't. Time is dilated by a factor

  $$g_{tt}^{-1/2} = 1 - \frac{2GM}{c^2 r}. \tag{1.2}$$

  GPS satellites are sensitive to this shift and take it into account in order to function accurately.

- **Light deflection** The deflection angle of a null ray is

  $$\Delta\phi = \frac{4GM}{b}. \tag{1.3}$$

  The extra-delay induced in the arrival time of a packet of light compared to had it travelled in a straight line is called the Shapiro delay (Shapiro, 1964), and has been well-tested in the solar system(Shapiro et al., 1968) and in binary pulsar systems(Stairs, 2003).

- **Leading-order precession** Another of the classic tests of relativity is the weak-field precession, and is due to the first perturbation after the Keplerian. These higher order terms shift Mercury's perihelion by

  $$\Delta\omega = \frac{6GM\pi}{L} \quad /\text{revolution}, \tag{1.4}$$

  where $L = a\left(1 - e^2\right)$ is the orbital angular momentum. This type of precession has also been measured on binary pulsar systems.

[2] In fact, by keeping in mind that we are probing the metric, and not the field equations, the conclusions of our tests are permitted to entertain the possibility that Sgr A* might not even be a black hole.

Figure 1.4: Creetchas sit idly by, minding their own business, while Van Honks duels the devil out yonder.

- **Precession due to spin** The Einstein Field equations admit an axially symmetric vacuum solution; in which the spatial part of the metric becomes oblate spheroidal. The oblateness of the metric can be parametrized by s, the spin parameter. Effects due to the now-nonzero $dtdx_i$ metric components are attributed to *frame-dragging*, and are proportional to the spin parameter. A frame-dragged geodesic experiences a tug in the spin direction. As a perturbation to a Keplerian orbit, if the spin is the same direction as the orbital angular momentum, the cumulative part of this tugging manifests as a retrograde precession of the orbit - both in the nodal angle and the argument of periapsis. This precession is equal to

$$\Delta\phi = -\kappa\frac{GM\pi}{L^{3/2}} \quad /\text{revolution}, \tag{1.5}$$

  where κ is a constant which depends on the axiality of the metric. If (1.5) is derived from the Kerr metric, then in the asymptotic region $r \to \infty$, it can be shown that κ is related to the angular momentum per unit mass, namely $\kappa = 8s \equiv 8J/M$(Kerr, 1963; Weinberg, 1972; Misner et al., 1973). On the other hand, if using frame-dragging induced precession as a test of relativity, s, is simply absorbed into κ, and becomes nothing more than a parameter to be measured. Without a model, the angular momentum of a black hole cannot be inferred.

  Using laser ranging to accurately determine the orbit of the Lageos satellites, this spin-induced precession (1.5) is claimed to have been measured (Ciufolini and Pavlis, 2004; Iorio, 2010). The recently launched LARES satellite aims to measure the effect to an accuracy of 1%(Ciufolini et al., 2009).

The square of the spin parameter also enters the metric, in the dt^2 and $dx_i dx_j$ components. As I shall show, in the weak-field, spin-squared effects enter the dynamics of timelike trajectories one

order higher than frame-dragging. As such, experiments so far have been sensitive to the latter and not yet the former. s^2-dependent effects have not yet been detected.

Each of the timelike effects mentioned here is cumulative, and are each due to one (or more) metric terms. These terms impart transient effects also, whose inclusions are unnecessary for solar system tests. Short-period galactic center stars and pulsars will be sensitive to all the relativistic effects mentioned here, along with their transient complements, as well as a plethora of higher-order effects, detailed in the coming sections. The abundance of new relativistic observables which will be available through monitoring S stars and S pulsars is such that most of these phenomena have remained unnamed.

It ought to be mentioned there is a way to find the metric components around a source in the weak field not by looking at the trajectory of the geodesic, but rather at how a vector attached to a geodesic is parallel transported. The parallel transport of a vector depends on the connection coefficients and therefore the metric. A vector attached to a satellite on a circular orbit moves by an amount (Fließbach, 1990)

$$\Delta\phi = \frac{3GM\pi}{r} \ \text{/orbit.} \tag{1.6}$$

Gravity probe B has measured this effect, sometimes called the geodetic effect (Everitt et al., 2011). The parallel transport of a vector along a geodesic is also influenced by frame-dragging. This is called the Lens-Thirring effect, and was also detected by gravity probe B. (Everitt et al., 2011). Galactic center orbits will likely not be sensitive to effects of this nature. However, it's possible that the spin axis of a pulsar be parallel transported enough to change the pulse profile.

In the next section, I will look at the orbits of massive particles around the galactic center black hole. I shall force the weak-field metric parameters to those expected from the Kerr metric. Were I solving the inverse problem, these coefficients could be replaced by arbitrary parameters, to be inferred through data fitting.

1.3 Relativistic time delays and redshifts

As in Angélil and Saha (2010), I use Hamiltonians to describe geodesics. The effects from the various terms are more easily interpreted when the Hamiltonian is written in Boyer-Lindquist coordinates, and so this is where I begin: taking the metric inverse, all freely-falling trajectories have Hamiltonian

$$H = \frac{1}{2} g^{\mu\nu} p_\mu p_\nu, \tag{1.7}$$

with $p_\mu = (p_t, p_r, p_\theta, p_\phi)$. Working in the weak-field enables us to toggle effects more easily. I shall make an expansion in r^{-1} around infinity, and so must be mindful of how the momenta behave with r. This dependency changes whether the trajectory is timelike (for stars or pulsars) or null (signal propagation). Of all the terms to pop out, because we're interested in those that depend on the square of the spin parameter, I truncate my series at the order at which they first feature. Table 1.3 breaks the Hamiltonian up order-by-order for timelike and null paths.

	Orbits	Light paths
$-\frac{p_t^2}{2}$	Static	Rømer $\Delta t \propto P^{2/3}$
$+\frac{p_\phi^2}{2r^2\sin^2\theta}+\frac{p_r^2}{2}+\frac{p_\phi^2}{2r^2}$	Kepler $\Delta t \propto P^{2/3}$	
$-\frac{p_t^2}{r}$		Shapiro $\Delta t \propto P^{0}$
$-\frac{p_r^2}{r}$	Schwarzschild $\Delta t \propto P^{0}$	
$-\frac{2p_t^2}{r^2}$		Spin (both), More Shapiro $\Delta t \propto P^{-2/3}$
$-\frac{2sp_tp_\phi}{r^3}$	Spin (odd) $\Delta t \propto P^{-1/3}$	
$+s^2\left(\frac{p_r^2\sin^2\theta}{2r^4}-\frac{p_\theta^2\cos^2\theta}{2r^4}-\frac{p_\phi^2}{2r^4\sin^2\theta}\right.$ $\left.+\frac{p_t^2\cos^2\theta}{r^3}\right)-\frac{4p_t^2}{r^3}$	Spin (even), Schwarzschild $\Delta t \propto P^{-2/3}$	not included

Each Hamiltonian term gives rise to effects on the orbit as well as on the signal propagation paths. These affect the observed light frequency and the times of arrival of pulsar flashes. The scaling relation for the timing delay of clock signals for each term is given in the boxes. For the orbit, the leading-order (or Keplerian) delay is simply $\sim$ orbit size, or $P^{2/3}$. Enter relativity, and each $p_r, p_\theta/r$ and p_ϕ/r contribute a factor $\sim P^{-1/3}$. The leading-order signal propagation effect is simply photons on a Minkowksi metric - meaning the signals do not propagate instantly. The corresponding delay from this is the time the light takes to cross the orbit, or, the Rømer delay $\sim$ orbit size. For the higher-order effects, each p_θ and p_ϕ contribute a further $P^{2/3}$.

To get the redshift residual for each effect from the timing residual, I simply take

$$\Delta z = \frac{\Delta t}{P}. \tag{1.8}$$

While exploring the effects that these terms give rise to, I split the Hamiltonians each into three parts,

$$H_{clock} = H_{sch} + H_s + H_{s^2}, \quad \text{and} \quad H^{signal} = H^{sch} + H^s + H^{s^2}, \tag{1.9}$$

no spin dependence, spin-odd, and spin-even.

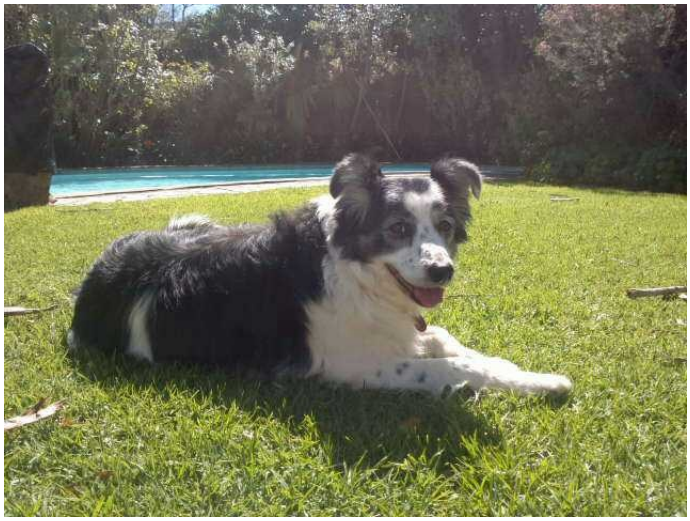

Figure 1.5: *Ay, in the catalogue ye go for men; As hounds, and greyhounds, mongrels, spaniels, curs, Shoughs, water-rugs, and demi-wolves, are 'clept All by the name of dogs: the valued file Distinguishes the swift, the slow, the subtle, The housekeeper, the hunter, every one According to the gift which bounteous nature Hath in him closed.*

It is convenient to be able to set the black hole spin direction without having to rotate the observer and the orbit. However, the Kerr geometry in Boyer-Lindquist coordinates necessarily aligns the axis of symmetry of the coordinate system with the axis of symmetry of the space-time geometry itself, and it is therefore not possible to disentangle the preferred direction of the coordinates with that of the spin in these coordinates. So, I first canonically transform the Hamiltonian to cartesian coordinates, and then generalize the spin direction. I make the transformation

$$\begin{aligned} x_\mu &= (t, r, \theta, \phi) \longrightarrow (t, \mathbf{x}) && (1.10)\\ p_\mu &= (p_t, p_r, p_\theta, p_\phi) \longrightarrow (p_t, \mathbf{p})\,. && (1.11) \end{aligned}$$

Under the generating function

$$S = r\sin\theta\cos\phi p_x + r\sin\phi\sin\theta p_y + r\cos\theta p_z, \tag{1.12}$$

the canonical momenta in the two bases are related by

$$\begin{aligned} p_r &\equiv \frac{\partial S}{\partial r} = \frac{\mathbf{x}\cdot\mathbf{p}}{r}, && (1.13)\\ p_\phi &\equiv \frac{\partial S}{\partial \theta} = (\mathbf{x}\times\mathbf{p})_z\,, && (1.14)\\ p_\theta &\equiv \frac{\partial S}{\partial \phi} = \frac{-1}{\sqrt{1-\left(\frac{z}{r}\right)^2}}\left(p_z r - \frac{z\mathbf{x}\cdot\mathbf{p}}{r}\right). && (1.15) \end{aligned}$$

Inserting these into H, I have the Hamiltonian in Cartesian coordinates.

$$
\begin{aligned}
H &= -\frac{p_t^2}{2}, && (1.16)\\
&+ \mathbf{p}^2 - \frac{p_t^2}{r}, && (1.17)\\
&+ -\frac{\mathbf{x}\cdot\mathbf{p}}{r} - \frac{2p_t^2}{r^2} && (1.18)\\
&+ -\frac{2sp_t(\mathbf{x}\times\mathbf{p})_z}{r^3} && (1.19)\\
&+ -4\frac{p_t^2}{r^3} + \underbrace{\frac{s^2p_t^2}{r^3}\frac{x^2+y^2}{r^2}}_{❶} + \underbrace{\frac{s^2}{2}\frac{1}{r^6}\left(x^2+y^2\right)\left(xp_x+yp_y+yp_z\right)^2}_{❷}\\
&\quad \underbrace{-\frac{s^2}{2}\frac{1}{r^4}\frac{1}{1-\frac{z^2}{r^2}}\left(p_zr - \frac{z\left(xp_x+yp_y+zp_z\right)}{r}\right)^2\left(1-\frac{x^2+y^2}{r^2}\right)}_{❸}\\
&\quad \underbrace{-\frac{s^2}{2}\frac{1}{r^2}\frac{\left(xp_y-yp_x\right)^2}{x^2+y^2}}_{❹}
\end{aligned}
$$

To generalize the spin direction I need to promote the scalar s to a 3-vector $\mathbf{s}$. Because the Kerr metric in Boyer-Lindquist coordinates aligns the spin direction along the axis-of symmetry of the coordinate system, the spin points in the $z-$direction. Written in the cartesian basis, I generalize it to $\mathbf{s} = (s_x, s_y, s_z)$. For simplicity's sake, I set the spin maximal, $|\mathbf{s}| = 1$.

Moving from the $z-$direction to the $\mathbf{s}-$direction, the frame-dragging term (1.19) becomes

$$-\frac{2p_t\mathbf{p}\cdot(\mathbf{s}\times\mathbf{x})}{r^3}. \tag{1.20}$$

The spin-squared terms, slightly more complicated are

❶
$$\frac{p_t^2}{r^3}s_\perp^2, \tag{1.21}$$

❷
$$\frac{1}{2}\frac{s_\perp^2}{r^4}\left(\mathbf{x}\cdot\mathbf{p}\right)^2, \tag{1.22}$$

❸
$$-\frac{1}{2}\frac{1}{r^4}\frac{1-s_\perp^2}{1-s_\parallel^2}\left(\left(\mathbf{p}\cdot\mathbf{s}\right)r - \frac{\left(\mathbf{x}\cdot\mathbf{s}\right)\left(\mathbf{x}\cdot\mathbf{p}\right)}{r}\right)^2, \tag{1.23}$$

❹
$$-\frac{1}{2}\frac{1}{r^4}\frac{\left(\mathbf{p}\cdot\mathbf{s}\times\mathbf{x}\right)^2}{s_\perp^2}, \tag{1.24}$$

with

$$s_\perp \equiv \frac{\mathbf{s}\times\mathbf{x}}{r} \qquad \text{and} \qquad s_\parallel \equiv \frac{\mathbf{s}\cdot\mathbf{p}}{r}.$$

Using these expressions I can integrate the associated Hamilton equations and find the orbits of timelike trajectories in the weak field Kerr geometry with arbitrary spin-direction. Figures 1.6, 1.7 and 1.8 show what the relativistic terms H_{sch}, H_s, and H_{s^2} respectively are capable of doing, each as perturbations to Keplerian orbits. Time axes in these plots represent the coordinate time of a distant observer, which has been integrated over proper time, along with the star's 3-position and 4-momentum. The independent variable here is the proper time, or, the time that the clock reports to an observer falling with it.

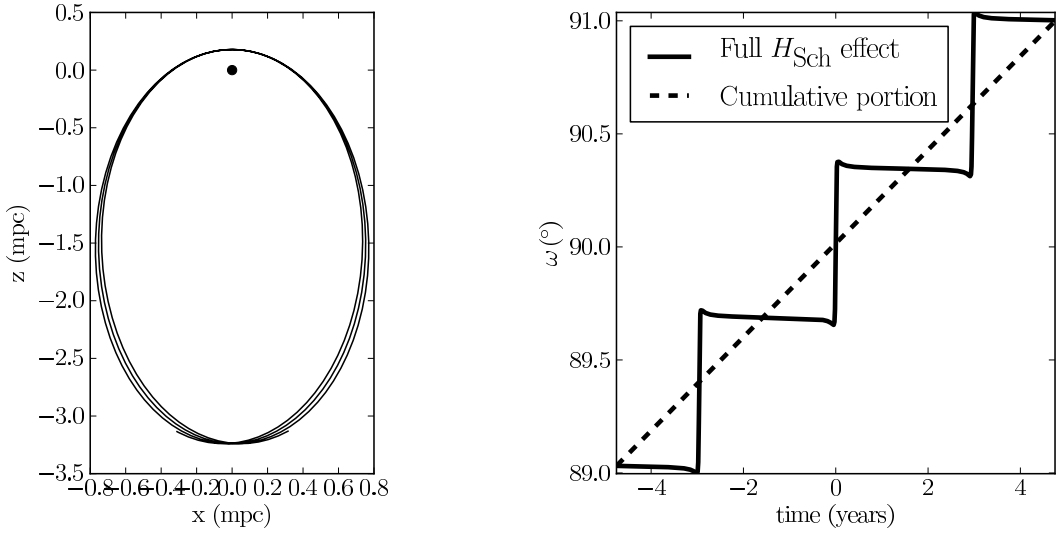

Figure 1.6: This orbit has eccentricity 0.9, and a semi-major axis of 1.6mpc (or $\sim 8.8\cdot 10^3$ gravitational radii), essentially the star S2, albeit pushed in by a factor of three. Here we view it face-on. The inclusion of H_{sch} in the dynamics perturbs the orbit from that of an ellipse. The almost-staircase curve is the instantaneous argument of pericenter evaluated at each point on the orbit. Naturally, relativistic effects are strongest at pericenter, at which time the perturbation imparts the most influence. The cumulative portion of the perturbation culminates in a prograde precession of $\sim 0.7°$/revolution, as estimated by the straight dashed line (1.4). The rosetta shape the orbit traces out is barely visible in the left panel. Note the curious behavior of the instantaneous angular element ω around pericenter. The information contained in this perturbed staircase is more valuable than that contained in the cumulative portion alone. After yet more orbits, the two curves diverge due to higher-order cumulative effects due not only to higher order dynamical effects at $H_{sch} \sim \mathcal{O}\left(r^{-2}\right)$, but also due to the higher order term in $H_{sch} \sim \mathcal{O}\left(r^{-3}\right)$. For the analytical cumulative line to account for this and keep it from drifting, equation (1.4) would need to be modified with terms $\sim L^{-2}$. Although technically, if in this regime, the leading order contributions H_{sch} and H_{s^2} would also have to be included.

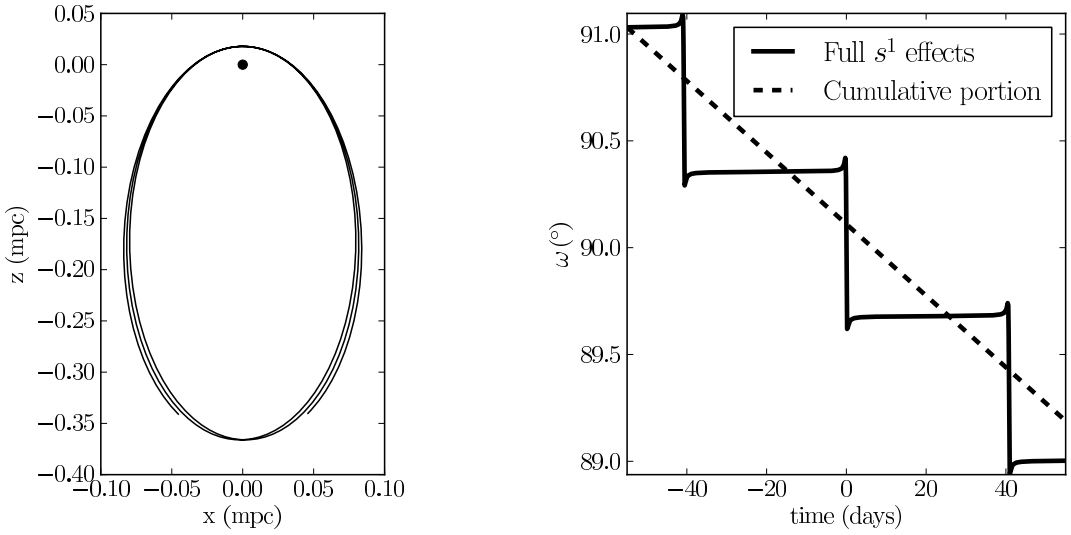

Figure 1.7: The orbital effects due to the spin term - H_s - as a perturbation to a Keplerian orbit. The orbit is the same as that in Fig. 1.6., albeit further pushed in by a factor of 10, so as to keep the cumulative precession per orbit approximately the same. The black hole spin is maximal, and points perpendicular to the orbital plane. Were the spin direction not perpendicular to the orbital plane, we would see orbital plane itself also precessing about the spin axis.

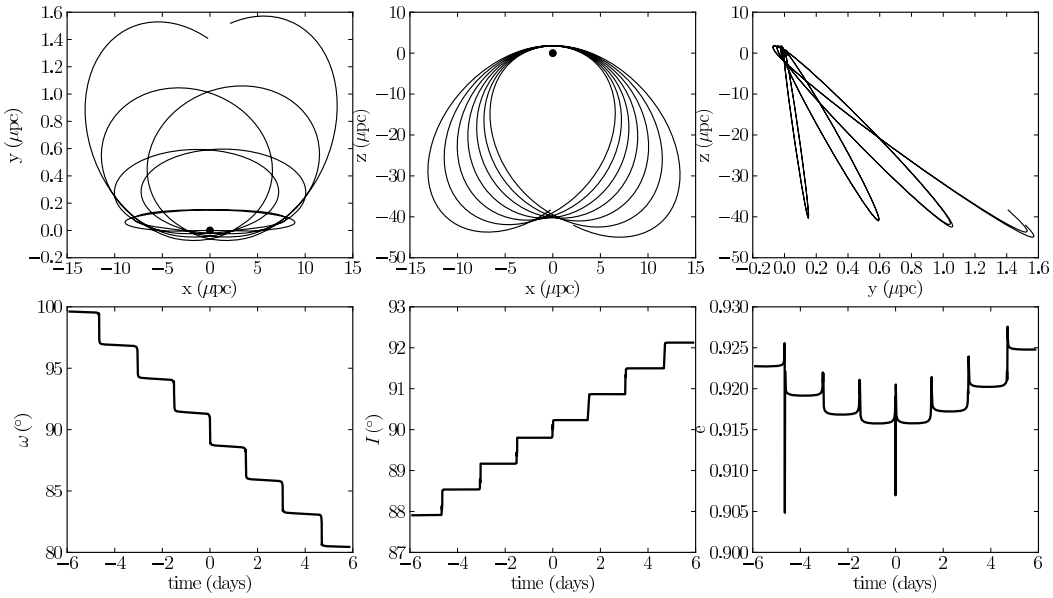

Figure 1.8: Here we look at the s^2 perturbations to a Keplerian orbit. To make them visible, I have scaled the orbit size down by a factor of 10 from that in Fig 1.7. The initial orbit orientation is the same as that in the previous examples - in the z-x plane. The spin direction though now points in the x-direction. In this demonstration none of the Keplerian orbital elements are exempt from change. Keep in mind that because the true orbit at $H_{orbit} \sim \mathcal{O}\left(r^{-3}\right)$ warrants the inclusion of H_{sch} and H_s, which are not included here, the orbit would look quite different. In this strong field the time per revolution would be far lower and most semblance of its Keplerian origins would be visually lost.

Knowing how to calculate the orbits of the stars and pulsars, I can then have them tick in equal intervals of proper time, and, using the same Hamiltonian, propagate these signals along null paths to the observer. This is a boundary value problem, whose implementation is explained in Angélil and Saha (2010) - null geodesics are shot in equal intervals of proper time and terminate at the observer, who is placed effectively at infinity. This gives us the pulse times of arrival. The derivative of the arrival times with respect to proper time (1.1) yields the observable in the case of spectroscopy. In an example orbit, Fig. 1.9 shows the propagation signal residuals due to Schwarzschild, and Fig. 1.10 due to the spin and spin-squared metric terms.

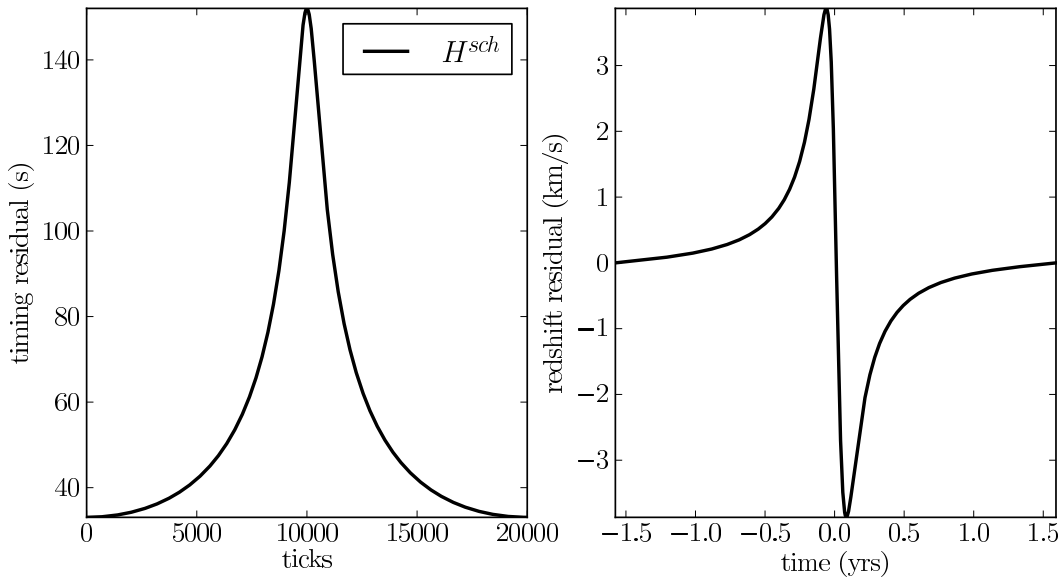

Figure 1.9: Here we look at the signal residuals due to the Schwarzschild propagation effects. Because I wish to look at each effect in isolation, these signals are emitted from clocks on Keplerian orbits. In this example, I have lowered the eccentricity of the orbit to 0.6 so that the interesting behavior does not overcrowd pericenter passage. The left panel shows pulsar timing residuals, and the second the redshift of a stellar spectral line. The signals are shot from a Keplerian orbit with semi-major axis ~ 1.6mpc (the same as the example in Fig. 1.6). The Schwarzschild residual is largely dominated by the $H^{sch} \sim \mathcal{O}\left(r^{-1}\right)$ Schwarzschild term. The effect illustrated here is sometimes called the Shapiro delay. Were the orbit size changed, the curve in the left panel would remain unchanged, as the leading-order Shapiro delay contribution is constant over period. However, the same effect, viewed with a stellar spectral line, grows with decreasing period.

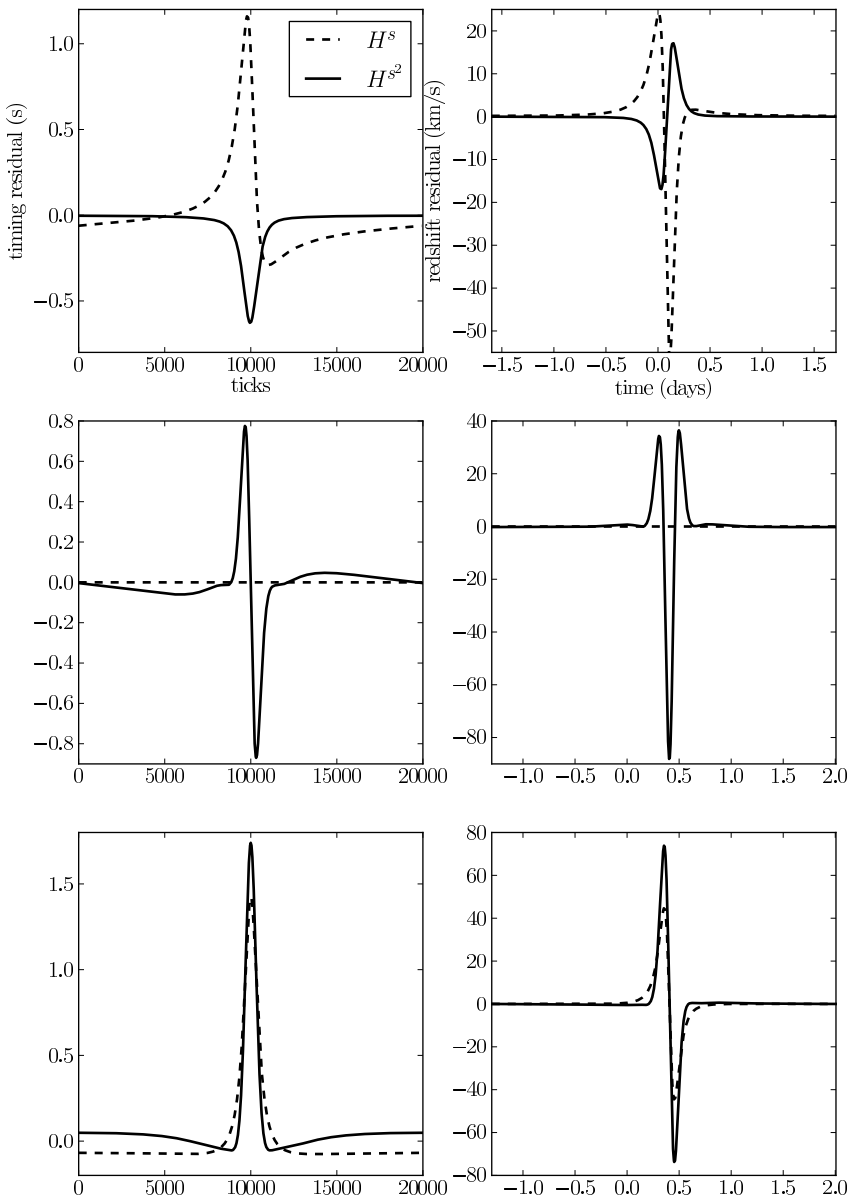

Figure 1.10: The propagation effects due to spin. All orbits are the same Keplerian one, and have the same geometry as that in Fig. 1.6 and Fig. 1.9, except here the orbit has semi-major axis 50 times smaller. Only the spin direction changes in each row, and affects only the light-ray trajectories. In the first panel, the spin is $\mathbf{s} = (1, 1, 1)/\sqrt{3}$. In the second, the spin vector points towards the observer, and so the frame-dragging signal drops to zero, while the s^2 signal remains. In the last row, the spin points in the direction perpendicular to the observer-black hole line. The s^2 signals on both the timing and redshift residuals are capable a wide variety of signal shapes, which depend on the orbit geometry relative to the observer and the spin-direction.

Fig. 1.11, in a numerical experiment, plots the residual redshift and timing delay against orbital period, confirming the expected orbit scaling relationships. Fig. 1.12. does the same for propagation effects. Intriguing is that the leading-order Schwarzschild effects, both on the orbit and on signal propagation (from H_{sch} and H^{sch}) make for timing residuals which remain constant as the orbital size deceases. For the propagation part alone, this characteristic is well-known, but less so for the orbit. This holds only for timing only though, and not for a spectral line shift - for the redshift I expect the signal to be larger on smaller orbits, in expectation with (1.8). In fact, since all redshift-signals have a P-dependence steeper by a factor of the period; prospects for testing relativity as period sizes decrease improve quicker for stellar orbits than pulsar orbits.

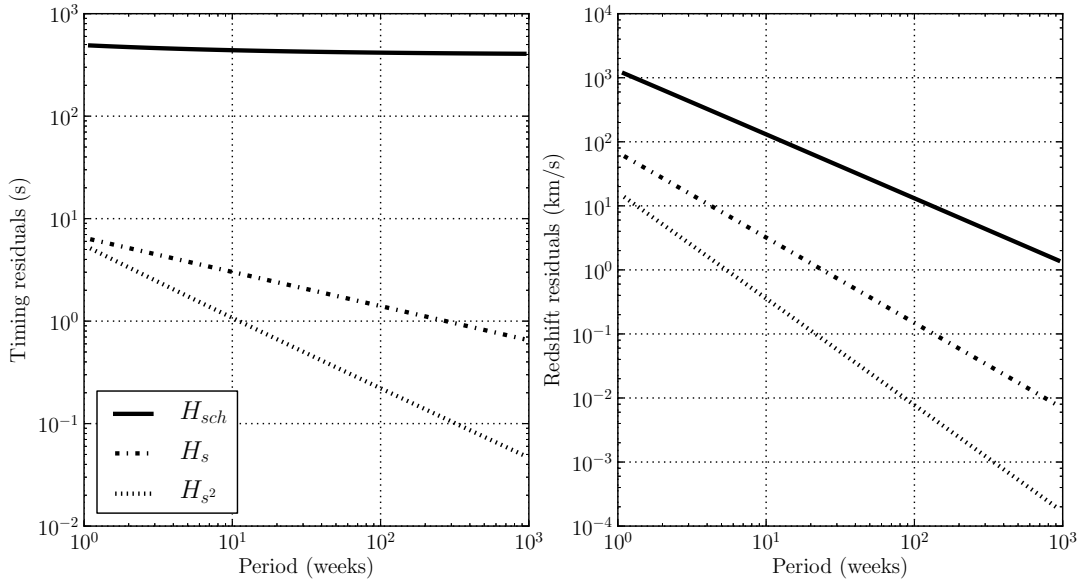

Figure 1.11: Here I show the size of the residuals on orbit perturbations. As in Fig 1.1., the eccentricity of the orbit is 0.6, and has an inclination with respect to the observer of $I = 45°$. The left panel shows the redshift residual, and the right the timing residual. Relativistic effects cause the orbit shape to change, and here the residual is the size of the residual observable at pericenter, after one orbit. These curves therefore show only the cumulative orbital effects. The leading order Schwarzschild contribution has $H_{sch} \sim \mathcal{O}\left(r^{-2}\right)$, and is flat. This is unlike the $\sim \mathcal{O}\left(r^{-3}\right)$ term in H^{sch}, whose contribution bends the both the timing and redshift H_{sch} residual curve for short-period orbits.

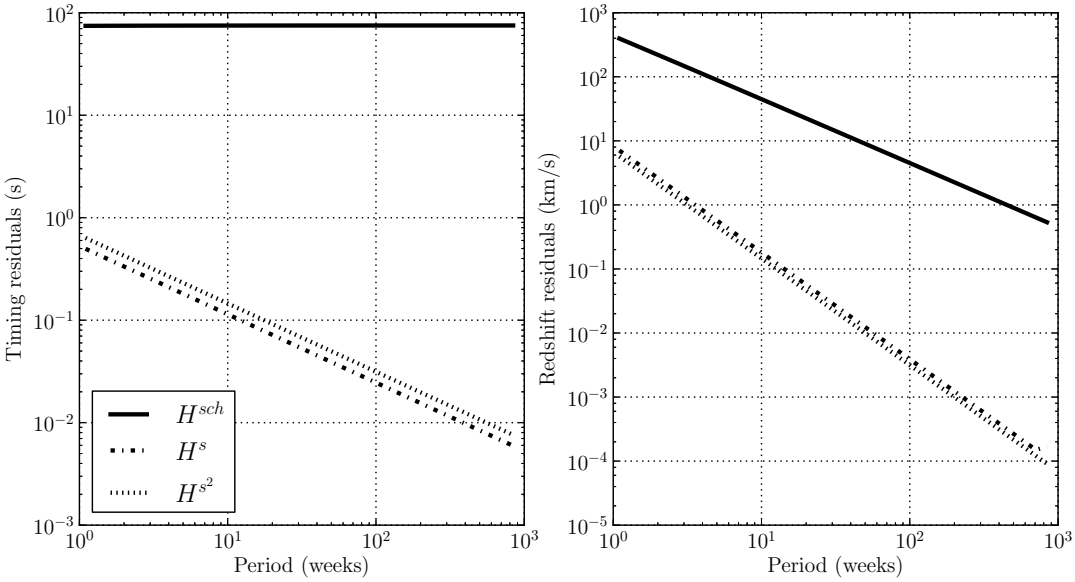

Figure 1.12: These are the residuals due to signal propagation. I show here the magnitudes of the curves in Fig 1.9. and Fig 1.10. for a range of orbit sizes. The orbit geometry is the same as that in Fig 1.11. Comparison of these residuals with those on the orbit, in Fig 1.11. help indicate which effects need to be included in the analysis when interested in a particular effect type. For instance, if a prospective experiment is interested in measuring the spin s^1, then its manifestation on the signal propagation may be neglected. On the other hand, for s^2 experiments, its consequences on neither the orbits nor propagation paths may be neglected.

1.4 Multipole moments are not hair

The statement that "Black holes have no hair" is the general notion that a black hole event horizon allows no physical properties of what fell into it to be measured, other than total mass, angular momentum and electric charge. Or, in other words, any gravitational experiment performed outside a vacuum, stationary black hole depends only the mass and spin. There are a number of results that can be considered some version of no-hair theorem. For example, Robinson (1975) shows that the Kerr metric is the only stationary solution of the vacuum Einstein field equations $R_{\mu\nu} = 0$. Thus, in Einstein gravity, an uncharged stationary black hole is not only hairless, but always Kerr.

While the mass M, the spin parameter s, and the orientation of the spin are the only properties of a Kerr black hole, they enter into the metric in a rather complicated way. In particular, spin appears in both odd powers (giving rise to frame dragging) and in even powers (producing torque-like effects). So it is natural to seek a simpler way of describing the dependence on M and s by analogy with a classical multipole expansion.

In Newtonian physics, given an isolated source with an arbitrary mass distribution, the multipole expansion of the potential is a sum over spherical harmonic basis functions. This sum is a solution

to the Poisson equation far enough away from the isolated source. In general relativity, the analogue to the potential are the components of a rank two tensor, the metric. Despite this analogy, how we move from these fields to equations of motion in each framework is completely different. Because of these differences there is no clear way to generalize or transform the notion of a multipole expansion to general relativity. R. O. Hansen (1974) proposes a definition for multipole moments in general relativity, and outlines the procedure by which they may be calculated. He goes on to calculate them for the Kerr metric, and with his choice of definition finds a monopole moment equal to m, a spin-pole proportional to ms, and a mass-quadrupole proportional to ms^2. There is no mass-dipole moment nor a spin-quadrupole moment. Janis and Newman (1965); Kundu (1981); Simon and Beig (1983); Fodor et al. (1989) propose other methods and definitions for quadruple moments, which in some case turn out to reduce to the same result in the Kerr-case. Newman and Janis (1965), after computing the multipole structure of the Kerr metric using their definition in Janis and Newman (1965), conclude that because their multiple moments are the same as those for the electrodynamic system of a ring of charges rotating about its axis of symmetry, that the full Kerr solution must describe a rotating ring of mass[3]. The rotating ring explanation was promptly shown to be erroneous.

Given the Kerr multipole relation, if a metric solution to the field equations, far enough away from a source possesses a multipole structure which was the same or similar to some Newtonian system, we could tentatively interpret the metric as a relativistic generalization. The relation between M, s and the quadrupole of a Kerr metric has been highlighted by several several authors in the context of S-star system (Liu et al., 2012; Will, 2008; Sadeghian and Will, 2011; Johannsen, 2012; Johannsen and Psaltis, 2012, 2011; Kramer et al., 2004; Merritt et al., 2010; Iorio, 2011). It is argued that the Kerr multiple relation is potentially a test of no-hair theorems.

Such claims must be taken with a grain of salt for several reasons.

- First, a test of the Kerr multipole relations is a test of Kerr, but not of no-hair. What if the Universe gives black holes no hair, but does not obey Einstein gravity and as a result, no black holes are Kerr.
- Second, if the goal is to test the Kerr metric, and hence Einstein gravity, why restrict attention to the Kerr quadrupole relations? The form of the Kerr metric provides much more detailed predictions than multipoles. Furthermore, there are terms in the metric which are artifacts of Schwarzschild, and so do not depend on spin. As shown in Table 1.3, they occur at the same order as the spin terms. As far as tests of the field equations go, effects that are sensitive to s or s^2 are no more special than those that aren't. This because the Schwarzschild solution is no less remarkable than the Kerr, as both descend from the same field equations.
- Finally, the R. O. Hansen (1974) definition of multipoles is anyway not unique. Janis and Newman (1965), Newman and Janis (1965), Kundu (1981), Simon and Beig (1983), and Fodor et al. (1989) propose other definitions for multipole moments, which in some cases turn out to reduce to the same results for the Kerr-case. Thorne (1980) consolidated various approaches, and introduced the definitions now standard in gravitational wave theory.

The supposed 'tests of no-hairness' seen in the literature are really 'tests of one aspect of Kerrness'. I stress that because all relativistic effects, spin-dependent or not, descend from the same field equations, are of equal significance in testing gravity around a compact source. Let us not forget that discussion on galactic center tests of Kerrness is somewhat overshadowed by the fact that regardless of the nature of the galactic center black hole, we should *expect* tests of Kerrness to fail.

[3]This was before the Kerr geometry had been written Boyer-Linquist coordinates, which greatly aided the physical interpretation.

By this, I mean that should the Einstein equations show themselves faithful to our expectations, we can still expect deviations from freely-falling test particles in the Kerr field, because the space-time is no vacuum, nor are the clocks true test particles. Because of the uncertainties in the stellar mass distribution around Sgr A*, we are somewhat oblivious as to what the deviations might look like.

1.5 Wrapping up

S stars and if existent, S pulsars, travel upon the most relativistic orbits known. With them, completely unexplored characteristics of general relativity will become accessible. Transient shape-changes, signal propagation delay, intrinsic redshifting, all either due to already-tested metric terms, or higher-order ones are to be expected and reveled. If the observed dynamics are not in agreement with that predicted from Einstein gravity even after taking the surrounding astrophysical environment into account, then it may be challenging to work out what went wrong. It's possible that the intense gravitational field is not due to a black hole at all, but rather some other kind of dense matter. Apparent general relativity-failure could be attributed to two fundamental reasons: the field equations are wrong, or, the principle of equivalence does not hold and the gravitational laws of physics are non-metric. (Of course, in either case, the no-hair conjecture could still hold true.)

The relativistic effects which will be observable on galactic center geodesics are extensions of similar experiments in the solar system and in binary pulsars. If general relativity is to be trusted, then galactic center stars and pulsars, if found further in to the black hole, will test the same metric, albeit in fields orders of magnitude stronger. The combination of the strong field as well as long period orbit timescales push otherwise invisible or irrelevant features into the observables. Solar system and binary pulsar methods will not work. Precession is not gradual, but rather a shock that happens at pericenter. The consequence of pericenter passage is especially true for terms which crop up at higher order, like those proportional to the spin or its square.

This regime expects the full 4-dimensional relativistic equations to be solved. Few effects can be captured by analytical formulae like (1.3), (1.4) and (1.5). Analytical versions for many of the expected effects are not known, and those that are available tend to strip them down by shunning transient phenomena. Furthermore, all effects are all coupled, which places further burden on analytical approaches.

The spectrometers of the Keck and VLT telescopes have independently observed the spectra of the S stars, managing to achieve spectral resolution up to $\sim 10\text{km} \cdot \text{s}^{-1}$. The European Extremely Large Telescope project will be able to perform these measurements at $1\text{km} \cdot \text{s}^{-1}$, and so will also play an important role in future experiments. Angélil et al. (2010) argue that the Schwarzschild effects discussed in this thesis, both on the orbit and on the photon paths, will be resolvable by these instruments for the known S stars. Higher order effects however will necessitate the discovery of stars further in to the black hole.

Were S-pulsars to be detected around Sgr A*, the Parkes observatory, Green Bank, and Effelsberg radio telescopes will be among the facilities capable of performing accurate timing. Liu et al. (2012) estimate a timing accuracy for such arrays to be $\sigma_{\text{TOA}} \sim 1\text{ms}$. The high frequency component of the Square Kilometer Array will be expected to achieve accuracies an order of magnitude better. In a pure Kerr field, measurements at this accuracy level would likely be capable of resolving even spin-squared effects on S-pulsar orbits and propagation signals, with orbital periods ~ 10 years. Of course, the extended mass distribution of as-yet unseen stars orbiting Sgr A* will obscure these

signals. For orbits with such periods, the leading-order Schwarzschild contributions, transient and cumulative, might be resolvable. However higher order ones will likely be obscured by red noise due to the extended mass distribution. Unless compelling techniques capable of extracting relativistic signals drowned out by this noise are developed, stars and pulsars closer in to the black hole than those yet discovered are needed.

Bibliography

R. Angélil and P. Saha. Relativistic Redshift Effects and the Galactic-Center Stars. *The Astrophysical Journal*, 711:157–163, March 2010. doi: 10.1088/0004-637X/711/1/157.

Raymond Angélil and Prasenjit Saha. Galactic-center s stars as a prospective test of the einstein equivalence principle. *The Astrophysical Journal Letters*, 734(1):L19, 2011. URL `http://stacks.iop.org/2041-8205/734/i=1/a=L19`.

Raymond Angélil, Prasenjit Saha, and David Merritt. Toward relativistic orbit fitting of galactic center stars and pulsars. *The Astrophysical Journal*, 720(2):1303, 2010. URL `http://stacks.iop.org/0004-637X/720/i=2/a=1303`.

V. Bozza and L. Mancini. Gravitational Lensing of Stars Orbiting the Massive Black Hole in the Galactic Center. *Astrophysical Journal*, 696:701–705, May 2009. doi: 10.1088/0004-637X/696/1/701.

I. Ciufolini and E. C. Pavlis. A confirmation of the general relativistic prediction of the Lense-Thirring effect. *Nature*, 431:958–960, October 2004. doi: 10.1038/nature03007.

I. Ciufolini, A. Paolozzi, E. C. Pavlis, J. C. Ries, R. Koenig, R. A. Matzner, G. Sindoni, and H. Neumayer. Towards a One Percent Measurement of Frame Dragging by Spin with Satellite Laser Ranging to LAGEOS, LAGEOS 2 and LARES and GRACE Gravity Models. *Space Science Reviews*, 148:71–104, December 2009. doi: 10.1007/s11214-009-9585-7.

J. M. Cordes and T. J. W. Lazio. Finding Radio Pulsars in and beyond the Galactic Center. *The Astrophysical Journal*, 475:557, February 1997. doi: 10.1086/303569.

A. Eckart, R. Schödel, J. Moultaka, C. Straubmeier, T. Viehmann, S. Pfalzner, and J.-U. Pott. The Galactic Center: The Stellar Cluster and the Massive Black Hole. In S. Hüttmeister, E. Manthey, D. Bomans, & K. Weis, editor, *The Evolution of Starbursts*, volume 783 of *American Institute of Physics Conference Series*, pages 17–25, August 2005. doi: 10.1063/1.2034961.

A. Eckhart, R. Schödel, and C. Straubmeier. *The Black Hole at the center of the Milky Way*. 2005.

F. Eisenhauer, R. Schödel, R. Genzel, T. Ott, M. Tecza, R. Abuter, A. Eckart, and T. Alexander. A Geometric Determination of the Distance to the Galactic Center. *Astrophysical Journal Letters*, 597:L121–L124, November 2003. doi: 10.1086/380188.

C. W. F. Everitt, D. B. Debra, B. W. Parkinson, J. P. Turneaure, J. W. Conklin, M. I. Heifetz, G. M. Keiser, A. S. Silbergleit, T. Holmes, J. Kolodziejczak, M. Al-Meshari, J. C. Mester, B. Muhlfelder, V. G. Solomonik, K. Stahl, P. W. Worden, Jr., W. Bencze, S. Buchman, B. Clarke, A. Al-Jadaan, H. Al-Jibreen, J. Li, J. A. Lipa, J. M. Lockhart, B. Al-Suwaidan, M. Taber, and S. Wang. Gravity Probe B: Final Results of a Space Experiment to Test General Relativity. *Physical Review Letters*, 106(22):221101, June 2011. doi: 10.1103/PhysRevLett.106.221101.

T. Fließbach. *Allgemeine Relativitätstheorie.* 1990.

G. Fodor, C. Hoenselaers, and Z. Perjés. Multipole moments of axisymmetric systems in relativity. *Journal of Mathematical Physics*, 30:2252, 1989.

S. Gillessen, F. Eisenhauer, T. K. Fritz, H. Bartko, K. Dodds-Eden, O. Pfuhl, T. Ott, and R. Genzel. The Orbit of the Star S2 Around SGR A* from Very Large Telescope and Keck Data. *Astrophysical Journal Letters*, 707:L114–L117, December 2009a. doi: 10.1088/0004-637X/707/2/L114.

S. Gillessen, F. Eisenhauer, S. Trippe, T. Alexander, R. Genzel, F. Martins, and T. Ott. Monitoring Stellar Orbits Around the Massive Black Hole in the Galactic Center. *The Astrophysical Journal*, 692:1075–1109, February 2009b. doi: 10.1088/0004-637X/692/2/1075.

L. Iorio. Perturbed stellar motions around the rotating black hole in sgr a* for a generic orientation of its spin axis. *Phys. Rev. D*, 84:124001, Dec 2011. doi: 10.1103/PhysRevD.84.124001. URL `http://link.aps.org/doi/10.1103/PhysRevD.84.124001`.

Lorenzo Iorio. Conservative evaluation of the uncertainty in the lageos-lageos ii lense-thirring test. *Central European Journal of Physics*, 8:25–32, 2010. ISSN 1895-1082. URL `http://dx.doi.org/10.2478/s11534-009-0060-6`. 10.2478/s11534-009-0060-6.

A. I. Janis and E. T. Newman. Structure of Gravitational Sources. *Journal of Mathematical Physics*, 6:902, 1965.

T. Johannsen. Testing the No-Hair Theorem with Sgr A*. *Advances in Astronomy*, 2012:486750, 2012. doi: 10.1155/2012/486750.

T. Johannsen and D. Psaltis. Metric for rapidly spinning black holes suitable for strong-field tests of the no-hair theorem. *Physical review D*, 83(12):124015, June 2011. doi: 10.1103/PhysRevD.83.124015.

T. Johannsen and D. Psaltis. Testing the No-Hair Theorem with Observations in the Electromagnetic Spectrum. IV. Relativistically Broadened Iron Lines. *ArXiv e-prints*, February 2012.

R. Kannan and P. Saha. Frame Dragging and the Kinematics of Galactic-Center Stars. *Astrophysical Journal*, 690:1553–1557, January 2009. doi: 10.1088/0004-637X/690/2/1553.

Roy P. Kerr. Gravitational field of a spinning mass as an example of algebraically special metrics. *Phys. Rev. Lett.*, 11:237–238, Sep 1963. doi: 10.1103/PhysRevLett.11.237. URL `http://link.aps.org/doi/10.1103/PhysRevLett.11.237`.

M. Kramer, B. Klein, D. Lorimer, P. Müller, A. Jessner, and R. Wielebinski. The Effelsberg Search for Pulsars in the Galactic Centre. In M. Kramer, N. Wex, & R. Wielebinski, editor, *IAU Colloq. 177: Pulsar Astronomy - 2000 and Beyond*, volume 202 of *Astronomical Society of the Pacific Conference Series*, page 37, 2000.

M. Kramer, D.C. Backer, J.M. Cordes, T.J.W. Lazio, B.W. Stappers, and S. Johnston. Strong-field tests of gravity using pulsars and black holes. *New Astronomy Reviews*, 48(11?12):993 – 1002, 2004. ISSN 1387-6473. doi: 10.1016/j.newar.2004.09.020. URL `http://www.sciencedirect.com/science/article/pii/S1387647304000909`. ¡ce:title¿Science with the Square Kilometre Array¡/ce:title¿ ¡xocs:full-name¿Science with the Square Kilometre Array¡/xocs:full-name¿.

P. Kundu. Multipole expansion of stationary asymptotically flat vacuum metrics in general relativity. *Journal of Mathematical Physics*, 22:1236, 1981.

K. Liu, N. Wex, M. Kramer, J. M. Cordes, and T. J. W. Lazio. Prospects for Probing the Spacetime of Sgr A* with Pulsars. *The Astrophysical Journal*, 747:1, March 2012. doi: 10.1088/0004-637X/747/1/1.

J.-P. Macquart, N. Kanekar, D. A. Frail, and S. M. Ransom. A high-frequency search for pulsars within the central parsec of sgr a*. *The Astrophysical Journal*, 715(2):939, 2010. URL `http://stacks.iop.org/0004-637X/715/i=2/a=939`.

F. Martins, S. Gillessen, F. Eisenhauer, R. Genzel, T. Ott, and S. Trippe. On the Nature of the Fast-Moving Star S2 in the Galactic Center. *Astrophysical Journal Letters*, 672:L119–L122, January 2008a. doi: 10.1086/526768.

F. Martins, S. Gillessen, F. Eisenhauer, R. Genzel, T. Ott, and S. Trippe. On the Nature of the Fast-Moving Star S2 in the Galactic Center. *Astrophysical Journal Letters*, 672:L119–L122, January 2008b. doi: 10.1086/526768.

David Merritt, Tal Alexander, Seppo Mikkola, and Clifford M. Will. Testing properties of the galactic center black hole using stellar orbits. *Phys. Rev. D*, 81:062002, Mar 2010. doi: 10.1103/PhysRevD.81.062002. URL `http://link.aps.org/doi/10.1103/PhysRevD.81.062002`.

C. W. Misner, K. S. Thorne, and J. A. Wheeler. *Gravitation*. 1973.

E. T. Newman and A. I. Janis. Note on the Kerr Spinning Particle Metric. *Journal of Mathematical Physics*, 6:915, 1965.

E. Pfahl and A. Loeb. Probing the Spacetime around Sagittarius A* with Radio Pulsars. *The Astrophysical Journal*, 615:253–258, November 2004. doi: 10.1086/423975.

M. Preto and P. Saha. On Post-Newtonian Orbits and the Galactic-center Stars. *Astrophysical Journal*, 703:1743–1751, October 2009. doi: 10.1088/0004-637X/703/2/1743.

R. O. Hansen. Multipole moments of stationary space times. *Journal of Mathematical Physics*, 15:46, 1974.

D. C. Robinson. Uniqueness of the kerr black hole. *Phys. Rev. Lett.*, 34:905–906, Apr 1975. doi: 10.1103/PhysRevLett.34.905. URL `http://link.aps.org/doi/10.1103/PhysRevLett.34.905`.

G. F. Rubilar and A. Eckart. Periastron shifts of stellar orbits near the Galactic Center. *Astronomy and Astrophysics*, 374:95–104, July 2001. doi: 10.1051/0004-6361:20010640.

N. Sabha, A. Eckart, D. Merritt, M. Zamaninasab, G. Witzel, M. García-Marín, B. Jalali, M. Valencia-S., S. Yazici, R. Buchholz, B. Shahzamanian, and C. Straubmeier. The S-Star Cluster at the Center of the Milky Way: On the nature of diffuse NIR emission in the inner tenth of a parsec. *ArXiv e-prints*, March 2012.

Laleh Sadeghian and Clifford M Will. Testing the black hole no-hair theorem at the galactic center: perturbing effects of stars in the surrounding cluster. *Classical and Quantum Gravity*, 28(22): 225029, 2011. URL `http://stacks.iop.org/0264-9381/28/i=22/a=225029`.

R. Schödel, T. Ott, R. Genzel, R. Hofmann, M. Lehnert, A. Eckart, N. Mouawad, T. Alexander, M. J. Reid, R. Lenzen, M. Hartung, F. Lacombe, D. Rouan, E. Gendron, G. Rousset, A.-M. Lagrange, W. Brandner, N. Ageorges, C. Lidman, A. F. M. Moorwood, J. Spyromilio, N. Hubin, and K. M. Menten. A star in a 15.2-year orbit around the supermassive black hole at the centre of the Milky Way. *Nature*, 419:694–696, October 2002. doi: 10.1038/nature01121.

I. I. Shapiro, G. H. Pettengill, M. E. Ash, M. L. Stone, W. B. Smith, R. P. Ingalls, and R. A. Brockelman. Fourth Test of General Relativity: Preliminary Results. *Physical Review Letters*, 20:1265–1269, May 1968. doi: 10.1103/PhysRevLett.20.1265.

Irwin I. Shapiro. Fourth test of general relativity. *Phys. Rev. Lett.*, 13:789–791, Dec 1964. doi: 10.1103/PhysRevLett.13.789. URL `http://link.aps.org/doi/10.1103/PhysRevLett.13.789`.

W. Simon and R. Beig. The multipole structure of stationary space?times. *Journal of Mathematical Physics*, 24:1163, 1983.

Ingrid H. Stairs. Testing general relativity with pulsar timing. *Living Reviews in Relativity*, 6(5), 2003. URL `http://www.livingreviews.org/lrr-2003-5`.

K. S. Thorne. Multipole expansions of gravitational radiation. *Reviews of Modern Physics*, 52: 299–340, April 1980. doi: 10.1103/RevModPhys.52.299.

S. Weinberg. *Gravitation and Cosmology: Principles and Applications of the General Theory of Relativity*. July 1972.

Clifford M. Will. Testing the general relativistic "no-hair" theorems using the galactic center black hole SgrA*. *THE ASTROPHYSICAL JOURNAL LETTERS*, 674:L25, 2008. URL `doi:10.1086/528847`.

S. Zucker, T. Alexander, S. Gillessen, F. Eisenhauer, and R. Genzel. Probing Post-Newtonian Physics near the Galactic Black Hole with Stellar Redshift Measurements. *Astrophysical Journal Letters*, 639:L21–L24, March 2006. doi: 10.1086/501436.

2 first publication

The Astrophysical Journal Letters, 734:L19 (4pp), 2011 June 10 doi:10.1088/2041-8205/734/1/L19

GALACTIC-CENTER S STARS AS A PROSPECTIVE TEST OF THE EINSTEIN EQUIVALENCE PRINCIPLE

Raymond Angélil and Prasenjit Saha
Institute for Theoretical Physics, University of Zürich, Winterthurerstrasse 190, CH-8057 Zürich, Switzerland
Received 2011 January 31; accepted 2011 May 2; published 2011 May 20

ABSTRACT

The S stars in the Galactic-center region are found to be on near-perfect Keplerian orbits around presumably a supermassive black hole, with periods of 15–50 yr. Since these stars reach a few percent of light speed at pericenter, various relativistic effects are expected and have been discussed in the literature. We argue that an elegant test of the Einstein equivalence principle should be possible with existing instruments, through spectroscopic monitoring of an S star concentrated during the months around pericenter, supplemented with an already-adequate astrometric determination of the inclination. In essence, the spectrum of an S star can be considered a heterogeneous ensemble of clocks in a freely falling frame, which near pericenter is moving at relativistic speeds.

Key words: Galaxy: center – relativistic processes

1. INTRODUCTION

The equivalence of gravitational and inertial mass, or that gravity can be canceled by transforming to a freely falling frame, was tested within classical celestial mechanics to high precision by the end of the nineteenth century. After all, if Mercury had a gravitational constant differing from (say) Jupiter's by one part per million, Mercury's orbit would not have fitted classical dynamics well enough to highlight the anomalous precession ($43''$ per century, or 10^{-7}) that was later explained by general relativity.

The Einstein equivalence principle (EEP) adds to the classical or weak equivalence principle the further physical postulate that special relativity holds locally in a freely falling frame. A consequence of the EEP is that the effects of gravity on test particles are fully described by endowing spacetime with a Riemannian metric, and having the particles follow geodesics of that metric. A further consequence of the EEP is that the temporal metric component is, to leading order, given by $g_{tt} = 1 + 2\Phi$, where Φ is the Newtonian potential. Hence, gravity causes time dilation.

Different aspects of the EEP have been verified by multiple experiments, as reviewed extensively by Will (2006). In particular, null-redshift experiments test that gravity—whatever it does—does the same to clocks of different types. Pound–Rebka experiments verify that, in a static gravitational field, time is dilated by a factor $g_{tt}^{-1/2} \simeq 1 - \Phi$. GPS satellites and binary pulsars are effectively freely falling clocks moving at[1] $\sim 10^{-5}$ and $\sim 10^{-3}$, respectively, and exhibit time dilation of $g_{tt}^{-1} \simeq 1 - 2\Phi$.

As excellent as the existing experiments on the EEP are, it would be even nicer to have a laboratory with experiments on multiple materials, the whole freely falling at relativistic speeds. In this Letter, we suggest that the S stars in the Galactic-center region approximate such a laboratory. Stellar spectra contain absorption lines from different atomic species, which can be regarded as different clocks. The EEP asserts that special relativity holds in the star's frame for all atomic processes (local Lorentz invariance), irrespective of where the star is (local position invariance), and these can be tested by observations of a single star. The remaining ingredient of the EEP, namely, that a freely falling frame does not itself depend on the composition of the star (universality of free fall, UFF) requires multiple stars. The nature of a violation of the UFF is difficult to speculate on, however, one could imagine, for example, fits from different S stars' redshift curves all yielding different values for the black hole (BH) mass. Such a deduction would signal a violation of the UFF.

Going beyond the EEP, yet another possibility is that a star with a relativistically significant gravitational self energy, i.e., a pulsar, may give different results. Such a result would be a violation of the strong equivalence principle. It is expected that a significant number of pulsars inhabit the inner milliparsec, and although none have yet been found, searches are currently underway (Macquart et al. 2010).

The S stars achieve the highest speeds of any known geodesics. For example, S2 reaches $v > 0.03$ at pericenter, which it last passed in 2002 and will again in 2018. The pericenter speed is an order of magnitude faster than for known binary pulsars. The spatial scales at pericenter are of order a light day. Hence, even if the quantitative constraints are initially modest, the S stars would test the EEP at velocity and spatial scales not reached by other experiments.

Astrometric and redshift observations of the S stars show them to be on orbits (so far) indistinguishable from pure Keplerian (Gillessen et al. 2009a; Ghez et al. 2008; Gillessen et al. 2009b). Keplerian elements are known to high accuracy for many stars. For example, for S2 the orbital inclination is measured to be $135^\circ \pm 1^\circ$. Expected relativistic effects have been discussed extensively in the literature. These include not only time dilation (Zucker et al. 2006), but also secular orbit precession (Rubilar & Eckart 2001; Will 2008) plus Newtonian perturbations from other stars (Merritt et al. 2010), kinematic effects due to space curvature and frame dragging (Kannan & Saha 2009; Preto & Saha 2009), and composite redshift perturbations including light-path effects (Angélil & Saha 2010; Angélil et al. 2010).

The EEP implies a time dilation of $1 + 2/r$. Hence, a spectral line intrinsically at ν_0 will be redshifted to ν, where

$$\frac{\nu_0}{\nu} = (1 + v_{\rm los})\left(1 + \frac{2}{r}\right). \quad (1)$$

Redshift is conventionally defined as $\nu_0/\nu - 1$. It is, however, somewhat more convenient if one defines $\ln(\nu_0/\nu)$ as the redshift, and we will do so. In any case, the $2/r$ term constitutes a redshift perturbation of $\mathcal{O}(v^2)$ and is the strongest relativistic perturbation. In other words, the leading-order perturbation due to relativity is time dilation on a Keplerian orbit. Space curvature

[1] We use geometrized units: $GM = c = 1$, where M is the black hole mass.

perturbs the redshift at $\mathcal{O}(v^3)$, frame dragging due to BH spin at $\mathcal{O}(v^4)$, with additional physical effects continuing at higher orders (Angélil et al. 2010). One way to test the EEP would be to replace $2/r$ in Equation (1) by α/r and fit observed redshift curves for the parameter α. In fact, this has already been attempted (Zucker et al. 2006) but the available data appeared not yet sufficiently accurate to overcome systematic uncertainties. We argue below that observations concentrated near pericenter will be particularly useful.

Relativistic perturbations to the S stars increase with decreasing pericenter distance. In orbit fitting from spectroscopy, as one looks to stars with longer periods, the perturbations to the redshift from relativity become overwhelmed by perturbations due to massive perturbers. Of all the compact objects orbiting the central BH, we see only the brightest stars. Thousands of solar masses worth of compact objects and a possibly significant dark matter component are expected to inhabit the inner arcseconds. Our lack of understanding of the form of this extended system may play a significant role in obscuring relativistic perturbations for large orbits. However, current models for the Newtonian perturbations are estimated to most likely be weaker than the time dilation effect for the shortest-period stars such as S2 (Schödel et al. 2009; Merritt et al. 2010). Hence, we will disregard the extended-mass component in our analysis.

2. OBSERVABLES

Consider a star on a pure Keplerian orbit. Elementary celestial mechanics gives the position of the star parametrically, that is, both coordinates and time are expressed as functions of the so-called eccentric anomaly ψ. At time

$$t = \frac{P}{2\pi}\left(\psi - e\sin\psi\right), \tag{2}$$

the position of the star in its orbital plane is

$$(x, y, z) = \frac{P}{2\pi\sqrt{a}}(\cos\psi - e, \sqrt{1-e^2}\sin\psi, 0). \tag{3}$$

Here P is the period, e is the eccentricity, while a is the semimajor axis in units of the gravitational radius of the BH.

We now rotate the coordinate system, first by the argument of periapsis ω about the z-axis, then by the inclination I about the new x-axis. The observer is now along the new z-axis. The redshift is

$$\ln\frac{\nu_0}{\nu} = \frac{dz}{dt} + \frac{\alpha}{r} = \frac{A_C\, f(e,\omega,\psi) + A_R}{1 - e\cos\psi}, \tag{4}$$

where

$$f(e,\omega,\psi) \equiv \sqrt{1-e^2}\cos\omega\cos\psi - \sin\omega\sin\psi \tag{5}$$

and we have introduced the coefficients

$$A_C \equiv \frac{\sin I}{\sqrt{a}} \quad \text{and} \quad A_R \equiv \frac{\alpha}{a}, \tag{6}$$

which can be interpreted as the amplitudes of the classical and relativistic contributions to the redshift. We also note that t above is the coordinate time of emission. The time of observation is, of course, t plus the light travel time, whose varying part is the Rømer time delay, which is the z-coordinate of the star

$$A_C\frac{P}{2\pi}[(\cos\psi - e)\sin\omega + \sqrt{1-e^2}\sin\psi\cos\omega], \tag{7}$$

and can also be interpreted as the time integral of the redshift.

Classically, the redshift curve determines only the combination $\sin I/\sqrt{a}$, leaving the inclination unknown. Hence, for a given redshift curve, the inferred orbital speed becomes infinite if the orbit is face-on. Not surprisingly, relativity prevents that happening. From Equations (4) and (6) it follows that

$$\sin^2 I = \frac{A_C^2}{A_R}\alpha. \tag{8}$$

Hence, time dilation breaks the inclination degeneracy if α is known, or allows α to be measured if I is known from astrometry.

It is worth mentioning that another way in which relativity can break the inclination degeneracy is through the well-known precession of

$$\Delta\omega = \frac{6\pi}{a(1-e^2)} \tag{9}$$

per orbit. For binary pulsars, the cumulative ω precession amounts to several degrees per year, allowing a and hence I to be inferred (Brumberg et al. 1975). For Galactic-center stars, however, the ω precession builds up much more slowly. Over a single orbit the redshift due to precession is $\sim\mathcal{O}(v^3)$ because $\Delta\omega \sim \mathcal{O}(v^2)$ over one orbit.

3. PARAMETER RECOVERY

We treat the following seven parameters as unknown.

1. The period P.
2. An additive constant on t.
3. The eccentricity e.
4. The argument of pericenter ω, which along with the inclination I sets the orbit orientation with respect to the observer. Since the observer is on the z-axis, the nodal angle Ω corresponds to a rotation around the line of sight, which leaves the redshift curve invariant.
5. The intrinsic frequency ν_0. This is the absolute line calibration plus any offset due to the observer's radial velocity. Changing ν_0 shifts the redshift curve vertically. The tangential motion of the observer is neglected here, since the Sun's orbital speed of $\sim$200 km s^{-1} in the Galaxy would contribute no significant Doppler shift.
6. A classical redshift amplitude A_C.
7. A relativistic redshift amplitude A_R. In fact, a, I, α form a degenerate trio and are absorbed into the non-degenerate dummy parameters A_C and A_R via Equation (6).

Astrometry independently measures the first four of these, as well as I. Astrometric observations also involve six other parameters: the position and proper motion of the Galactic center on the sky, the distance to the Galactic center, and Ω. The mass of the BH is not an independent parameter, since it is a function of P and a. For our purposes, only I from astrometry is essential. In testing the EEP, while we shall argue that observation of the star over a short time around pericenter suffices for spectroscopy, recovery of the inclination via astrometry can be done anywhere on the orbit.

It is important to note ν_0 and ν need not refer to a single spectral line. The spectra of S stars (see, e.g., Martins et al. 2008) contain multiple features. Most are early-type stars with H and He features, while about 10% are late-type stars with molecular and metal bands/lines and little or no H or He. Hence, S star spectra could, in principle, test the equivalence principle

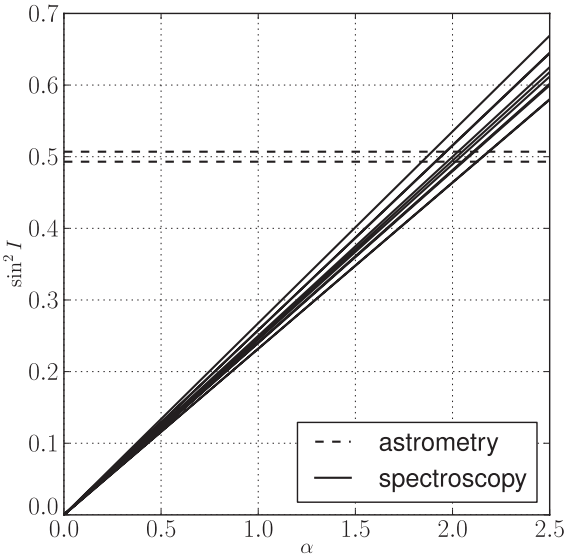

Figure 1. Recovery of α for 10 mock data sets. The ratio A_C^2/A_R is the slope of the lines in the above plot and is recovered from mock spectroscopic data of 14 data points with accuracy 10 km s^{-1}, concentrated around pericenter. The horizontal lines are the upper and lower confidence levels for the recovered inclination from astrometry, taken from Gillessen et al. (2009b). The intersection point corresponds to the value of α for which both data types agree on the inclination.

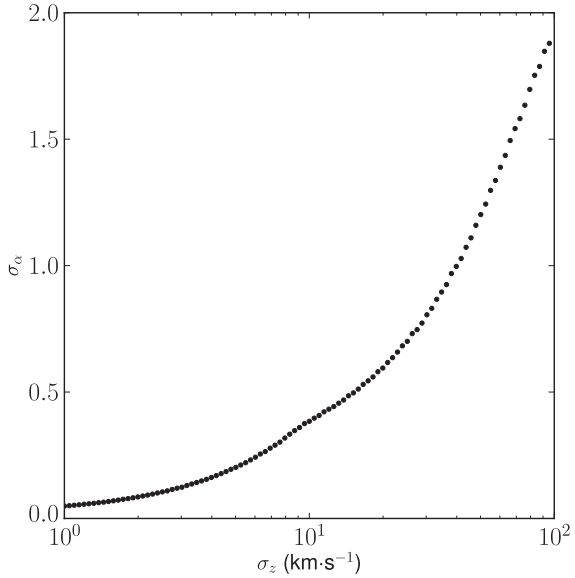

Figure 2. 1σ level in the recovered value of α for spectroscopic data of different accuracy. At each data accuracy level, we have performed the same procedure illustrated in Figure 1, except that 60,000 mock data realizations have been used.

for multiple atomic processes. If the stellar atmosphere does not change appreciably over an orbit, an observed spectrum can be cross-correlated on a logarithmic wavelength scale with a spectrum observed at some other epoch, and the cross-correlation peak would directly give the redshift $\ln(\nu_0/\nu)$ with ν_0 an unknown constant. If different atomic/molecular species behave differently in a freely falling frame, the shape of the cross-correlation curve would change. Alternatively, multiple spectral features could be fitted simultaneously with variable redshift. We do not, however, attempt to model the observable spectra explicitly in this Letter.

We now simulate the recovery of α as follows. We generate 10 mock redshift data points of S2 taken over two months at pericenter, plus four additional data points, at ± 1, ± 2 yr around pericenter. The data are generated with $\alpha = 2$ and orbital parameters taken from Gillessen et al. (2009b). To them we add Gaussian random noise at a dispersion of 10 km s^{-1} and then fit via the seven parameters. We then assume I has been measured by astrometry and use Equation (8) to recover α. Figure 1 shows an example for a few mock data realizations at a fixed accuracy and Figure 2 shows the dependency of the recovered value of alpha with the data accuracy.

4. DISCUSSION

Testing the equivalence principle using a combination of spectroscopy and astrometry seems possible in the near future. In comparing the spread in A_C^2/A_R from mock data to the recovered value for I from real astrometric data (illustrated in Figure 1), in testing the equivalence principle using S2, the current accuracy available from astrometry sits at a comfortable level. Spectroscopic accuracy of S2 at 10 km s^{-1} is not yet available, but seems plausible with future observations. For the late-type star S35, which has a more favorable spectrum, a fit error of 10 km s^{-1} has been achieved (Gillessen et al. 2009b). We remark that any systematic errors that do not change between observations are harmlessly absorbed into ν_0.

Naturally, in detecting relativistic effects on S stars, data during pericenter passage are of greatest value. With instrumentation currently available, an observation program concentrated over two months during S2's next pericenter passage (2018) will prove to be sufficient as a test for the EEP. Figure 2 argues that a small handful of spectral measurements of S2 at 10 km s^{-1} around pericenter imply a 1σ accuracy on α of $\sim$0.3.

The approach we have taken above focuses on the essentials. The degeneracy between α, I, and a for spectroscopy has been lifted by using astrometry only to provide I. In practice, all the parameters are fitted simultaneously to both astrometry and spectroscopy. We have done simulations to verify that when this is done, the degeneracy is implicitly broken by the mechanism highlighted in this Letter.

Relativistic effects can be expected to become increasingly important as corrections in other astrophysics relating to the S stars. Three areas where this can be expected are the following.

1. The combination of spectroscopic and astrometric S star data provides us with the distance to the center of the galaxy. Astrometry is sensitive to the angular size of the orbit, while spectroscopy on the physical size. The quotient is the distance to the galactic center (Eisenhauer et al. 2003).
2. The position of the observed line depends on the velocity of the BH-star system with respect to the Earth. Spectroscopy therefore has the power to determine our velocity with respect to the central BH (Angélil et al. 2010), thus constraining the U component of the Galactic local standard of rest.
3. The form of the mass distribution within the inner arcsecond affects the S star orbits. A better understanding of the density profile will provide insight into the region's star capture and formation history, and to the central dark matter distribution (Ghez et al. 2008; Gillessen et al. 2009b).

In exploring (1) and (2), one cannot easily avoid relativity simply by considering stars with larger orbit sizes (3), as perturbations due to the enclosed mass become a problem. With the accuracy regime that spectroscopy will enter in the coming decade, one of two types of perturbations to the redshift must

be faced: either those from the extended mass distribution, for S stars with large orbits, or, those perturbations from relativity, for smaller orbit S stars. While effects due to relativity are well understood in principle, and can be easily treated, the constitution of the extended system is poorly understood and requires a more grueling treatment. In the coming decade, spectroscopic S star accuracy at $\sim$10 km s^{-1} is expected to be available, and the discovery of stars closer in to the BH is anticipated. In light of these prospects, so that constraints on these quantities may be improved, relativistic perturbations, while interesting in their own right, can no longer be ignored and must be faced.

The authors thank S. Gillessen, G. F. R. Ellis, and J.-P. Uzan for discussion and comments.

REFERENCES

Angélil, R., & Saha, P. 2010, ApJ, 711, 157
Angélil, R., Saha, P., & Merritt, D. 2010, ApJ, 720, 1303
Brumberg, V. A., Zeldovich, I. B., Novikov, I. D., & Shakura, N. I. 1975, Pis'ma Astron. Zh., 1, 5
Eisenhauer, F., Schödel, R., Genzel, R., Ott, T., Tecza, M., Abuter, R., Eckart, A., & Alexander, T. 2003, ApJ, 597, L121
Ghez, A. M., et al. 2008, ApJ, 689, 1044
Gillessen, S., Eisenhauer, F., Fritz, T. K., Bartko, H., Dodds-Eden, K., Pfuhl, O., Ott, T., & Genzel, R. 2009a, ApJ, 707, L114
Gillessen, S., Eisenhauer, F., Trippe, S., Alexander, T., Genzel, R., Martins, F., & Ott, T. 2009b, ApJ, 692, 1075
Kannan, R., & Saha, P. 2009, ApJ, 690, 1553
Macquart, J., Kanekar, N., Frail, D. A., & Ransom, S. M. 2010, ApJ, 715, 939
Martins, F., Gillessen, S., Eisenhauer, F., Genzel, R., Ott, T., & Trippe, S. 2008, ApJ, 672, L119
Merritt, D., Alexander, T., Mikkola, S., & Will, C. M. 2010, Phys. Rev. D, 81, 062002
Preto, M., & Saha, P. 2009, ApJ, 703, 1743
Rubilar, G. F., & Eckart, A. 2001, A&A, 374, 95
Schödel, R., Merritt, D., & Eckart, A. 2009, A&A, 502, 91
Will, C. M. 2006, Living Rev. Rel., 9, 3
Will, C. M. 2008, ApJ, 674, L25
Zucker, S., Alexander, T., Gillessen, S., Eisenhauer, F., & Genzel, R. 2006, ApJ, 639, L21

3 second publication

The Astrophysical Journal, 711:157–163, 2010 March 1 doi:10.1088/0004-637X/711/1/157

RELATIVISTIC REDSHIFT EFFECTS AND THE GALACTIC-CENTER STARS

Raymond Angélil and Prasenjit Saha
Institute for Theoretical Physics, University of Zürich, Winterthurerstrasse 190, CH-8057 Zürich, Switzerland
Received 2009 October 7; accepted 2010 January 18; published 2010 February 8

ABSTRACT

The high pericenter velocities (up to a few percent of light) of the S stars around the Galactic-center black hole suggest that general relativistic effects may be detectable through the time variation of the redshift during pericenter passage. Previous work has computed post-Newtonian perturbations to the stellar orbits. We study the additional redshift effects due to perturbations of the light path (what one may call "post-Minkowskian" effects), a calculation that can be elegantly formulated as a boundary-value problem. The post-Newtonian and post-Minkowskian redshift effects are comparable: both are $\mathcal{O}(\beta^3)$ and amount to a few km s^{-1} at pericenter for the star S2. On the other hand, the post-Minkowskian redshift contribution of spin is $\mathcal{O}(\beta^5)$ and much smaller than the $\mathcal{O}(\beta^4)$ post-Newtonian effect, which would be $\sim$0.1 km s^{-1} for S2.

Key words: Galaxy: nucleus – gravitation – stars: kinematics and dynamics

Online-only material: tar file

1. INTRODUCTION

Over the past decade, dozens of fast-moving stars orbiting a large compact mass (thought to be a supermassive black hole with mass $\approx 4.4 \times 10^6\, M_\odot$) have been discovered (Ghez et al. 2008; Gillessen et al. 2009). The highly eccentric orbits and the low pericenter distances of these stars ($\sim 3 \times 10^3$ of the gravitational radius in the case of S2) provide a lucrative testing ground for general relativistic perturbations to Keplerian orbits. High resolution spectral and astrometric measurements of such stars would also aid in the modeling of the mass distribution in the Galactic center. Other consequences of general relativity, the possible form of the metric itself (and the corresponding theories to which the metric is a solution) could be studied.

The prospect for measuring general relativistic pericenter precession, an $\mathcal{O}(\beta^2)$ effect (where β is the pericenter velocity in light units) for the Galactic-center stars is widely appreciated (see, for example, Jaroszynski 1998; Fragile & Mattews 2000) and is anticipated to be observable by interferometric instruments currently under development (Eisenhauer et al. 2009). Should stars further in be detected in the future, precession effects at $\mathcal{O}(\beta^4)$ would become measurable, enabling tests of no-hair theorems (Will 2008).

Relativity also perturbs the kinematics of a star. Zucker et al. (2006) drew attention to the rapid velocity changes that stars undergo around pericenter passage, and argued that the $\mathcal{O}(\beta^2)$ effect of time dilation in the star's frame would be measurable as a perturbation of the redshift. Kannan & Saha (2009) calculated the $\mathcal{O}(\beta^3)$ kinematic contribution of space curvature g_{ij} and $\mathcal{O}(\beta^4)$ effect of black hole spin g_{0j}, suggesting that even the latter may become measurable with future interferometric instruments. Preto & Saha (2009) presented a new orbit integration method in the presence of space curvature, spin, and Newtonian Galactic perturbations.

In this paper, we extend previous work to include the redshift contributions that come from the effect of space curvature and spin on the light path between the star and the observer. Specifically, we will compute the redshift of a moving point source in a weak-field approximation of a Kerr metric, identify the various contributions, and investigate the scaling of these signals with orbital size.

We formulate the problem as two photons emitted from a stellar orbit, an infinitesimal proper time interval $\Delta\tau$ apart. Both photons hit the observer, but with a difference Δt in arrival time. The redshift z is then

$$\Delta t = (1 + z)\Delta\tau. \tag{1}$$

The physical process is the same as in the calculation of the spectrum of an accretion disk (e.g., Müller & Camenzind 2004), only the computational strategy needed is different. In the accretion-disk case, photons are shot backward from the observer in a range of directions, but in the general direction of the extended source (the disk). By considering the collision events of each ray with the source surface, the quantities of interest may be read off. In the stellar-source case, however, it is necessary to solve for the initial direction of a photon so that it will reach the observer. Hence we have a boundary-value problem.

Figure 1 is a schematic illustration of our method. Photons are emitted from nearby spacetime points on the stellar orbits and travel to the observer. In the left-hand picture, the star emits "Minkowski photons", which feel no space curvature and travel in straight lines; redshift depends only on the velocity and time dilation of the star. This is in effect the approximation used in previous work. In the middle picture, the star emits "Schwarzschild photons", which feel space curvature. In the right-hand picture, the star emits "frame-dragging photons", which feel spin as well as space curvature.

Below, Section 2.1 details the problem to be solved and the method used for calculation of the redshift. The Matlab scripts implementing our algorithm are available as an online supplement. Then Section 2.2 presents the black hole model and associated metrics which we use in our approach, and Section 2.4 derives how the various effects scale with orbit size. We apply our algorithm to the star S2, and detail the results in Section 3.

2. THE REDSHIFT-CALCULATION METHOD

2.1. A Boundary-value Problem

In order to calculate the redshift of a moving star as observed by a fixed observer, we need to solve the geodesic equations for

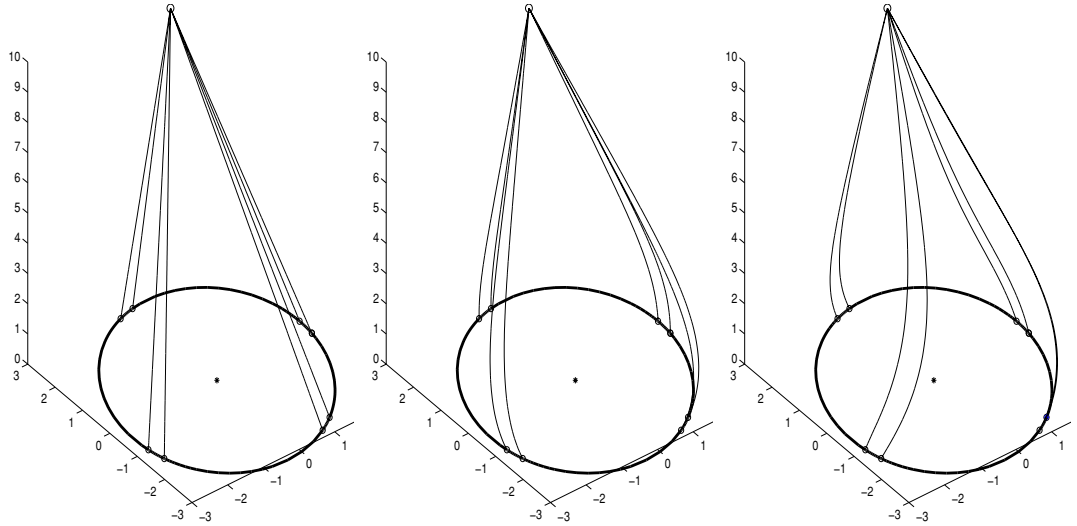

Figure 1. Schematic illustration of the method. Pairs of photons are emitted at slightly different proper times along the orbit, in precisely the right direction to reach the observer. Finding these photons is a boundary-value problem, and once found, each photon pair allows us to calculate the redshift at that point on the orbit by evaluating Equation (5). Left: Minkowski photons, which move in straight lines. Middle: Schwarzschild photons, which are lensed. Right: frame-dragged photons. The time difference between the emission of each photon in a pair has been exaggerated here for visual clarity. Note that it is only the star's unrealistic proximity to the black hole that allows for such a visible depiction of the different effects.

both the star and photons. Geodesic equations are commonly expressed in terms of the Lagrangian,

$$\mathcal{L} = \tfrac{1}{2} g_{\mu\nu} \dot{x}^{\mu} \dot{x}^{\nu} \tag{2}$$

with dots denoting derivatives with respect to the affine parameter. But an equivalent formulation exists in terms of a Hamiltonian

$$\mathcal{H} = \tfrac{1}{2} g^{\mu\nu} p_{\mu} p_{\nu}. \tag{3}$$

We will follow the latter in this work. Numerically $\mathcal{H} = \mathcal{L}$. We will in fact employ two Hamiltonians[1] $\mathcal{H}_{\rm star}$ and $\mathcal{H}^{\rm null}$, which are really two different approximations for the same Hamiltonian. Numerically $\mathcal{H}^{\rm null} = 0$ of course. We will write λ for the affine parameter of the star, and σ for that of a photon.

Consider two photon trajectories, emitted at two points on the star's orbit $\Delta\lambda$ apart in the affine parameter, with both photons terminating at the observer and arriving at time Δt apart in the observer's frame. Since $d\tau = \sqrt{|g_{\mu\nu} dx^{\mu} dx^{\nu}|}$, we are able to express the proper time between the emission events in terms of the affine parameter as

$$\Delta\tau = \Delta\lambda \sqrt{|2\mathcal{H}_{\rm star}|}, \tag{4}$$

where $\mathcal{H}_{\rm star}$ is evaluated at either point of emission. Comparing with the definition (1) of the redshift, we have

$$z = \frac{\Delta t}{\Delta\lambda \sqrt{|2\mathcal{H}_{\rm star}|}} - 1. \tag{5}$$

We now need to compute Δt for a given $\Delta\lambda$. To do this, we begin by calculating the orbit of the star for some chosen initial conditions, by solving Hamilton's equations for $\mathcal{H}_{\rm star}$ with λ as the independent variable. The temporal component of the generalized momentum is set at $p_t = -1$. This amounts to choosing the units for λ such that $dt = d\lambda$ outside of gravitational fields. We then choose a point on the star's orbit whose observed redshift we wish to calculate, and from this point we seek a photon that will reach the observer.

Consider a function Φ^j, which effectively shoots a photon by integrating Hamilton's equations for $\mathcal{H}^{\rm null}$ with given initial conditions at affine parameter $\sigma = 0$ and returns the three-position at $\sigma = 1$. We write

$$\Phi^j(t, x^i, p_i) = x^j|_{\sigma=1}, \tag{6}$$

where $i, j = 1, 2, 3$ and the initial p_t is chosen such that $\mathcal{H}^{\rm null} = 0$. We pass the function Φ^j to a root finder, and solve for the root of

$$f(p_i) = \Phi^j - x^j_{\rm obs} \tag{7}$$

by varying the initial three-momentum p_i. Naturally, we may not adjust the x^i, as we are interested in a specific point on the star's orbit.

The root-finding algorithm requires a set of initial guesses for the initial p_i of the photon. On this account, we shoot an initial-guess photon from the star position in the direction of the observer, that is, we evaluate Φ^j with trivial initial conditions. These initial-guess values for the p_i shoot in the direction of the observer ignoring curvature. However, because the spacetime is indeed curved, this photon will *not* hit the observer. It serves only to start the root-finding algorithm.

Once the root finder reports a solution within specified tolerance level, we move the star a very short distance ($\Delta\lambda$ in affine parameter) along its orbit, and repeat the above procedure, now solving for the sought-after trajectory at the star's new position. The difference in arrival times of the two photons is Δt, which we insert into Equation (5) to evaluate the redshift.

Thus far we have solved for two photon trajectories. This computation has enabled us to calculate the redshift at a chosen point on the orbit. We may then repeat this process at further points along the orbit, garnering results as much as the required resolution demands.

[1] In an effort to keep the distinctions between effects on the star orbit and those on the light path as perspicuous as possible, we adopt subscripts for orbital effects and superscripts for light-path effects. This notation may be found on Hamiltonians $\mathcal{H}$ and redshifts z, and has nothing to do with covariant/contravariant indices.

2.2. Post-Newtonian and Post-Minkowskian Approximations

The spacetime outside a spinning black hole is described by the Kerr metric. Since the Galactic-center stars are far from the horizon, approximations valid only at large r can be used to study general relativistic effects. Accordingly, we first derive two perturbative Hamiltonians, a post-Newtonian $\mathcal{H}_{\rm star}$ for stars, and a post-Minkowskian[2] approximation $\mathcal{H}^{\rm null}$ for photons. Different physical effects come into play at different orders of the perturbation parameter[3] ϵ, and we will show these numerically by toggling different terms on and off.

Taking the Kerr metric in Boyer–Lindquist coordinates with geometric units $GM = c = 1$ (leaving us with a unit of length equal to the gravitational radius $GM/c^2 \simeq 5 \times 10^6$ km for the Galactic-center black hole) we have the full Hamiltonian

$$\mathcal{H}_{\rm Kerr} = \frac{(r^2+s^2)^2 - s^2\Delta\sin^2\theta}{2\rho^2\Delta}p_t^2 - \frac{\Delta}{2\rho^2}p_r^2 - \frac{1}{2\rho^2}p_\theta^2 - \frac{\Delta - s^2\sin^2\theta}{2\Delta\rho^2\sin^2\theta}p_\phi^2 + \frac{2sr}{2\rho^2\Delta}p_t p_\phi, \tag{8}$$

where

$$\Delta \equiv r^2 - 2r + s^2 \quad \text{and} \quad \rho^2 \equiv r^2 + s^2\cos^2\theta \tag{9}$$

and s denotes the black hole spin parameter.

Let us first consider the dynamics of the star. Sufficiently far from the black hole, the post-Newtonian approximation

$$v^2 \sim 1/r \tag{10}$$

applies. If we choose $v \sim \mathcal{O}(\epsilon)$ then by Equation (10) r is $\mathcal{O}(\epsilon^{-2})$. Correspondingly, we force the velocity terms p_r, p_θ/r, and p_ϕ/r to be $\mathcal{O}(\epsilon)$. Making the following replacements in Equation (8),

$$r \to \epsilon^{-2}r, \quad p_r \to \epsilon p_r, \quad p_\theta \to \epsilon^{-1}p_\theta, \quad \text{and} \quad p_\phi \to \epsilon^{-1}p_\phi \tag{11}$$

and keeping terms to $\mathcal{O}(\epsilon^5)$, we obtain

$$\mathcal{H}_{\rm star} = -\frac{p_t^2}{2} + \left(\frac{p_r^2}{2} + \frac{p_\theta^2}{2r^2} + \frac{p_\phi^2}{2r^2\sin^2\theta} - \frac{p_t^2}{r}\right)\epsilon^2 - \left(\frac{2p_t^2}{r^2} + \frac{p_r^2}{r}\right)\epsilon^4 - \frac{2sp_t p_\phi}{r^3}\epsilon^5. \tag{12}$$

We can abbreviate Equation (12) as

$$\mathcal{H}_{\rm star} = \mathcal{H}_{\rm static} + \epsilon^2\mathcal{H}_{\rm Kep} + \epsilon^4\mathcal{H}_{\rm Schw} + \epsilon^5\mathcal{H}_{\rm FD}. \tag{13}$$

Here $\mathcal{H}_{\rm static}$ produces motionless geodesics, $\mathcal{H}_{\rm Kep}$ gives the Keplerian phenomenology, $\mathcal{H}_{\rm Schw}$ is the weak-field Schwarzschild contribution that produces pericenter precession, while the angular-temporal term $\mathcal{H}_{\rm FD}$ produces the Lens–Thirring effect or frame dragging.

Continuing now to photon trajectories, we remark that by the equivalence principle, the full Hamiltonian is exactly the same for photons and stars. However, the same terms can have different orders in the two regimes, prompting approximation $\mathcal{H}^{\rm null}$. In particular, the approximation (10) obviously does not hold for photons, which have $v^2 = 1$, implying the scalings

$$r \to \epsilon^{-2}r, \quad p_\theta \to \epsilon^{-2}p_\theta \quad \text{and} \quad p_\phi \to \epsilon^{-2}p_\phi \tag{14}$$

with p_r being $\mathcal{O}(1)$. Expanding as before, we obtain

$$\mathcal{H}^{\rm null} = -\frac{p_t^2}{2} + \frac{p_r^2}{2} + \frac{p_\theta^2}{2r^2} + \frac{p_\phi^2}{2r^2\sin^2\theta} - \left(\frac{p_t^2}{r} + \frac{p_r^2}{r}\right)\epsilon^2 + - \left(\frac{2p_t^2}{r^2} + \frac{2sp_t p_\phi}{r^3} - \frac{s^2\sin^2\theta}{2r^2}p_r^2 + \frac{s^2\cos^2\theta}{2r^4}p_\theta^2\right)\epsilon^4, \tag{15}$$

a different selection of terms compared to the post-Newtonian case. There is no term at $\mathcal{O}(\epsilon^5)$. We may abbreviate Equation (15) as

$$\mathcal{H}^{\rm null} = \mathcal{H}^{\rm Mink} + \epsilon^2\mathcal{H}^{\rm S_{LO}} + \epsilon^4\left(\mathcal{H}^{\rm S_{NLO}} + \mathcal{H}^{\rm FD} + \mathcal{H}^{\rm torq}\right). \tag{16}$$

At zeroth order we have special relativistic or Minkowski photons. The leading-order Schwarzschild effect $\mathcal{H}^{\rm S_{LO}}$ gives the gravitational deflection of light. At $\mathcal{O}(\epsilon^4)$; however, there are three distinct effects: first $\mathcal{H}^{\rm S_{NLO}}$ gives a next-to-leading-order correction to the Schwarzschild effect, the off-diagonal term $\mathcal{H}^{\rm FD}$ gives frame dragging again but for photon trajectories, while $\mathcal{H}^{\rm torq}$ provides a torque proportional to s^2.

2.3. Pseudo-Cartesian Coordinates

The spatial Boyer–Lindquist coordinates r, θ, ϕ are convenient for computing stellar orbits, but not well suited for photon paths. The photon paths are nearly straight lines, but since the observer is much further from the black hole than the source, tiny variations in θ and ϕ at the observer imply large distances. As a result, both the integrator and the root finder become susceptible to roundoff error.

To cure the problem, we change to pseudo-Cartesian coordinates. They are not purely Cartesian, as the surface $x^2 + y^2 + z^2$ is not spherical:

$$x = r\sin\theta\cos\phi, \quad y = r\sin\theta\cos\phi, \quad z = r\cos\theta. \tag{17}$$

The corresponding momenta are readily derived by completing the canonical transformation, leading to the usual relations

$$p_r = \frac{\mathbf{x}\cdot\mathbf{p}}{r}, \quad p_\phi = (\mathbf{x}\times\mathbf{p})_z, \quad p_r^2 + \frac{p_\theta^2}{r^2} + \frac{p_\phi^2}{r^2\sin^2\theta} = \mathbf{p}^2. \tag{18}$$

The form of $\mathcal{H}^{\rm null}$ changes accordingly. The Minkowski part bears the familiar form

$$\mathcal{H}^{\rm Mink} = -\frac{p_t^2}{2} + \frac{\mathbf{p}^2}{2}. \tag{19}$$

The leading-order Schwarzschild terms are

$$\mathcal{H}^{\rm S_{LO}} = -\frac{p_t^2}{r} - \frac{(\mathbf{x}\cdot\mathbf{p})^2}{r^3}, \tag{20}$$

and the associated $\mathcal{O}(\epsilon^4)$ term retains its previous form of

$$\mathcal{H}^{\rm S_{NLO}} = -\frac{2p_t^2}{r^2}. \tag{21}$$

[2] The term "post-Minkowskian" is often used as a synonym for "weak-field metric." We are using it, however, to refer specifically to light paths that deviate slightly from special relativity.

[3] In this paper ϵ, ϵ^2 and so on are just labels to keep track of different orders. Numerically $\epsilon = 1$.

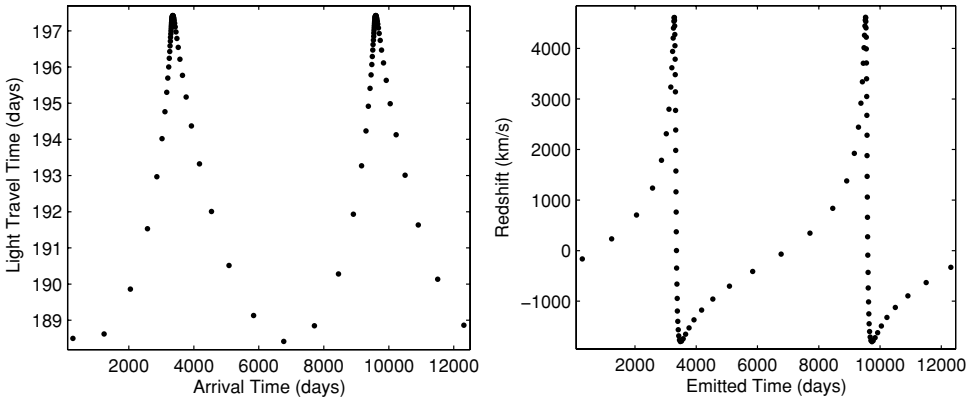

Figure 2. Redshift calculation for an S2-like star over two orbits. The left panel shows the time each photon takes to travel from the star to the observer. The star begins at the apocenter, which happens to be closer to the observer than the pericenter. Therefore, the light travel time naturally increases as the star moves toward its pericenter. The right panel shows the redshift. The peaks occur during pericenter passage due to the high pericenter passage velocities. The calculation includes post-Newtonian and post-Minkowskian effects, but these are too small to see in this figure.

Also at $\mathcal{O}(\epsilon^4)$ we have the frame-dragging term

$$\mathcal{H}^{\rm FD} = -\frac{2sp_t}{r^3}\,(\mathbf{x}\times\mathbf{p})_z\,, \tag{22}$$

and the torquing terms

$$\mathcal{H}^{\rm torq} = \frac{s^2}{2r^2}\left(1-\frac{z^2}{r^2}\right)\left(\frac{\mathbf{x}\cdot\mathbf{p}}{r}\right)^2 - \frac{s^2}{2z^2} \times\left[\mathbf{p}^2 - \left(\frac{\mathbf{x}\cdot\mathbf{p}}{r}\right)^2 - \frac{(\mathbf{x}\times\mathbf{p})_z^2}{r^2-z^2}\right]. \tag{23}$$

The torquing terms are the most difficult to integrate numerically. This is because while the terms themselves are at $\mathcal{O}(\epsilon^4)$, they involve quotients of particularly high powers. Taking derivatives of $\mathcal{H}^{\rm torq}$ further bloats these bottom and top heavy fractions, and provokes roundoff errors. We argue below that the torquing terms are in any case unimportant for the known Galactic-center stars. Hence, we omit these terms in our numerical work.

2.4. Scaling Properties of Redshift Contributions

We can infer the scaling with orbital size a of the redshift contributions Δz of the various perturbative terms in $\mathcal{H}_{\rm star}$ with the following deliberation. Consider a perturbative term

$$\Delta\mathcal{H}_{\rm star} \sim a^{-n}. \tag{24}$$

Since $\mathcal{H}_{\rm star}$ is constant along the orbit, any variation in $\Delta\mathcal{H}_{\rm star}$ has to be balanced by a variation in the unperturbed Hamiltonian. Since the latter scales as $\mathcal{H}_{\rm star} \sim 1/a$, we have $\Delta\mathcal{H}_{\rm star} \sim \Delta a/a^2$, giving

$$\Delta a \sim a^{2-n}. \tag{25}$$

Furthermore, since the orbital velocity scales as $v \sim a^{-1/2}$, we have $\Delta v \sim a^{-3/2}\,\Delta a$ and hence the redshift signal

$$\Delta z\,(\Delta H_{\rm star}) \sim a^{\frac{1}{2}-n}. \tag{26}$$

A similar argument can be made for the perturbative terms $\Delta\mathcal{H}^{\rm null}$. In this case we compare photons emitted from the same point, only with different Hamiltonians. While the redshift signal from the previous case necessitated our consideration of the stellar velocity only, in analyzing the gravitational redshift signal, we are naturally interested in the time difference Δt due to ΔH. Let the perturbation be

$$\Delta\mathcal{H}^{\rm null} \sim r^{-n}. \tag{27}$$

Since the light travel time is an integrated quantity, we expect the change in the light travel time to scale as

$$\Delta t_{\rm trav} \sim r^{1-n}. \tag{28}$$

The change $\Delta t_{\rm trav}$ in light travel time must not be confused with the difference Δt in arrival time of two photons. For the latter quantity we get $\Delta t \sim \Delta r/r^n$ and since Δr between two photons is $\sim v \sim a^{-1/2}$ we derive

$$\Delta z(\Delta\mathcal{H}^{\rm null}) \sim a^{-\frac{1}{2}-n}. \tag{29}$$

Using Equations (26) and (29) and recalling that each power of ϵ in the Hamiltonians represents a scaling factor of $r^{-1/2}$ we can read off the following scalings:

$$\begin{pmatrix} & \mathcal{H}_{\rm Schw} & \\ & \mathcal{H}_{\rm FD} & \\ & \mathcal{H}^{\rm SLO} & \\ \mathcal{H}^{\rm SNLO} & \mathcal{H}^{\rm torq} & \mathcal{H}^{\rm FD} \end{pmatrix} \Rightarrow \Delta z \propto \begin{pmatrix} a^{-3/2} \\ a^{-2} \\ a^{-3/2} \\ a^{-5/2} \end{pmatrix}. \tag{30}$$

3. APPLICATION TO S2-LIKE ORBITS

We select S2 for a case study, since S2 has the shortest orbit and one of the highest pericenter velocities of all the known stars orbiting Sagittarius A*, and hence provides us with perhaps the best opportunity to observe general-relativistic effects.

Figure 2 shows a redshift calculation for a star with S2's orbital parameters. These are taken from Gillessen et al. (2009). The gravitational radius is taken as 5×10^6 km. For definiteness, we take the spin to be maximal, and pointing toward Galactic North. Disk seismology models (Kato et al. 2009) put the spin at $s \approx 0.44$. The direction however, remains unknown.

All the contributions to $\mathcal{H}_{\rm star}$ in Equation (13) are included for the orbit calculation. The photon trajectories include all contributions to $\mathcal{H}^{\rm null}$ in Equation (16) except for $\mathcal{H}^{\rm torq}$.

Naturally we would like to compute the redshift contributions of the various relativistic terms, and verify that they follow the expected scalings (30). In order to do this, we examine the

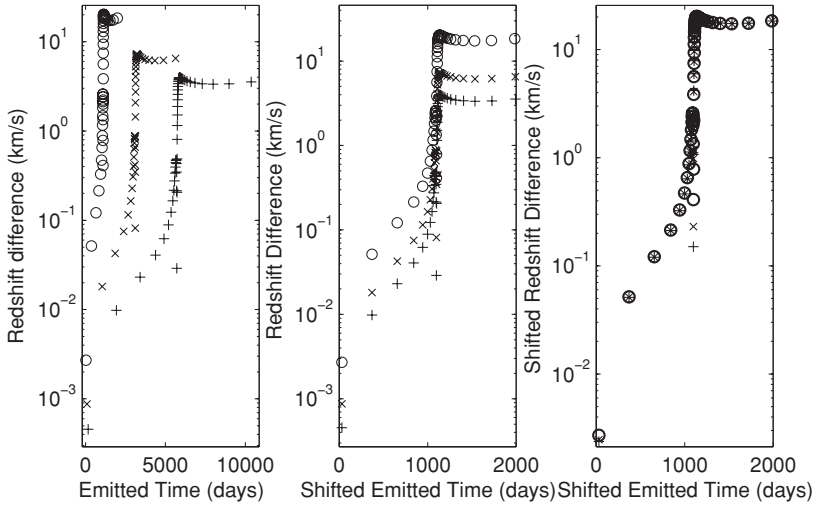

Figure 3. Redshift difference $z^{\rm Mink}_{\rm Schw} - z^{\rm Mink}_{\rm Kep}$ showing the contribution of $\mathcal{H}_{\rm Schw}$. The left panel shows the redshift difference for three orbits, one with the parameters of S2, and the other two with a doubled or halved. In the middle panel, the horizontal scale is stretched $(a/a_{\rm S2})^{-3/2}$. In the right panel, the redshift difference is scaled by $(a/a_{\rm S2})^{-3/2}$.

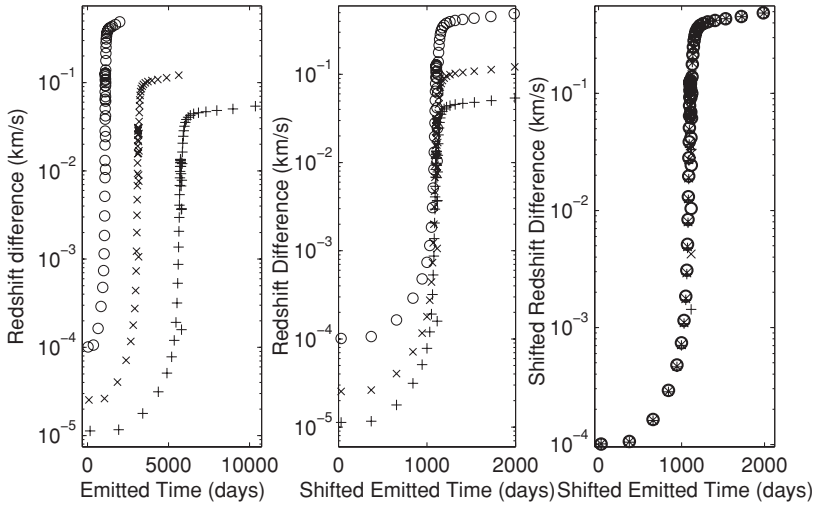

Figure 4. Redshift difference $z^{\rm Mink}_{\rm FD} - z^{\rm Mink}_{\rm Schw}$ showing the contribution of $\mathcal{H}_{\rm FD}$. The scheme follows Figure 3 except that the redshift difference is scaled by $(a/a_{\rm S2})^{-2}$.

differences between redshifts computed from different post-Newtonian and post-Minkowskian cases. This allows us to isolate the effects of $\mathcal{H}_{\rm Schw}$, $\mathcal{H}_{\rm FD}$, $\mathcal{H}^{\rm S_{LO}}$, and $\mathcal{H}^{\rm S_{NLO}} + \mathcal{H}^{\rm FD}$, as follows.

1. To isolate $\mathcal{H}_{\rm Schw}$ we compute the redshift difference $z^{\rm Mink}_{\rm Schw} - z^{\rm Mink}_{\rm Kep}$. By $z^{\rm Mink}_{\rm Schw}$ we mean that the star is followed using terms in $\mathcal{H}_{\rm star}$ up to $\mathcal{H}_{\rm Schw}$ and the photons are followed using $\mathcal{H}^{\rm null}$ up to $\mathcal{H}^{\rm Mink}$. The same naming convention applies to $z^{\rm Mink}_{\rm Kep}$ and to other expressions of this type below.

   Figure 3 shows the redshift difference, calculated for three orbits going from apocenter to apocenter. One orbit has the parameters of S2; the two others have $a = 2a_{\rm S2}$ and $\frac{1}{2}a_{\rm S2}$ with the other orbital parameters being the same. The redshift difference increases till pericenter and then declines somewhat, but not to its previous apocentric value, because the relativistic orbit experiences prograde Schwarzschild precession whereas the Keplerian orbit does not, and the resulting phase change in the orbit gives an increasing contribution to the redshift.

   For S2 parameters, the maximum redshift contribution of $\mathcal{H}_{\rm Schw}$ is found to be $\simeq 7$ km s^{-1}. For the other two stars, upon rescaling the redshift differences by $(a/a_{\rm S2})^{-3/2}$ and the orbital time also by $(a/a_{\rm S2})^{-3/2}$, the results can be overlaid almost perfectly on those of the S2-like star.

2. To isolate $\mathcal{H}_{\rm FD}$ we then compute the redshift difference $z^{\rm Mink}_{\rm FD} - z^{\rm Mink}_{\rm Schw}$. For an S2-like orbit the signal is around 0.1 km s^{-1} at pericenter, and as Figure 4 shows, the signal scales as a^{-2}.

3. To isolate $\mathcal{H}^{\rm S_{LO}}$ we compute $z^{\rm S_{LO}}_{\rm Schw} - z^{\rm Mink}_{\rm Schw}$ and illustrate this difference in Figure 5. There is no precession-related redshift effect involved, because the photon types being compared refer to the same stellar orbits. The signal scales as $a^{-3/2}$ and for the S2-like orbit the maximum is $\simeq 2$ km s^{-1}.

   We see that the Schwarzschild terms in the stellar orbit and in the light path give comparable contributions to the redshift. To detect the Schwarzschild effect, it is necessary to take both into account.

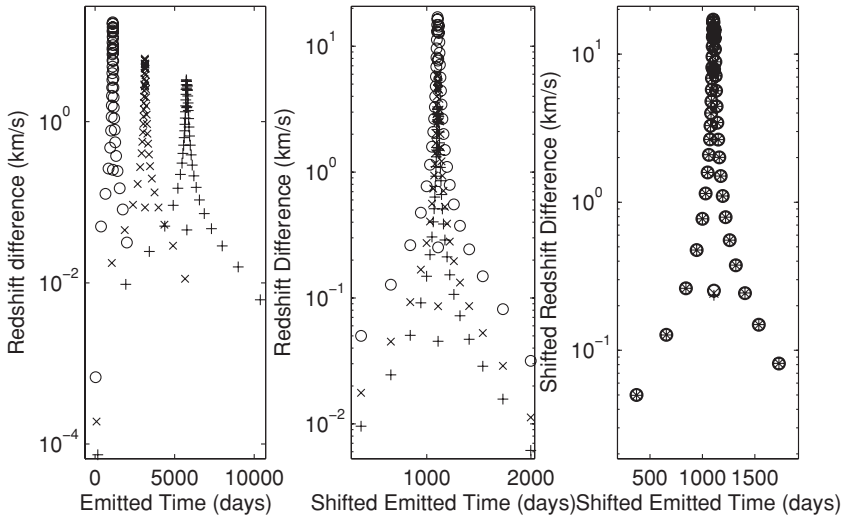

Figure 5. Redshift difference $z^{\mathrm{S_{LO}}}_{\mathrm{Schw}} - z^{\mathrm{Mink}}_{\mathrm{Schw}}$ showing the contribution of $\mathcal{H}^{\mathrm{S_{LO}}}$. The scheme follows Figure 3, the redshift difference being scaled again $(a/a_{\mathrm{S2}})^{-3/2}$.

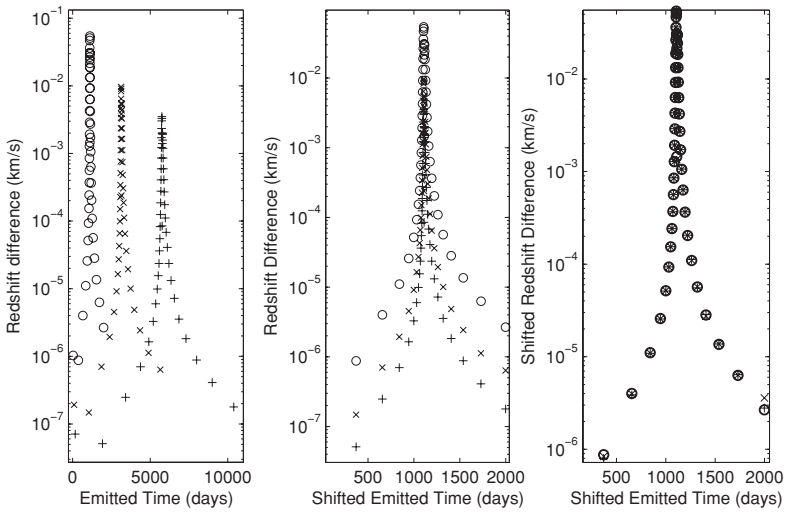

Figure 6. Redshift difference $z^{\mathrm{FD}}_{\mathrm{FD}} - z^{\mathrm{S_{LO}}}_{\mathrm{FD}}$ showing the contribution of $\mathcal{H}^{\mathrm{S_{NLO}}} + \mathcal{H}^{\mathrm{FD}}$. The scheme follows Figures 3–5, with the redshift difference scaled by $(a/a_{\mathrm{S2}})^{-5/2}$. Here we have taken the spin as maximal, $s = 1$. This signal is exactly proportional to s.

4. Finally, we isolate $\mathcal{H}^{\mathrm{S_{NLO}}} + \mathcal{H}^{\mathrm{FD}}$ by computing $z^{\mathrm{FD}}_{\mathrm{FD}} - z^{\mathrm{S_{LO}}}_{\mathrm{FD}}$. Figure 6 verifies the expected $a^{-5/2}$ scaling and shows that the maximum signal for S2 parameters is $\sim 10^{-2}$ km s^{-1}. Thus, we see that the frame-dragging on photons is much smaller than on stars. Similarly, $\mathcal{H}^{\mathrm{S_{NLO}}}$ makes a much smaller contribution than $\mathcal{H}_{\mathrm{FD}}$. We expect that the contribution of $\mathcal{H}^{\mathrm{torq}}$ would be similarly small, though we have not calculated it.

   We see that in order to measure the leading-order frame-dragging effect on Galactic-center stars, it is sufficient to consider Schwarzschild photons.

Of course, the computation method for weak redshift signals contains numerical errors, especially for higher-order effects being evaluated at large distances from the black hole. The numerical noise in our implementation drowns out the leading-order Schwarzschild effect for scaled S2-like orbits with $a \approx 3 \times 10^8$—at which point the pericenter redshift signal is $\approx 5 \times 10^{-6}$ km s^{-1}. Numerical noise would overwhelm the frame-dragging signal for scaled S2-like orbits with at $a \approx 1.2 \times 10^5$. This being an order of magnitude larger than a_{S2}, and so we are in good shape to calculate the frame-dragging redshift contribution. For redshift signal contributions beyond those of frame-dragging, the numerical noise in our Matlab implementation of the algorithm is intolerable for a_{S2}. Were we calculating these effects for stars closer to the SBH, the higher-order signals would be stronger, and therefore less prone to round-off. In summary, for the known Galactic-center stars, the numerical noise in calculating relativistic redshifts will be well within the observational errors, even with the next generation spectral instrumentation.

4. SUMMARY AND OUTLOOK

Some stars in orbit around the Galactic-center black hole reach velocities of a few percent light at pericenter, and the time-varying redshift of these stars during pericenter passage has small but distinctive perturbations from general relativity.

The redshift is dominated by the line of sight velocity, which for the star S2 reaches $v \sim 5 \times 10^3$ km s^{-1} at pericenter. The

leading perturbations are from time dilation because (1) the star is moving and (2) because it is in a potential well. Both of these make $\mathcal{O}(\beta^2)$ contributions to the redshift (where v is the stellar velocity in light units) and are well understood (Zucker et al. 2006). In this paper, we have calculated additional perturbations from general relativity, which are the following.

1. The weak-field Schwarzschild effect on the stellar orbit, which contributes to redshift at $\mathcal{O}(\beta^3)$. For S2 it is $\simeq 7$ km s^{-1}.[4]
2. The frame-dragging effect of black hole spin on the stellar orbit, which perturbs the redshift at $\mathcal{O}(\beta^4)$. For S2 it would be $\sim 10^{-1}$ km s^{-1} for maximal spin.
3. The weak-field Schwarzschild effect on the light traveling from the star to us, which gives a redshift perturbation at $\mathcal{O}(\beta^3)$. For S2 it is $\simeq 2$ km s^{-1}.
4. Frame dragging plus next-order Schwarzschild perturbation of the photon paths. These contribute at $\mathcal{O}(\beta^5)$ to the redshift, and we estimate these as $\sim 10^{-2}$ km s^{-1} for S2.

Of these, the first two are orbital effects and have been considered in previous work (Kannan & Saha 2009; Preto & Saha 2009). The last two are light-path effects, known about but not previously computed in the context of Galactic-center stars.

Clearly, in order to measure the Schwarzschild effects via the redshift, the effects of general relativity on both the stellar orbit and the light path must be computed, as they are of the same order. On the other hand, to leading order, frame dragging needs to be considered only in the orbit and can be neglected in the light path.

In order to test for the presence and form of the NLO and NNLO terms in the metric, the calculated redshift curve must be fitted to the spectral data via a range of parameters. These include the orbital parameters and the black hole mass. In keeping these parameters variable, we can expect a requirement for spectroscopic accuracy less than the signal sizes themselves. Bear in mind however, that this depends on the number of data points. The inclusion of astrometric data to the fitting procedure will help relax the accuracy bound.

Observationally, the Galactic-center stars are of course observable only in infrared. For the most massive stars, including S2, the Brackett-γ line at 2.16 μm is the most prominent available spectral feature, and has an intrinsic dispersion of ~ 100 km s^{-1} (see, e.g., Martins et al. 2008). For low-mass stars, the edges of the CO molecular bands (the so-called CO band heads) are excellent sharp features for redshift measurements.

The SINFONI spectrograph, an instrument at the VLT, has a spectral resolution of 75 km s^{-1}. Redshift errors are currently estimated at 10 s of km s^{-1} (see Section 4.1 of Gillessen et al. 2009) but expected to improve. Measurements by this instrument during S2's next pericenter passage in 2016 could suffice to provide data from which the Schwarzschild signals could be extracted.

Spectral measurements seeking the spin-dependent signals are far beyond the capabilities of existing infrared spectrographs. On the other hand, recent developments such as laser-comb spectrographs (see, e.g., Steinmetz et al. 2008) suggest optimism that the spectral resolutions of next-generation instruments will prove adequate.

Meanwhile, there are some theoretical issues that require further research.

1. Given a model of gravity which is metric, and an associated energy–momentum distribution, for which we have a metric, we are able to calculate the general relativistic redshift as observed by the Earth. Should we wish to probe the agreement of measured redshift contributions with a model, an effective way of working backward needs to be formulated. Given redshift curve data of sufficient resolution, methods for determining the model from such must be developed.
2. The Kerr black hole metric is a vacuum solution to the Einstein field equations. The assumption of a "clean" metric is an oversimplification. An extended Newtonian mass distribution in the galactic center is anticipated. Accreting material, gas, and a possible accumulation of dark matter in the center could play a significant role in the dynamics. Such mass distributions need to be included in the metric.
3. The possibility of a non-Einsteinian black hole metric should not be disregarded. Alternative theories of gravity possess black hole solutions whose phenomenology differs potentially already at low order (Will 1993) from weak-field Einstein gravity. Suitable measurements, combined with the concession of extended mass distributions would allow for the identification of potentially revealing redshift contributions. Conclusive results of such studies would likely require spectral measurements with a resolution beyond that offered by present-day generation instruments.

We thank S. Gillessen and the referee for comments.

REFERENCES

Eisenhauer, F., et al. 2009, GRAVITY: Microarcsecond Astrometry and Deep Interferometric Imaging with the VLT (Dordrecht: Springer)
Fragile, P. C., & Mattews, G. J. 2000, ApJ, 542, 328
Ghez, A., et al. 2008, ApJ, 689, 1044
Gillessen, S., Eisenhauer, F., Trippe, S., Alexander, T., Genzel, R., Martins, F., & Ott, T. 2009, ApJ, 692, 1075
Jaroszynski, M. 1998, Acta Astron., 48, 653
Kannan, R., & Saha, P. 2009, ApJ, 690, 1553
Kato, Y., Miyoshi, M., Takahashi, R., Negoro, H., & Matsumoto, R. 2009, arXiv:0906.5423
Martins, F., Gillessen, S., Eisenhauer, F., Genzel, R., Ott, T., & Trippe, S. 2008, ApJ, 672, L119
Müller, A., & Camenzind, M. 2004, A&A, 413, 861
Preto, M., & Saha, P. 2009, ApJ, 703, 1743
Steinmetz, T., et al. 2008, Science, 321, 1335
Will, C. M. 1993, Theory and Experiment in Gravitational Physics (Cambridge: Cambridge Univ. Press)
Will, C. M. 2008, ApJ, 674, L25
Zucker, S., Alexander, T., Gillessen, S., Eisenhauer, F., & Genzel, R. 2006, ApJ, 639, L21

[4] Note that these effects are not measurable separately, only the total redshift is. Hence values like 7 km s^{-1} depend on the choice of reference orbit and phase, and can change accordingly. Nevertheless, the stated numbers give an idea of the observational precision required.

Figure 3.1: *Cry 'Havoc!', and let slip the dogs of war!*

4 third publication

The Galactic Center: A Window to the Nuclear Environment of Disk Galaxies
ASP Conference Series, Vol. 439, ▬ 2011
M. R. Morris, Q. D. Wang, and F. Yuan, eds.

Testing General Relativity with Galactic-Centre Stars

Raymond Angélil[1] and Prasenjit Saha[1]

Abstract. The Galactic Centre S-stars orbiting the central supermassive black hole reach velocities of a few percent of the speed of light. The GR-induced perturbations to the redshift enter the dynamics via two distinct channels. The post-Newtonian regime perturbs the orbit from the Keplerian (Zucker et al., 2006, Kannan & Saha 2009), and the photons from the Minkowski (Angélil & Saha 2010). The inclusion of gravitational time dilation at $\mathcal{O}\left(v^2\right)$ marks the first departure of the redshift from the line-of-sight velocities. The leading-order Schwarzschild terms curve space, and enter at $\mathcal{O}\left(v^3\right)$. The classical Keplerian phenomenology dominates the total redshift. Spectral measurements of sufficient resolution will allow for the detection of these post-Newtonian effects. We estimate the spectral resolution required to detect each of these effects by fitting the redshift curve via the five Keplerian elements plus black hole mass to mock data. We play with an exaggerated S2 orbit - one with a semi-major axis a fraction of that of the real S2. This amplifies the relativistic effects, and allows clear visual distinctions between the relativistic terms. We argue that spectral data of S2 with a dispersion $\sim 10\,\mathrm{km\ s^{-1}}$ would allow for a clear detection of gravitational redshift, and $\sim 1\,\mathrm{km\ s^{-1}}$ would suffice for leading-order space curvature detection.

1. Introduction

The stars orbiting the supermassive black hole ($M \approx 4.4 \cdot 10^6 M_\odot$) within the central arcsecond are on highly relativistic orbits. In comparison, the velocity of a geosynchronous Earth satellite is $v_{\mathrm{satell}} \approx 0.00005c$. Mercury, whose orbital Schwarzschild precession has been measured has $v_{\mathrm{merc}} \approx 0.00016c$. Binary pulsar systems manage to reach $v_{\text{binary pulsar}} \sim 0.003c$, while the galactic centre S-Stars boast $v_{\mathrm{S2}} \sim 0.03c$. This, due to their proximity to the black hole during pericenter passage (down to ~ 3000 gravitational radii), make this class of stars the fastest resolvable ballistic objects known, and allow for the prospect of detecting post-Newtonian effects.

The dynamics of the orbit and light trajectories provide an opportunity to test the form of the metric, and in doing so, General Relativity. The Kerr metric is the external solution to the Einstein Field Equations for a rotating body. The geodesics of such a space-time exhibit some well-known features: gravitational time dilation, prograde precession, lensing, and frame-dragging. Gravitational time dilation and precession are orbital effects. The former due to a temporal stretching, and the latter due to space curvature. Such a curvature also affects photon trajectories — veering the trajectories away from those of straight lines.

[1]Institute for Theoretical Physics, University of Zürich,
Winterthurerstrasse 190, CH-8057 Zürich, Switzerland

Each of these effects contributes to the redshift of the Galactic-centre stars in a distinct manner.

These features, although markedly distinct, are all due to the same metric. The post-Newtonian formalism, valid provided $r \gg 0$, allows us to cleanly disentangle these effects, and investigate the detection of each separately. Not only are the stars on post-Keplerian orbits, but the photons must travel through spacetime on nontrivial paths before arriving at Earth. This nontrivial path through spacetime affects the time of arrival, and therefore the redshift.

2. Model

The star's orbit can be described by the Hamiltonian (Angélil & Saha 2010)

$$\begin{aligned}
\mathcal{H}_{star} = \quad & -\frac{p_t^2}{2} && \propto v^1 && \text{No gravity} \\
& +\frac{p_r^2}{2} + \frac{p_\theta^2}{2r^2} + \frac{p_\phi^2}{2r^2 \sin^2\theta} - \frac{p_t^2}{r} && \propto v^1, v^2 && \text{Kepler + Time-dilation} \\
& -\frac{p_t^2}{r^2} - \frac{p_r^2}{r} && \propto v^3 && \text{space curvature} \\
& + \text{frame dragging, torquing, ...}
\end{aligned} \tag{1}$$

At leading order, the system is spatially invariant, and the star feels no acceleration. At next-to-leading order, gravity debuts. Classically, the potential term is $1/r$. GR however demands the modification to p_t^2/r, which results in gravitational time-dilation $\propto v^2$, a consequence of the Einstein Equivalence Principle. Spatially the problem has remained unchanged. However, because the time-dilation term affects the photon arrival times, the redshift is affected. Space curvature enters one order higher. This is the leading-order Schwarzschild term, and causes the orbit to precess. Higher order effects, such as frame-dragging and torquing, we choose not to delve into here.

The Hamiltonian governing photon paths, being null, contains a different selection of pre-truncation terms.

$$\begin{aligned}
\mathcal{H}^{\text{null}} = \quad & -\frac{p_t^2}{2} + \frac{p_r^2}{2} + \frac{p_\theta^2}{2r^2} + \frac{p_\phi^2}{2r^2 \sin^2\theta} && \propto v^0 && \text{Minkowski} \\
& -\frac{p_t^2}{r} - \frac{p_r^2}{r} && \propto v^3 && \text{space curvature} \\
& + \text{frame dragging, torquing, ...}
\end{aligned} \tag{2}$$

At leading order, the trajectories are straight lines. Lensing occurs at $\mathcal{O}\left(v^3\right)$ via the leading order Schwarzschild contribution. There is no contribution at $\mathcal{O}\left(v^4\right)$. For photons, the frame-dragging term debuts at $\mathcal{O}\left(v^5\right)$ along with higher-order Schwarzschild terms, and spin-induced torquing terms. In this work, we consider effects only up to $\mathcal{O}\left(v^3\right)$ for both the null and timelike cases[1].

[1]For a maximally spinning black hole, the frame-dragging *photon* signal on S2's redshift at pericenter is $\sim 10\,\text{m s}^{-1}$ — two orders of magnitude weaker than the Schwarzschild photon

3. Calculating the Redshift

To calculate the redshift curve of the star, we integrate the star's orbit using timelike solutions to (1), and then, on chosen points along the star's orbit, we find the paths of *those particular photons emitted by the star which hit the observer* (Figure 1). To do this, the initial angular momentum of the trajectories (corresponding to null solutions of 2) is varied until the termination position of the photon converges on the observer position. Once the trajectories of these photons are known, the redshift may then be calculated directly from the definition:

$$z = \frac{t_{a_2} - t_{a_1}}{\tau_{e_2} - \tau_{e_1}} - 1, \tag{3}$$

where τ_{e_1} and τ_{e_2} are the proper times of a pair of photons emitted at neighbouring points on the star's orbit, and t_{a_1} and t_{a_2} are their respective arrival times.

4. Post-Newtonian Detection

The redshift curve of a galactic centre star is dependent on a handful of parameters. These include the Keplerian elements, the black hole mass, as well as discrete parameters which toggle the post-Newtonian terms. We proceed as follows. In order to put upper bounds on the spectral resolution required to detect the post-Newtonian effects, we generate mock spectral data consisting of 200 data points with a chosen dispersion, using relativistic terms up to $\mathcal{O}\left(v^3\right)$ for both the null and timelike metrics, and determine whether or not we are able recover the parameter values by fitting with these effects turned off. For illustrative purposes, we consider an exaggerated S2 orbit. For the semi-major axis, we take $a = a_{\mathrm{S2}}/100$. In doing so, $v = 10v_{\mathrm{S2}}$ — the classical contribution to the redshift is raised 10-fold. The redshift due to gravitational time dilation, which enters the dynamics at $\mathcal{O}\left(v^2\right)$ is increased 100-fold. The space curvature redshift contribution, entering at $\mathcal{O}\left(v^3\right)$, is enhanced 1000-fold. Figure 2 shows the results of the fitting procedure. The classical fit manages a $\chi^2_{\mathrm{red}} = 4.88$, the time dilation fit $\chi^2_{\mathrm{red}} = 2.68$, and the space curvature fit $\chi^2_{\mathrm{red}} = 1.07$. Hence, a spectral dispersion of $10^3\,\mathrm{km\ s^{-1}}$ suffices for clear visual and numerical distinction of these relativistic effects. In undoing our exaggeration of the orbit, we argue that a spectral dispersion of $\sim 10\,\mathrm{km\ s^{-1}}$ would allow for a clear detection of gravitational redshift for the real S2, and $\sim 1\,\mathrm{km\ s^{-1}}$ would yield a test for space curvature.

References

R. Angélil and P. Saha. Relativistic redshift effects and the Galactic-center stars. *The Astrophysical Journal*, In Press, arXiv 1001.1957.

---

signal. It is unlikely that the next generation of instruments will possess the capability to probe such deeper, weaker terms. We feel morally obligated not to raise the heartbeat of the observer reading this.

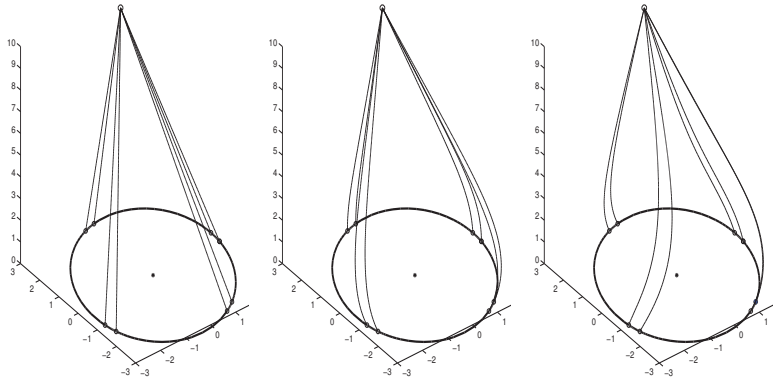

Figure 1. Schematic illustration of the redshift calculation method. Each photon shot by the star hits the observer. Each of the above cases yields four points on the redshift curve. The first panel shows Minkowski photons, the second space-curved photons, and the third frame-dragged photons.

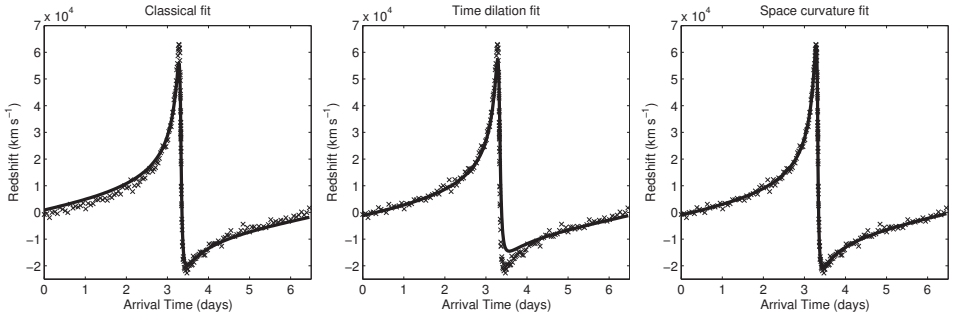

Figure 2. Our S2-like star has $a = a_{\rm S2}/100$. The mock redshift data in the above examples is generated all in the same way: 200 data points are distributed along the complete orbit with a dispersion of 10^3 km s^{-1}, gravitational time dilation and space curvature are all turned on. In the first panel, we fit with gravitational time dilation turned on, and space curvature turned off. For the second, we turn gravitational time dilation on, and for the third, we further turn space curvature on. The mismatch between the fit and the simulated data is discernable in the first two panels. Only in the last panel, when all the effects are included in the fit, is a satisfactory fit with $\chi^2_{\rm red} \approx 1$ obtained.

S. Zucker, T. Alexander, S. Gillessen, F. Eisenhauer, and R. Genzel. Probing post-newtonian physics near the galactic black hole with stellar redshift measurements. *The Astrophysical Journal Letters*, 639(1):L21–L24, 2006.

R. Kannan and P. Saha. On post-Newtonian orbits and the Galactic-center stars. *Astrophysical Journal 690 (2009) 1553-1557*, September 2008.

5 fourth publication

The Astrophysical Journal, 720:1303–1310, 2010 September 20 doi:10.1088/0004-637X/720/2/1303

TOWARD RELATIVISTIC ORBIT FITTING OF GALACTIC CENTER STARS AND PULSARS

Raymond Angélil[1], Prasenjit Saha[1], and David Merritt[2]
[1] Institute for Theoretical Physics, University of Zürich, Winterthurerstrasse 190, CH-8057 Zürich, Switzerland
[2] Department of Physics and Center for Computational Relativity and Gravitation, Rochester Institute of Technology, Rochester, NY 14623, USA
Received 2010 June 30; accepted 2010 July 15; published 2010 August 19

ABSTRACT

The S stars orbiting the Galactic center black hole reach speeds of up to a few percent the speed of light during pericenter passage. This makes, for example, S2 at pericenter much more relativistic than known binary pulsars and opens up new possibilities for testing general relativity. This paper develops a technique for fitting nearly Keplerian orbits with perturbations from the Schwarzschild curvature, frame dragging, and the black hole spin-induced quadrupole moment, to redshift measurements distributed along the orbit but concentrated around pericenter. Both orbital and light-path effects are taken into account. It turns out that absolute calibration of rest-frame frequency is not required. Hence, if pulsars on orbits similar to the S stars are discovered, the technique described here can be applied without change, allowing the much greater accuracies of pulsar timing to be taken advantage of. For example, pulse timing of 3 μs over 1 hr amounts to an effective redshift precision of 30 cm s^{-1}, enough to measure frame dragging and the quadrupole moment from an S2-like orbit, provided problems like the Newtonian "foreground" due to other masses can be overcome. On the other hand, if stars with orbital periods of order of a month are discovered, the same could be accomplished with stellar spectroscopy from the European Extremely Large Telescope at the level of 1 km s^{-1}.

Key words: Galaxy: nucleus – gravitation – stars: kinematics and dynamics

Online-only material: tar.gz file

1. INTRODUCTION

Tracing the orbits of the S stars in the Galactic center region reveals a central mass of $\sim 4 \times 10^6\, M_\odot$ (Ghez et al. 2008; Gillessen et al. 2009b), presumably a supermassive black hole. The roughly 20 known S stars are mostly main-sequence B stars, and it is likely that they share their environment with many fainter stars. Hence, discovery by the next generation of telescopes of stars far closer to the black hole is anticipated. The dynamics of the orbit and light trajectories provide an opportunity to test hitherto unobserved predictions of general relativity in the black hole neighborhood, and in doing so, confirm or revise our understanding of the nature of gravity (Gillessen et al. 2010). Meanwhile, searches for pulsars in the Galactic center region are also underway (e.g., Macquart et al. 2010). If pulsars on orbits similar to S stars are discovered, their time-of-arrival measurements may provide accuracies orders of magnitude beyond those available from optical spectroscopy.

It is interesting to compare S stars with other relativistic orbits. General relativistic perturbations of a nearly Keplerian orbit typically scale as an inverse power of the classical angular momentum $\sqrt{a(1-e^2)}$. Thus, a simple measure of the strength of relativistic effects in a nearly Keplerian orbit is the dimensionless pericenter distance.[3] Figure 1 plots pericenter distance against orbital period for a sample of S stars and binary pulsars together with Mercury and artificial satellites. At present, binary pulsars are the leading laboratories for general relativity. The principles are summarized in Taylor (1994). Taylor's Figure 11, depicting five intersecting curves, indicating four distinct tests of general relativity, is especially memorable, and descendants of this figure with newer data appear in recent work (e.g., Figure 3 in Kramer & Wex 2009). So, it is remarkable that the star S2 has a pericenter distance $\sim 3 \times 10^3$, an order of magnitude lower than the most relativistic binary-pulsar systems, and 4 orders of magnitude lower than Mercury. This suggests that Galactic center orbits may show relativistic effects not measured in binary pulsars, such as frame dragging. On the other hand, S2 has an orbital period of $\sim$15.9 yr versus 1 day or less for some binary pulsars. Thus, for the known S stars or pulsars on similar orbits, we cannot build up a relativistic signal over many orbits. A different strategy is needed, based on detailed observation of one or a few orbits, and paying special attention to pericenter passage, when relativistic effects are strongest.

Several different possibilities for observing relativistic effects have been discussed in the literature. To see how these relate to each other, let us consider the different physical effects involved in observing a relativistic orbit over time. These are illustrated in Figure 2. Shown schematically in this figure is a star on a precessing orbit, which emits photons (pulses, wavecrests) at a fixed frequency in proper time. These photons then take a curved path to the observer. When they arrive, both their frequency and their travel direction have been altered. What can the observer detecting these photons infer about the metric? This observer must take multiple physical processes into account.

1. *Time dilation* at the source is a consequence of the equivalence principle and is the strongest relativistic perturbation. Its measurability in the context of the Global Positioning System (GPS) is well known (Ashby 2003). The manifestation of time dilation in pulsar timing is known as the Einstein time delay. For the S stars, a spectroscopic detection of time dilation is expected around pericenter passage (Zucker et al. 2006).
2. *Orbit perturbations* are a test of space curvature, and at higher order, of black hole spin.
   (a) The leading-order precession of orbital periapse is well measured in binary pulsars. (For a discussion of how pulsar timing effects scale to the Galactic center region,

[3] In this paper, the semimajor axis a and the pericenter distance $a(1-e)$ are always expressed in units of GM/c^2 and are therefore dimensionless.

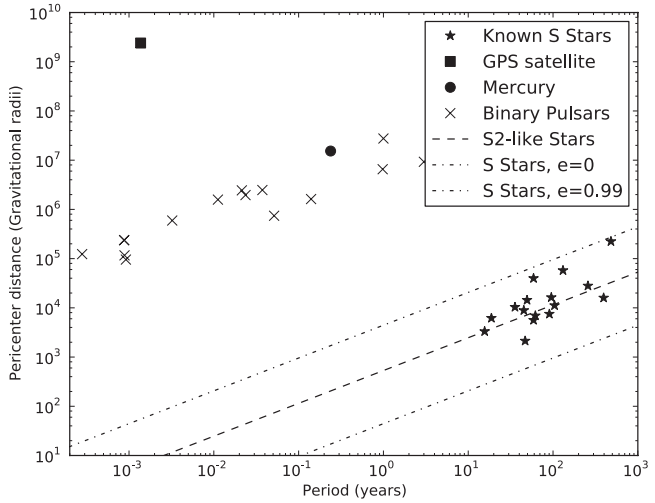

Figure 1. Pericenter distance (in units of GM/c^2) against orbital period for a variety of systems. The known S stars, having smaller pericenter distances, are more relativistic than known binary pulsars. But the long orbital periods of the S stars render it infeasible to measure cumulative effects over many orbits. Hence, other techniques must be devised. The pulsar examples are taken from Lorimer (2008). For the S stars, the orbital elements in Gillessen et al. (2009b) have been used. In this paper, we also treat fictitious stars that lie along the dashed line, that is, having a range of semimajor axis a values but with the same eccentricity and angular elements as S2.

see Pfahl & Loeb 2004.) Astrometric measurement of precession in the orbit of S2 is considered feasible with current instruments (Eisenhauer et al. 2009), but the long orbital period and the likelihood of Newtonian precession due to the distributed mass both present serious difficulties. If stars much further in are discovered, however, precession of orbital planes due to higher-order spin and quadrupole effects become accessible (Will 2008; Merritt et al. 2010).

(b) Orbital decay due to gravitational radiation is not considered measurable because of the long timescales and the extreme mass ratio between the star or pulsar and the supermassive black hole.

(c) In contrast to the above secular effects, there are also general-relativity-induced velocity perturbations, which vary along the orbit (Kannan & Saha 2009; Preto & Saha 2009). In binary pulsars, velocity perturbations are not considered especially interesting and are subsumed within Roemer delays. For Galactic center stars, however, the situation is different. First, the velocity perturbations are larger, and second, they are concentrated around pericenter passage, thus offering a better prospect for isolating relativistic perturbations from Newtonian ones.

3. *Light paths and travel times* are affected by the black hole mass, and again at higher order by spin.

(a) Strong deflection of starlight (Bozza & Mancini 2009) or a pulsar beam (Wang et al. 2009a, 2009b) would be a spectacular though rare event.

(b) Small perturbations of photon trajectories, too small to measure astrometrically, can nevertheless produce detectable changes in the light travel time. In the pulsar literature, this is known as the Shapiro delay. The analogous effect for S stars is a time-dependent redshift contribution (Angélil & Saha 2010), which for a star-like S2 is comparable to the velocity perturbations. Hence, in the Galactic center, relativistic perturbations on both orbits and light paths must be considered.

Later in this paper, we will group time dilation with the orbital effects.

Motivated by the above considerations, in this paper we develop a method to fit a relativistic model to observables. This strategy (1) takes relativistic perturbations on both the orbits and the light into account, (2) treats stellar spectroscopy and pulse timing in a unified way, and (3) is well suited to analyzing data obtained from a single orbital period or even less. We include the effects of time dilation, space curvature, frame dragging, and torquing-like effects induced by the quadrupole moment from the black hole spin. Some further issues remain, most importantly, how to include Newtonian perturbations (from mass other than the black hole's) in the fit—hence the "toward" in the title.

The observable we consider is the apparent frequency ν. As remarked above, this can refer to spectral lines or pulses. The source frequency ν_0 is in principle known for stars, but unknown for pulsars. Note that

$$c\ln(\nu_0/\nu) = c\ln(1+z) \simeq cz, \tag{1}$$

where z is redshift in the usual definition. For this paper, however, we will use "redshift" to mean $c\ln(\nu_0/\nu)$. The possibly unknown source frequency now appears as a harmless additive constant in the redshift. For the S stars, the current spectroscopic accuracy is $\approx$10 km s^{-1} under optimal conditions (Gillessen et al. 2009b). If a pulsar on a similar orbit is discovered, the accuracy would likely be much higher. Taking, as an example, a 1 hr observation with pulses timed to 3 μs (cf. Janssen et al. 2010) implies an accuracy of one part in 10^9, equivalent to a redshift accuracy of 30 cm s^{-1}. The same level of accuracy is not inconceivable from spectroscopy of S stars, since planet searches routinely achieve $\Delta v < 1$ m s^{-1} (e.g., Lovis et al. 2006), but would require some technical breakthroughs to achieve for faint infrared sources like the S stars.

For a given orbit and redshift accuracy, the principal quantities we will calculate are the signal-to-noise ratio (S/N) for different relativistic effects. For each of four relativistic effects—time dilation, space curvature, frame dragging, and quadrupole moment effects—we will present the results in two ways: (1) the redshift accuracy needed to reach some S/N for a given orbit and (2) the orbital parameters needed to reach some S/N for a given redshift accuracy.

2. MODEL

The main calculations in this paper will assume that the trajectories of both S stars (or pulsars) and photons are geodesic in a pure Kerr metric. Naturally, geodesics of the former are timelike, and of the latter, null. Even if Einstein gravity is correct, the pure Kerr metric is naturally an approximation because this solution to the field equations neglects all mass in the vicinity of the black hole (more on this later), and the mass of the star itself. In general relativity, geodesic motion is fully described by the super Hamiltonian

$$H = \tfrac{1}{2}\, g^{\mu\nu} p_\mu p_\nu, \tag{2}$$

with $H = 0$ for null geodesics.

Rather than carry out all computations with the Hamiltonian resulting from the full Kerr metric, it is useful to consider two different approximations for the cases of orbits and light paths.

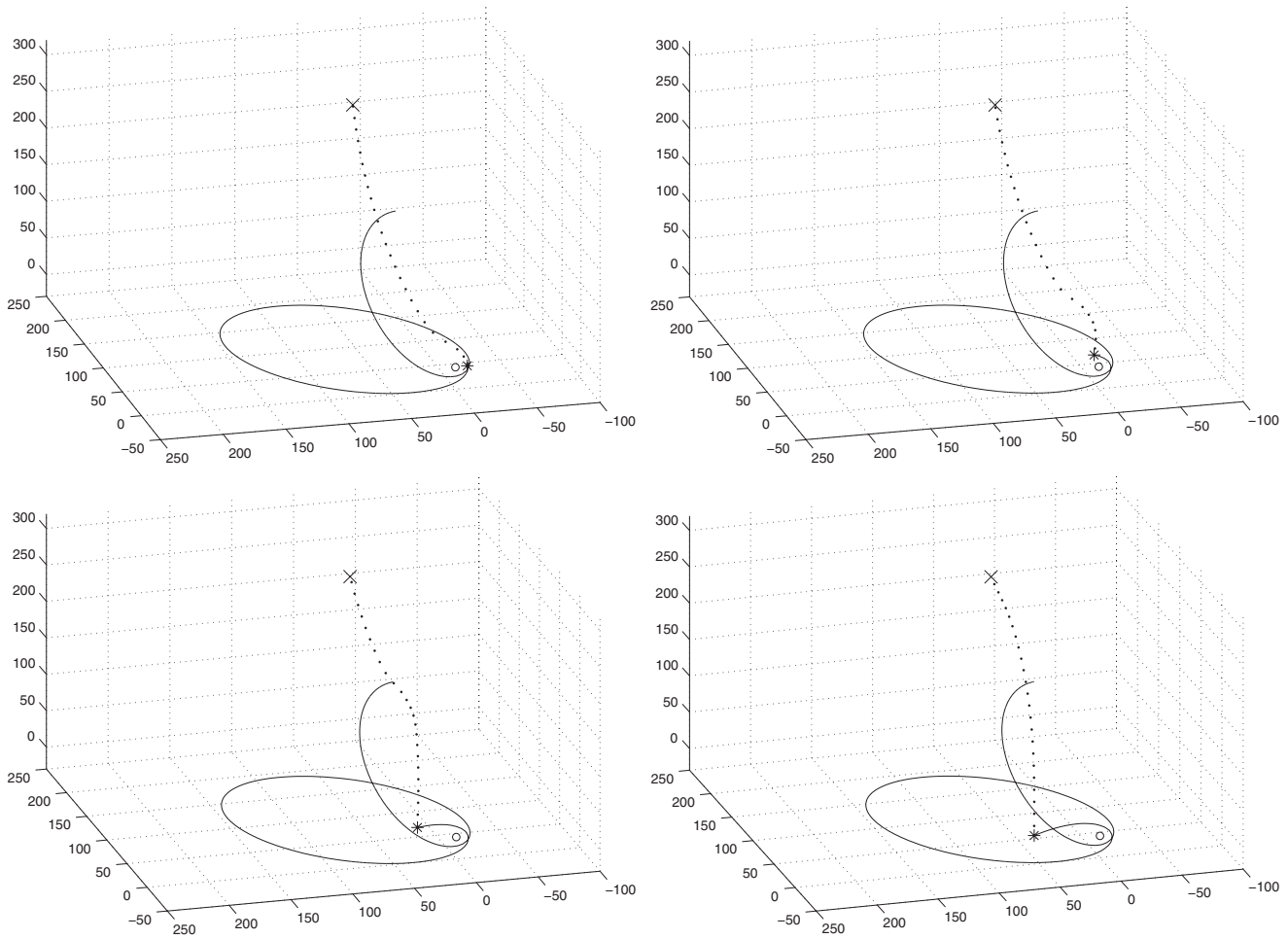

Figure 2. Depiction of the system we deal with, shown at four slices of coordinate time. The curve ending in a star symbol traces a stellar orbit, starting from apocenter, through its second pericenter passage. The star emits photons in all directions at equal intervals of proper time. Dots show photons which will reach the observer (marked "×"). Note that the dots represent a sequence of photons emitted at different places, hence joining the dots does not represent the path of any particular photon. Time dilation and Schwarzschild perturbations are included in this example, but not frame dragging or quadrupole. This means that the star's orbit precesses, and the photons are lensed. In order to make the relativistic effects visually discernible, the star has a very low value of $a = 100$. Such a star may, however, yet be discoverable by the E-ELT (Lyubenova & Kissler-Patig 2009). Also, the observer has been placed at an unrealistically close distance of 300.

These we will call $H_{\rm star}$ and $H^{\rm null}$. (Word labels in subscripts indicate orbits, in superscripts, light paths.) We express these approximate Hamiltonians perturbatively as

$$H_{\rm star} = H_{\rm static} + \epsilon^2 H_{\rm Kep} + \epsilon^4 H_{\rm Schw} + \epsilon^5 H_{\rm FD} + \epsilon^6 H_{\rm q}, \quad (3)$$

and

$$H^{\rm null} = H^{\rm Mink} + \epsilon^4 H^{\rm Schw} + \epsilon^6 \left(H^{\rm FD} + H^{\rm q}\right), \quad (4)$$

where the meanings of the various component Hamiltonians will be explained shortly. Note that ϵ is just a label to indicate orders: if ϵ^n appears, the term is of order v_n (where v is the stellar velocity in light units), but numerically $\epsilon = 1$. The series in Equations (3) and (4) actually consist of the same terms, but because $H_{\rm star}$ is to be applied only to trajectories that are strongly timelike, and $H^{\rm null}$ only to compute null geodesics, the orders of same terms are often different.

Expressions for all the Hamiltonian terms are derived perturbatively from the Kerr metric, using the basic method explained in Angélil & Saha (2010). We will not repeat the details here, but simply list the terms and their physical meanings.

First we consider the orbit (Equation (3)).

1. To leading order, the star feels no gravity and the clock simply ticks:
$$H_{\rm static} = -\frac{p_t^2}{2}. \quad (5)$$
2. At next-to-leading order, gravity first appears, with
$$H_{\rm Kep} = \frac{p_r^2}{2} + \frac{p_\theta^2}{2r^2} + \frac{p_\phi^2}{2r^2 \sin^2\theta} - \frac{p_t^2}{r}, \quad (6)$$
which is the classical Hamiltonian modified by $1/r \to p_t^2/r$. This modification leaves the problem spatially unchanged, but introduces a temporal stretching causing a gravitational time dilation. This is originally a consequence of the Einstein Equivalence Principle, and affects the redshift at $\mathcal{O}(v^2)$.
3. Appearing next are the leading-order Schwarzschild contributions,
$$H_{\rm Schw} = -\frac{2p_t^2}{r^2} - \frac{p_r^2}{r}, \quad (7)$$
of which the first term effects a further time dilation, and the second curves space, leading to orbital precession.

4. Next, the first spin term emerges with

$$H_{\rm FD} = -\frac{2sp_t p_\phi}{r^3}, \tag{8}$$

producing frame dragging, an r-dependent precession around the spin axis. Here, s is the spin parameter, which points in the $\theta = 0$ or $+z$ direction. Maximal spin is $s = 1$.

5. The last set of orbital terms we will consider are

$$H_{\rm q} = s^2\left(\frac{\sin^2\theta p_r^2}{2r^2} - \frac{p_\phi^2}{2r^4\sin^2\theta} + \frac{\cos^2\theta p_t^2}{r^3} - \frac{\cos^2\theta p_\theta^2}{2r^4}\right), \tag{9}$$

which are the leading-order quadrupole moment terms. These result in the orbit being torqued toward the spin plane as well as other less intuitive effects.

We then consider light paths (Equation (4)).

1. At leading order, we have

$$H^{\rm Mink} = -\frac{p_t^2}{2} + \frac{p_r^2}{2} + \frac{p_\theta^2}{2r^2} + \frac{p_\phi^2}{2r^2\sin^2\theta}, \tag{10}$$

which is to say, the spacetime is Minkowski and the photon trajectories are straight lines.

2. The leading-order Schwarzschild contribution

$$H^{\rm Schw} = -\frac{p_t^2}{r} - \frac{p_r^2}{r} \tag{11}$$

(which, notice, is not identical to $H_{\rm Schw}$) introduces lensing and time delays.

3. The frame-dragging term for photons

$$H^{\rm FD} = -\frac{2sp_t p_\phi}{r^3} \tag{12}$$

debuts at one order higher than $H_{\rm FD}$. Frame dragging lenses photons around the black hole in a twisted fashion. A ϕ-dependent time dilation also occurs.

4. Finally, we consider higher-order Schwarzschild terms and quadrupole moment terms

$$H^{\rm q} = -\frac{2p_t^2}{r^2} + \frac{s^2\sin^2\theta p_r^2}{2r^2} - \frac{s^2\cos^2\theta p_\theta^2}{2r^4} - \frac{s^2 p_\phi^2}{2r^4\sin^2\theta}, \tag{13}$$

which, as before, produce a torque toward the spin plane and as well as some more subtle effects.

The well-known separability properties of the Kerr metric (cf. Chandrasekhar 1983, p. 663) provide solutions up to quadratures, but not explicit solutions. Analytic solutions for geodesics and null geodesics are available for various special cases, for example, for the leading-order Schwarzschild case (D'Orazio & Saha 2010), but the present work uses the numerical integration of Hamilton's equations.

3. CALCULATING REDSHIFTS

Given a set of orbital parameters for the star, we calculate a redshift curve, meaning $\ln(\nu_0/\nu)$ against observer time or pulse arrival time, by the following method.

First, the orbit is calculated by numerically solving Hamilton's equations for $H_{\rm star}$ (Equation (3)). If desired, particular orbital relativistic effects can be isolated by omitting other relativistic terms from $H_{\rm star}$. The independent variable is, of course, not time but the affine parameter (say λ). Along this orbit, from pairs of points separated by $\Delta\lambda$, photons are sent to the observer. The difference in proper time between the emission of two photons is

$$\Delta\tau = \frac{\Delta\lambda}{\sqrt{-2\,H_{\rm star}}}. \tag{14}$$

The photons themselves travel along paths determined by $H^{\rm null}$ (Equation (4)) with the additional condition $H^{\rm null} = 0$. Again, one is free to isolate particular relativistic effects on the photons by discarding terms from $H^{\rm null}$. If Δt is the difference in the photons' times of arrival at the observer, then

$$\frac{\nu_0}{\nu} = \frac{\Delta t}{\Delta\tau}. \tag{15}$$

This calculation is carried out along the orbital path. Some snapshots of this procedure are illustrated in Figure 2.

Now, photons are emitted from the star in all directions, but we need to find exactly those photons which reach the observer. Solving this boundary value problem is the computationally intensive part. Our algorithm for doing so is explained in Angélil & Saha (2010). In stronger fields, the redshift curve takes longer to compute than in weaker ones, both because the orbit integration needs smaller step sizes over more relativistic regions, and because the boundary value problem requires more iterations before satisfactory convergence is reached.

The observable redshift is of course a combination of all the relativistic effects atop the classical redshift. One can, however, estimate the strengths of each effect in isolation by toggling each term in Equations (3) and (4) on and off, and then taking the difference in redshift. Figures 3 and 4 show relativistic redshift contributions measured in this way. These orbits refer to the pericenters of a range of orbits, varying in a but with e and the other orbital parameters fixed at the values of S2. These effects have simple scalings with the orbital period, readily deduced from the scaling properties of the Hamiltonians, and summarized in Table 1. Numerical results in Angélil & Saha (2010) verify that such scalings apply not only at pericenter but all along the orbit.

Table 1
Relativistic Effects Considered in this Paper, and How They Scale with the Orbital Period

Effect	Orbit	Light Path
Classical	$P^{-1/3}$	
Time dilation	$P^{-2/3}$	
Schwarzschild	P^{-1}	P^{-1}
Frame dragging	$P^{-4/3}$	$P^{-5/3}$
Quadrupole	$P^{-5/3}$	$P^{-5/3}$

The extended mass distribution in the Galactic center region, due to all the other stars, stellar remnants, and dark matter particles that are present, introduces Newtonian perturbations. The distribution and normalization of this mass are poorly constrained on the scales of interest (Schödel et al. 2009), although some upper limits exist (Gillessen et al. 2009a) and some numerical experiments have been done (Merritt et al. 2010). Assuming spherical symmetry for this distributed mass, models of the form

$$\rho(r) \propto r^{-\gamma} \tag{16}$$

are sometimes adopted. Such a model ignores the torques due to a nonspherical or discrete mass distribution, and the only change it implies in the orbital dynamics is an additional (prograde)

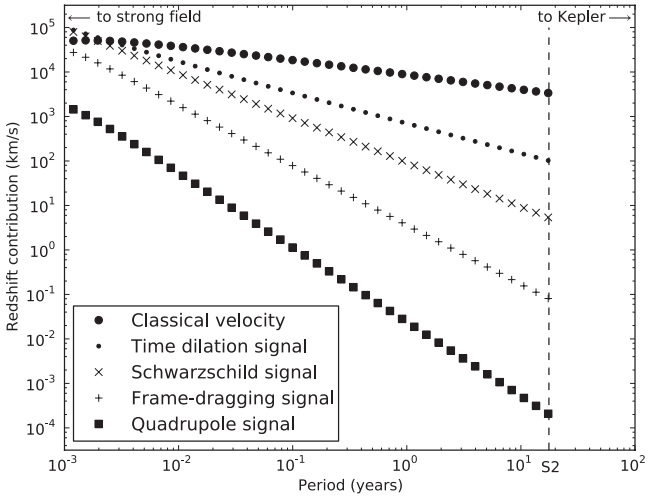

Figure 3. Redshift contributions of different orbital effects. Shown here are the contributions of each term in Equation (3) at pericenter, with the orbital period being varied and the other orbital parameters fixed at the S2 values. The pericenter distance varies from 3600 (approximately the value for S2) down to 6. Note that for the last two signals—the frame dragging and the quadrupole—we have taken the black hole spin to be maximal and to point perpendicular to the line of sight. The signal scalings are listed in Table 1. The curves begin to intersect as we move toward the strong field regime—attributable to the breakdown in our perturbative approximation for small r.

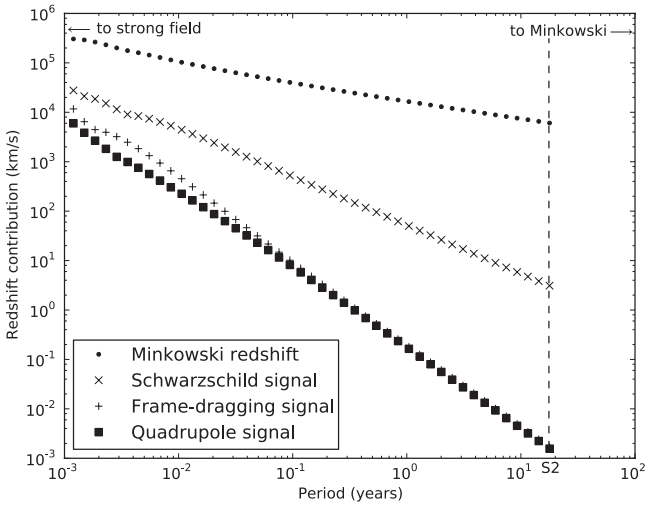

Figure 4. Same as Figure 3, but for photon propagation delays (Equation (4)). The Schwarzschild propagation signal is for the most part slightly smaller than the Schwarzschild orbital signal, and scales in the same way. The frame-dragging propagation signal is considerably smaller than the corresponding orbital signal, and scales like $z^{\rm FD} \propto P^{-5/3}$, as opposed to $z_{\rm FD} \propto P^{-4/3}$. The frame-dragging signal remains approximately an order of magnitude weaker on the photons than on the star. This suggests that in attempting to measure the spin of the black hole in the post-Newtonian regime, its manifestation on the orbit is what matters. Note, however, that this is not the case for the Schwarzschild effects—for which neither the photon nor orbit perturbations may be neglected.

pericenter advance. Figure 5 compares the orbital and photon signal strengths for each effect, including an extended mass distribution of the type (16). Note, however, that in the analysis which follows, we do not attempt to include the effects of the extended mass distribution.

4. FITTING

The computational demands for the present work are far greater than the calculations of a few redshift curves for given

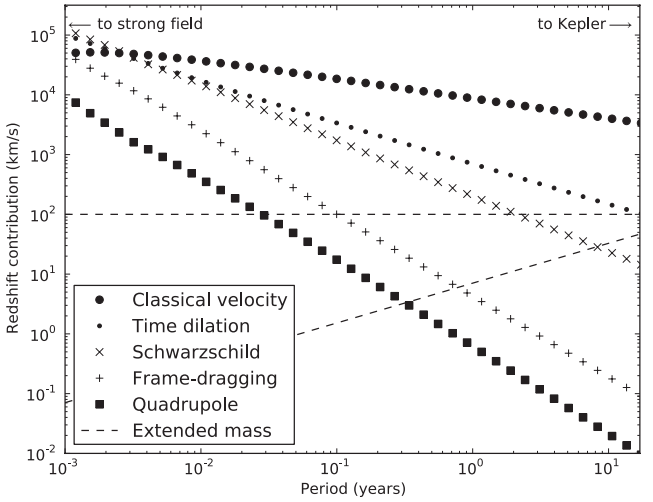

Figure 5. Relativistic redshift effects with orbital and light-path contributions summed. Two estimates for the signal due to the extended mass distribution are also shown, using the crude model (16) normalized so that the circular velocity at the $r = 10^5\, GM_{\rm BH}/c^2$ (or ~ 0.1 pc) is $\sim$100 km s^{-1} (cf. Gillessen et al. 2009b). The flat and sloping dashed curves correspond to $\gamma = 2.5$ and 1.5, respectively.

parameters (as in Angélil & Saha 2010), because *fitting* redshift curves in a multidimensional parameter space requires evaluations of up to tens of thousands of such curves. To this end, parallel functionality was added to the implementation. The work is distributed evenly among the available processors. A workload is the charge of calculating the redshift from a single position on the star's orbit, i.e., a single evaluation of Equation (15), calling for the finding of two photons traveling from star to observer. The program is available as an online supplement.

4.1. The Parameters

The redshift curve of an S star or pulsar depends on eight essential parameters, but there can be any number of additional parameters for secondary effects. In this paper, we consider nine parameters in all as follows.

1. The black hole mass $M_{\rm BH}$ sets the overall timescale, and accordingly we express it as time. Changing $M_{\rm BH}$ simply stretches or shrinks the redshift curve in the horizontal direction.
2. The intrinsic frequency ν_0 for pulsars is the pulse frequency in proper time, whereas for spectroscopy, it has the interpretation of absolute calibration. Altering ν_0 simply shifts the redshift curve vertically.
3. Then there are the Keplerian elements, referring to the instantaneous pure Keplerian orbit with the initial coordinates and momenta. Our orbit integrations all start at apocenter.
   (a) The semimajor axis a (or equivalently the period $P = 2\pi a^{3/2} M_{\rm BH}$) is the single most important parameter dictating the strength of the relativistic signals.
   (b) The eccentricity e sets how strongly peaked the redshift curve is at pericenter.
   (c) The argument of pericenter ω sets the level of asymmetry of the redshift curve.
   (d) The orbital inclination I changes the amplitude of the redshift. Classically, the inclination entering the redshift depends only on $M_{\rm BH} \sin^3 I$ (on $M_{\rm BH}^3/M_{\rm total}^2 \sin^3 I$ for finite mass ratio). In relativity, the degeneracy is broken, because time dilation is independent of I.

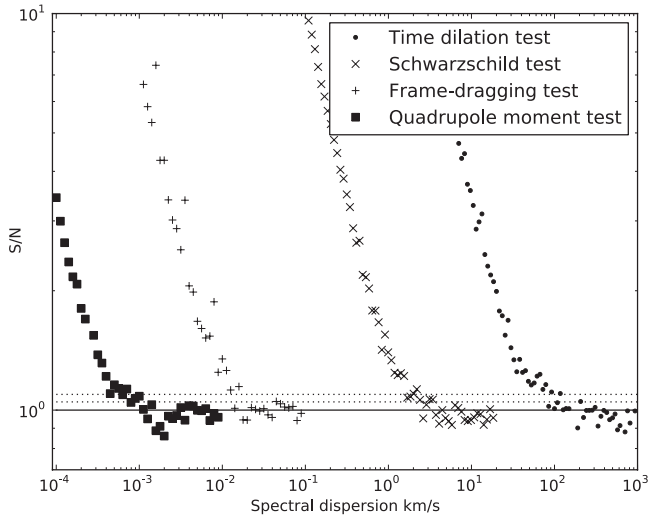

Figure 6. Signal-to-noise ratios (as defined by Equation (17)) for different relativistic effects in the orbit of S2 as a function of redshift accuracy. Each point on this figure corresponds to a simulated data set of 200 redshifts, distributed over the orbit but with the highest density around pericenter.

(e) The epoch ϵ_0 basically the zero of the observer's clock.

The longitude of the ascending node Ω does not appear, because in our chosen coordinate system, Ω rotates the whole system about the line of sight, which has no effect on the redshift. Formally, we simply fix $\Omega = 0$.

4. For the pulsar case, we include a simple spin-down model with a constant spin-down rate $\nu_0 \rightarrow \nu_0 - \dot{\nu}\,(t_a)$. Here, $\dot{\nu}$ is an additional parameter.

We take the black hole spin as maximal, and as pointing perpendicular to the line of sight. Proper motion of the black hole is not considered.

To fit, we use a quasi-Newton limited memory Broyden–Fletcher–Goldfarb–Shanno optimization routine with bounds (Zhu et al. 1997; Byrd et al. 1994).

4.2. Signal to Noise

With an orbit fitting algorithm in hand, we now need to quantify the notion of detectability of particular relativistic effects. One way would be to attach a coefficient to each term in the relativistic Hamiltonians and then see how accurately that coefficient can be recovered. For this paper, however, we take a simpler approach. Since, for now, we only aim to identify which effects and which regimes are promising, we will simply attempt to estimate the threshold for detecting the presence of each term in Hamiltonians (3) and (4). Accordingly, we proceed as follows.

1. For some chosen parameters, we generate a redshift curve including all Hamiltonian terms up to some $\mathcal{O}(\epsilon^n)$. These redshift curves are sampled at 200 points with dense sampling near pericenter.
2. We add Gaussian noise to the redshifts at some chosen level.
3. We then fit the parameters with a redshift curve *lacking* a particular Hamiltonian contribution. If the noise level is too high, a reduced $\chi^2 \simeq 1$ will be obtained, otherwise $\chi^2_{\rm red}$ will be higher. We define

$$\mathrm{S/N} \equiv \sqrt{\chi^2_{\rm red}} \tag{17}$$

as the signal-to-noise ratio.

Table 2
Summary of the Observational Thresholds at which Different Relativistic Effects are Exposed, Assuming a Source of Negligible Mass in a Pure Kerr Spacetime

Effect	Required Redshift Rccuracy for S2	Required Orbital Period (yr) for Given Redshift Accuracy		
		$10\,\mathrm{km\,s^{-1}}$	$1\,\mathrm{km\,s^{-1}}$	$30\,\mathrm{cm\,s^{-1}}$
Time dilation	$\sim 60\ \mathrm{km\ s^{-1}}$	~ 50	$\gg P_{S2}$	$\gg P_{S2}$
Schwarzschild	$\sim 3\ \mathrm{km\ s^{-1}}$	~ 13	~ 30	$\gg P_{S2}$
Frame dragging	$\sim 10\,\mathrm{m\ s^{-1}}$	~ 0.5	~ 0.8	$> P_{S2}$
Quadrupole	$\sim 50\,\mathrm{cm\ s^{-1}}$	~ 0.04	~ 0.1	$\sim P_{S2}$

Naturally, it is necessary to check that a large $\chi^2_{\rm red}$ is not the result of some algorithmic problem, by verifying that a good fit is obtained if the Hamiltonian term in question is consistently included.

4.3. Redshift-accuracy Demands for S2

Figure 6 shows the S/N of time dilation, space curvature, frame dragging, and quadrupole terms, all as a function of redshift accuracy, assuming the orbit of S2. Time dilation is well above the current spectroscopic threshold of $\approx 10\ \mathrm{km\ s^{-1}}$. Space curvature is somewhat below, while frame dragging and quadrupole are far below.

The detectability thresholds are summarized in the first part of Table 2.

4.4. Orbit-size Demands for Given Redshift Accuracy

In Figures 7, 8, and 9, the redshift accuracy is set to $10\,\mathrm{km\ s^{-1}}$, $1\ \mathrm{km\ s^{-1}}$, and $30\,\mathrm{cm\ s^{-1}}$, respectively, while the orbital period varies along the horizontal axis.

Table 2 summarizes the detectability thresholds.

5. SUMMARY AND OUTLOOK

This paper addresses the problem shown schematically in Figure 2, which is to infer orbital parameters and detect relativistic effects from redshifts or pulsar timings along an orbit. The specific observable of interest is the ratio of rest-frame to observed frequency ν_0/ν and how it varies along an orbit, especially around pericenter. It is not necessary to measure ν_0 separately; it can be treated as a parameter to be inferred. As a result, spectroscopic redshifts and pulsar timings can be treated in a unified way. We argue that redshift variation over one or a few orbits, with special attention given to pericenter passage, provides a possible route to testing relativity using Galactic center stars, or (if discovered) pulsars on similar orbits. There are two reasons why a different strategy is called for here than in the binary pulsar case. First, pericenter speeds of S stars are typically much higher than those of binary pulsars, and second, the orbital periods are too long for cumulative effects to build up.

The observable redshift contains several different relativistic contributions affecting the orbit of the star or pulsar and the light traveling to the observer. For calculations, we use a four-dimensional perturbative Hamiltonian formulation derived from the Kerr metric. Each relativistic effect appears conveniently as a Hamiltonian term that can be toggled on and off to examine its import. Computation of redshift curves using this Hamiltonian approach was demonstrated in a previous paper (Angélil & Saha 2010). In the present paper, we have developed a pipeline for solving the inverse problem of inferring the

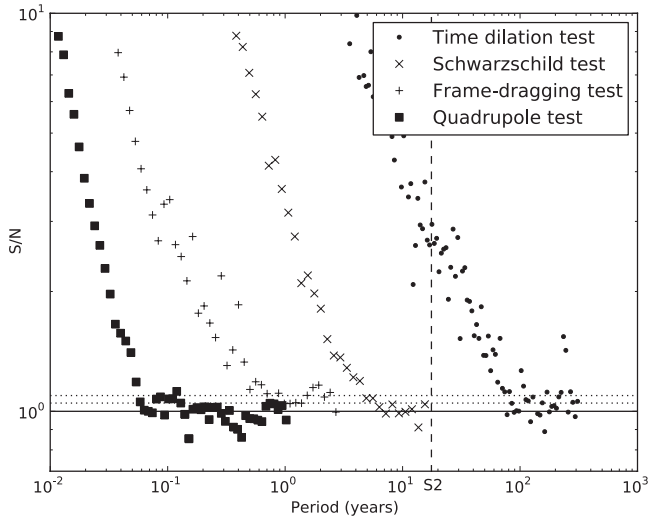

Figure 7. Similar to Figure 6, except that the redshift accuracy is fixed at 10 km s^{-1} and the orbits vary, being scaled-down and speeded-up versions of the orbit S2. For large S/N, these curves scale with the powers in Table 1. Current instrumentation, operating under optimum conditions, should manage an accuracy of 10 km s^{-1} indicating that gravitational time dilation should be able to be detected on some of the currently known S stars.

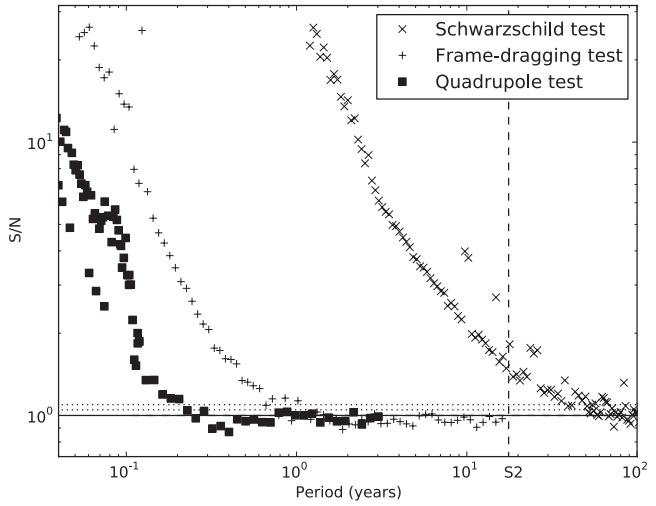

Figure 8. Same as Figure 7, but for a redshift accuracy of 1 km s^{-1}—matching the capabilities of the E-ELT (Lyubenova & Kissler-Patig 2009).

orbital parameters from a redshift curve. We then compute the redshift resolution needed to distinguish between redshift curves with and without each relativistic perturbation included, thus simulating the analysis of future observations. The redshift resolution needed to uncover each effect is a few times finer than the maximum contribution of that effect.

In our treatment, we have assumed that frequency data are the only observables at hand. The prospects for detection would be improved if astrometric information were included in the fitting procedure. Information provided by astrometry is particularly potent in constraining the angular Keplerian elements, and would alleviate the burden placed on spectroscopy or pulse timing.

A further way in which the detection prospects could be improved would be to obtain data from multiple orbits. The analysis of frequency data from stars or pulsars with periods <1 yr would not only benefit from the steep period dependence

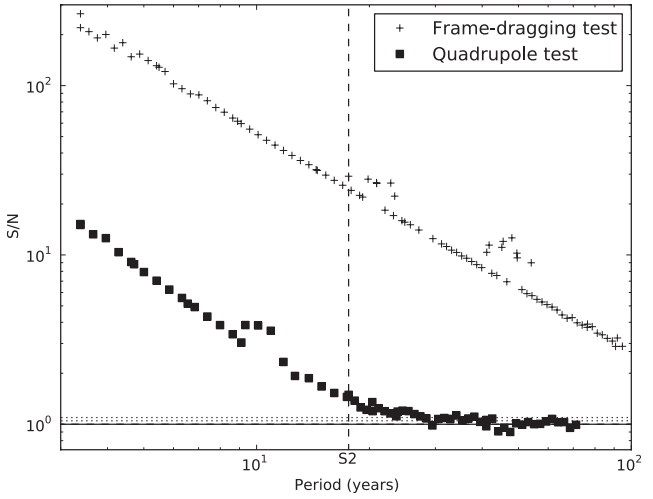

Figure 9. Same as Figures 7 and 8, but for a redshift accuracy of 30 cm s^{-1}. Pulse timing accuracies at this level are already available, known pulsars orbiting the black hole on suitably short orbits, however, are not.

of the relativistic effects, but would also boost our chances of resolving cumulative effects. Precession effects are naturally of this type.

Figure 6 illustrates the redshift accuracies required for S2. With current instrumentation, capable of ∼10 km s^{-1} accuracies, detecting time dilation appears comfortably feasible. Detecting space curvature appears feasible with a modest improvement in redshift resolution. On the other hand, the discovery of a pulsar on an orbit comparable to S2 could push the effective redshift accuracy to <1 m s^{-1} and, in principle, bring frame dragging and even quadrupole effects within reach, as shown in Figure 9.

This paper, however, assumes a source of negligible mass in pure Kerr spacetime. The finite mass of S2 (being $< 10^{-5} M_{\rm BH}$) would perturb the redshift by a similar factor via its effect on the motion of the supermassive black hole. This would be much smaller than the space-curvature effect, but more than the frame-dragging contribution. A potentially much more serious problem, however, is the Newtonian perturbations due to other mass in the Galactic center region. This Newtonian "foreground" is not necessarily fatal—the very specific time-dependence of the relativistic effects may enable them to be extracted from under a larger Newtonian perturbation (Merritt et al. 2010)—but further research is needed to assess this.

If sources inward of S2 are discovered—something we may hope for from the European Extra Large Telescope (E-ELT) and the Square Kilometer Array (SKA)—the prospects for relativity improve. Pfahl & Loeb (2004) argue that there may be 100 pulsars with orbital periods less than 10 yr, although the number may be much smaller (e.g., Merritt 2009). A large fraction of these are expected to be found by the SKA. Not only do the relativistic effects get stronger as we move closer to the black hole, but the Newtonian perturbations are likely to weaken. Figures 7 and 8 show the orbital periods at which one would need to find stars or pulsars, given redshift accuracies of 10 km s^{-1} and 1 km s^{-1}, respectively. If stars with a period of less than one year are discovered, the prospects become very exciting indeed.

We thank Antoine Klein and Daniel D'Orazio for discussion and comments. D.M. was supported by grants AST-0807910 (NSF) and NNX07AH15G (NASA).

REFERENCES

Angélil, R., & Saha, P. 2010, ApJ, 711, 157
Ashby, N. 2003, Living Rev. Rel., 6, 1
Bozza, V., & Mancini, L. 2009, ApJ, 696, 701
Byrd, R. H., Byrd, R. H., Lu, P., Lu, P., Nocedal, J., Nocedal, J., Zhu, C., & Zhu, C. 1994, SIAM J. Sci. Comput., 16, 1190
Chandrasekhar, S. 1983, The Mathematical Theory of Black Holes (International Series of Monographs on Physics. Volume 69; Oxford: Clarendon)
D'Orazio, D. J., & Saha, P. 2010, MNRAS, 406, 2787
Eisenhauer, F., et al. 2009, in Science with the VLT in the ELT Era, ed. A. Moorwood (Netherlands: Springer), 361
Ghez, A. M., et al. 2008, ApJ, 689, 1044
Gillessen, S., Eisenhauer, F., Bartko, H., Dodds-Eden, K., Fritz, T. K., Pfuhl, O., Ott, T., & Genzel, R. 2010, arXiv:1002.1224
Gillessen, S., Eisenhauer, F., Fritz, T. K., Bartko, H., Dodds-Eden, K., Pfuhl, O., Ott, T., & Genzel, R. 2009a, ApJ, 707, L114
Gillessen, S., Eisenhauer, F., Trippe, S., Alexander, T., Genzel, R., Martins, F., & Ott, T. 2009b, ApJ, 692, 1075
Janssen, G. H., Stappers, B. W., Bassa, C. G., Cognard, I., Kramer, M., & Theureau, G. 2010, A&A, 514, A74
Kannan, R., & Saha, P. 2009, ApJ, 690, 1553
Kramer, M., & Wex, N. 2009, Class. Quantum Grav., 26, 073001
Lorimer, D. R. 2001, Living Rev. Rel., 4, 5
Lovis, C., et al. 2006, Proc. SPIE, 6269, 23
Lyubenova, M., & Kissler-Patig, M. 2009, An Expanded View of the Universe—Science with the European Extremely Large Telescope (ESO: Garching)
Macquart, J., Kanekar, N., Frail, D. A., & Ransom, S. M. 2010, ApJ, 715, 939
Merritt, D. 2010, ApJ, 718, 739
Merritt, D., Alexander, T., Mikkola, S., & Will, C. M. 2010, Phys. Rev. D, 81, 062002
Pfahl, E., & Loeb, A. 2004, ApJ, 615, 253
Preto, M., & Saha, P. 2009, ApJ, 703, 1743
Schödel, R., Merritt, D., & Eckart, A. 2009, A&A, 502, 91
Taylor, J. H., Jr. 1994, Rev. Mod. Phys., 66, 711
Wang, Y., Creighton, T., Price, R. H., & Jenet, F. A. 2009a, ApJ, 705, 1252
Wang, Y., Jenet, F. A., Creighton, T., & Price, R. H. 2009b, ApJ, 697, 237
Will, C. M. 2008, ApJ, 674, L25
Zhu, C., Byrd, R. H., Lu, P., & Nocedal, J. 1997, ACM Trans. Math. Softw., 23, 550
Zucker, S., Alexander, T., Gillessen, S., Eisenhauer, F., & Genzel, R. 2006, ApJ, 639, L21

Figure 5.1: *This is the way the world ends, this is the way the world ends, this is the way the world ends, not with a bark, but a whimper.*

6 unsubmitted addendum

Using wavelets to identify relativistic vs. stochastic newtonian perturbations to S star orbits.

Raymond Angélil & Prasenjit Saha

August 18, 2011

1 Introduction

The galactic center S stars are the most relativistic ballistic objects yet observed. The strong gravitational field offers the opportunity to infer the metric by observing S Star redshift curves. There are expected to be thousands of solar masses worth of stars and black holes orbiting the central supermassive black hole. Of these, we see but a small handful. The gravitational newtonian perturbations from these on an observed redshift curve may well be significant in clouding relativistic perturbations. In this text we focus on picking up the leading-order relativistic space-time curvature perturbations. The extended mass perturbations however are expected to influence the redshift curve in markedly different ways. Relativistic contributions to the redshift curve are most significant at pericenter, while such a clear dependence is not expected for the newtonian perturbations.

2 Perturbations from a Keplerian line-of-sight redshift

To leading order, the redshift is completely classical - the line-of-sight velocity of a star on a Keplerian orbit. Because the field in the S-Star regime is always weak, in our numerical experiments, this contribution always dominates. There are two classes of perturbations to this, namely, those from relativistic effects, and those from classical perturbations due to the extended mass distribution.

- *Relativistic perturbations* Perturbations to the redshift from relativity enter the system in two ways. Either via the star orbit, or via the photon trajectories. In Einstein gravity, in the weak-field limit, the exterior stationary metric reads

$$ds^2 = -\left(1^{(\bigcirc,\mathrm{I})} - \frac{2M}{r}^{(-,\mathrm{II})}\right)\mathrm{d}t^2 + \left(1^{(-,\mathrm{I})} + \frac{2M}{r}^{(=,\mathrm{II})} + \mathcal{O}\left(\frac{2M}{r^2}\right)^{(\equiv,\mathrm{III})}\right)\mathrm{d}\mathbf{x}^2, \quad (1)$$

  where the superscripts denote the order at which they enter the dynamics. Chinese numerals for the star dynamics, and roman for photon trajectories.

  - The effect of the perturbation on the star metric from Newtonian, enters the metric as an additional space-curvature and induces a prograde precession, marginally increasing the velocities. This effect scales like $z \sim P^{-1}$.[1] This manifests in the redshift curve as a doppler perturbation. The orbital precession is cumulative, and is therefore most easily detected over multiple orbits.

[1] This precession has been observed on Mercury's orbit and is in agreement with relativity.

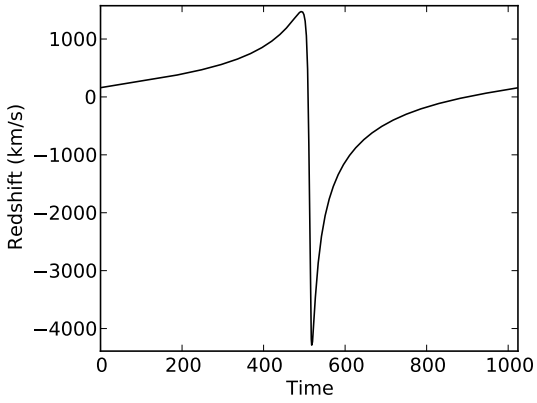

Figure 1: Classical redshift curve over one orbit, no perturbers

  - The perturbation for photons from Minkowski paths curves the space-time in the vicinity of the black hole, lensing the photons, and further increasing the redshift. This contribution to the redshift curve also scales like P^{-1}.

- *Classical Perturbations* The perturbations on the redshift curve from the extended mass distribution are purely classical, and at this point do not perturb the central black hole itself. These perturbers are on Keplerian orbits. The perturbers perturb the orbit which we observe, and on long enough timescales, induce a prograde precession.

A redshift curve of a galactic center star is generated using the following ingredients.

1. *Orbital parameters* semi-major axis a, eccentricity e, mean anomaly ω, inclination I, and epoch τ_0. The choices for ω and I implicitly set the position of the observer.

2. Black hole mass M.

3. *Perturbers* The number of perturbers, their total mass as a fraction of the supermassive black hole mass, and their distribution.

4. *Relativistic effects* The metric terms which induce relativistic perturbations to orbits and photons can be toggled. In what follows, when we refer to relativistic effects being *on* or *off*, they are either on for both orbits and photon trajectories, or off for both.

In this text, as an example, we consider a redshift curve of a galactic center S Star, and see what the perturbation types do to the wavelet transformation. The star we choose has a semi-major axis $a = 10000$ in gravitational radii (three times less than that of the the galactic center star S-2), and an eccentricity $e = 0.9$. When we include the effects of the perturbing stars, we include 200 in total, with a total mass 1% of the supermassive black hole mass. So far, we have chosen an extremely simple distribution - uniformly random semi-major axes over the range $0 - 20000$, eccentricities uniformly distributed $0.0 - 0.8$, and uniformly random orbit orientations.

Figure 1 shows this star's classical redshift curve over one orbit. Here, there are no perturbers, and the relativistic effects are turned off. Let's call this z_{Kepl}. We recalculate the redshift curve twice. First, with the perturbers on and relativity off (z_{Pert}), and second, with perturbers off,

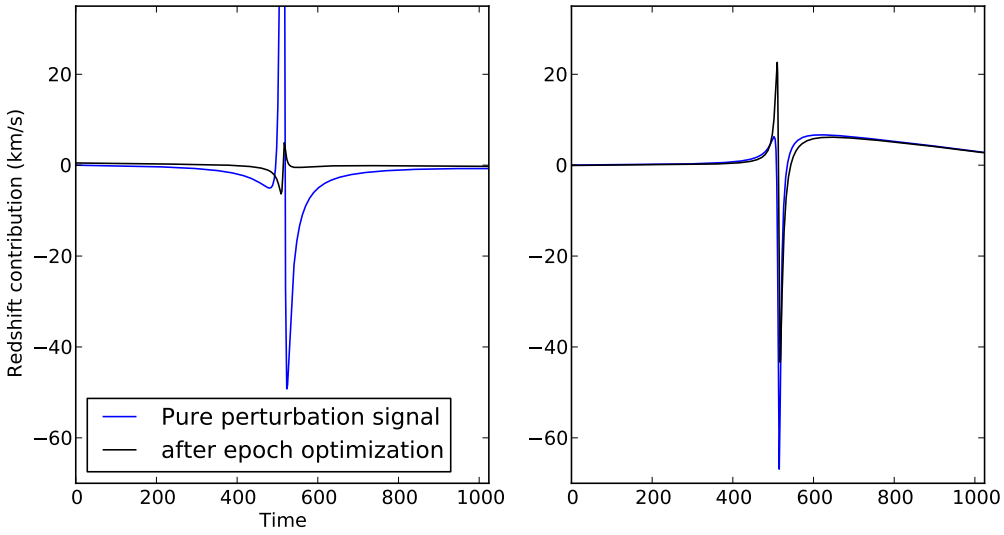

Figure 2: The left panel shows extended mass redshift signal before and after optimizing the area under the curve by shifting epochs. The right panel does the same, albeit for relativistic perturbations.

and relativity on (z_{GR}). From each of these curves we subtract the previously-calculated classical redshift, and are left with the blue curves in Figure 2. These are the signal strengths. Now both recalculated redshift curves have precessed with with respect to the original ones. This means that at a specific time at which the difference is taken, the two orbits are phase-shifted with respect to one another. To minimize this artificial effect as much as possible, we find the relative epoch such that the difference is minimal. The black curves in Figure 2. show the signal sizes after optimization.

3 Wavelets

Unlike a Fourier transformation, in which signals are represented as a sum of sinusoidal functions, each localized in frequency only, the wavelet transformation preserves frequency and localization. Relativistic perturbations, and perturbations due to the extended mass affect the dynamics in different ways, at different frequencies and different localizations. We would like to design a procedure which removes extended-mass perturbations. Because redshift curves over a single orbit have no periodicity, and because relativistic perturbations are most prevalent around pericenter, wavelets, preserving frequency and location information are a natural choice for designing a filter. Because relativistic effects are most pronounced around pericenter, we can expect high-frequency coefficients, localized around pericenter passage, to be of greatest value in retaining information from relativistic effects.

3.1 Structure of the wavelet transformation

The n-th frequency mode of the wavelet transformation contains contains 2^{n-1} coefficients. (Save for the zeroth, or constant mode, which has no localization.) Each coefficient thereof corresponds to a different localization.

n	$C_{n,m}$
0	$C_{0,1}$
1	$C_{1,1}$
2	$C_{2,1}, C_{2,2}$
3	$C_{3,1}, C_{3,2}, C_{3,3}, C_{3,4}$
4	$C_{4,1}, \quad \ldots \quad , C_{4,8}$
5	$C_{5,1}, \quad \ldots \quad , C_{5,16}$

Table 1: Wavelet transformation coefficient structure.

4 Redshift curves and wavelets

We have three redshift curves. One with neither perturbation type turned on (z_{Kepl}), one with perturbation from the extended mass distribution (z_{Pert}), and the third with perturbations from relativity (z_{GR}). We take the wavelet transformation W of each curve. Now we do the following. For each frequency mode, we take the inverse transformation of the coefficients in that mode, while keeping the others zero. The import that the n^{th}-mode coefficients on the total redshift curve is $F_n(z) \equiv W^{-1}(W(z))_n$. Figure 4. plots $F_n(z_{\mathrm{Pert}}) - F_n(z_{\mathrm{Newt}})$ in the first column, and $F_n(z_{\mathrm{GR}}) - F_n(z_{\mathrm{Newt}})$ down the second, for $n = 1 \ldots 8$.

We compute the associated power spectra (the sum of the square of the coefficients for each frequency mode), $P[W(z_{\mathrm{Kepl}})]$, $P[W(z_{\mathrm{Pert}})]$ and $P[W(z_{\mathrm{GR}})]$. The differences $P[W(z_{\mathrm{Pert}})] - P[W(z_{\mathrm{Newt}})]$ and $P[W(z_{\mathrm{GR}})] - [W(z_{\mathrm{Newt}})]$ are shown in panels 1 and 2 of Figure 5. respectively. The power spectra differences show us the worth of coefficients at a particular frequency insofar as they deviate from the classical, perturberless case. Our experiments show that relativistic signals have more power at high frequency modes than extended-mass perturbations at the same mode. This is because the eccentricity forces the relativity to 'happen' over a shorter timescale (higher frequency), while extended-mass signals are more noise-like - uniform over the orbit regardless of the eccentricity of the observed redshift curve.

5 Building a filter

If we wish to isolate certain frequencies over a specific locality in a redshift curve, we can choose the corresponding grouping of coefficients, and use them as a filter. Figure 6. shows the locality relationship a redshift curve, and the coefficients of its wavelet transformation.

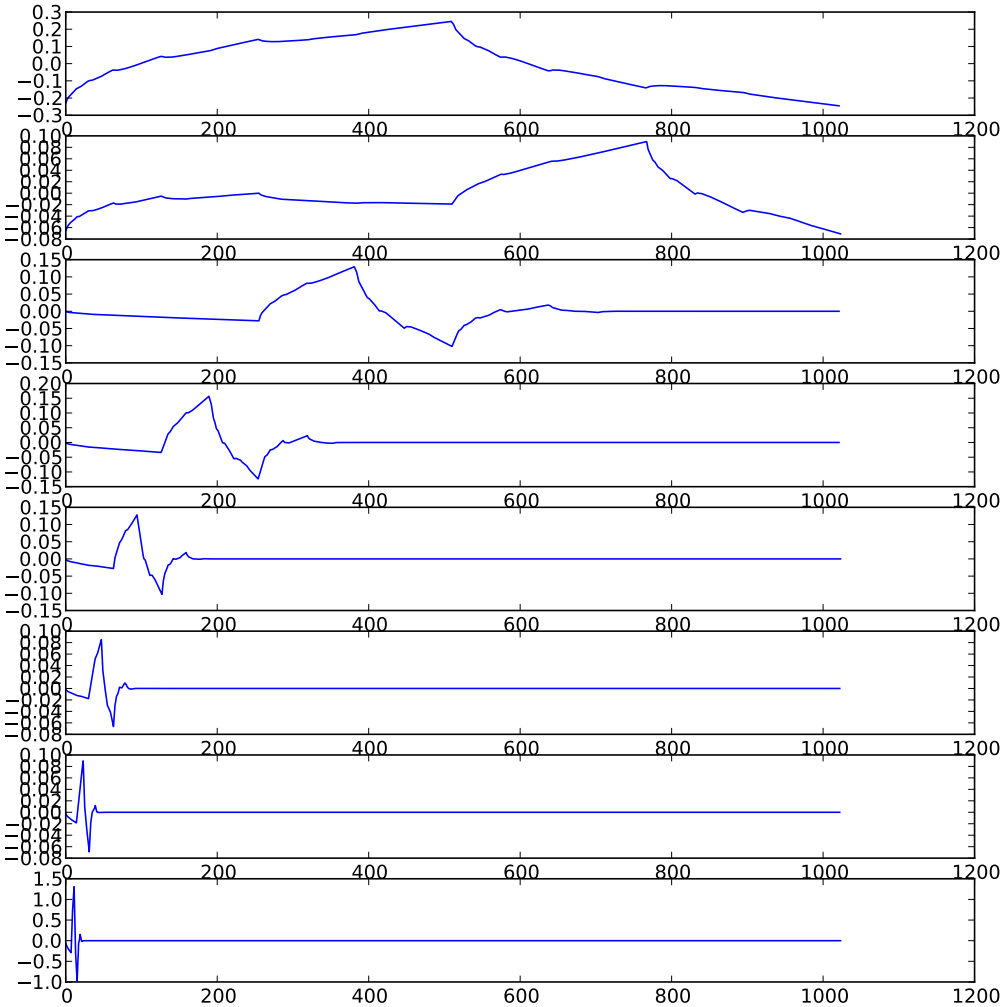

Figure 3: Wavelet structure. Each shows the inverse transformation of a single coefficient, revealing the shape of the basis function. Each panel shows one mode higher than the previous.

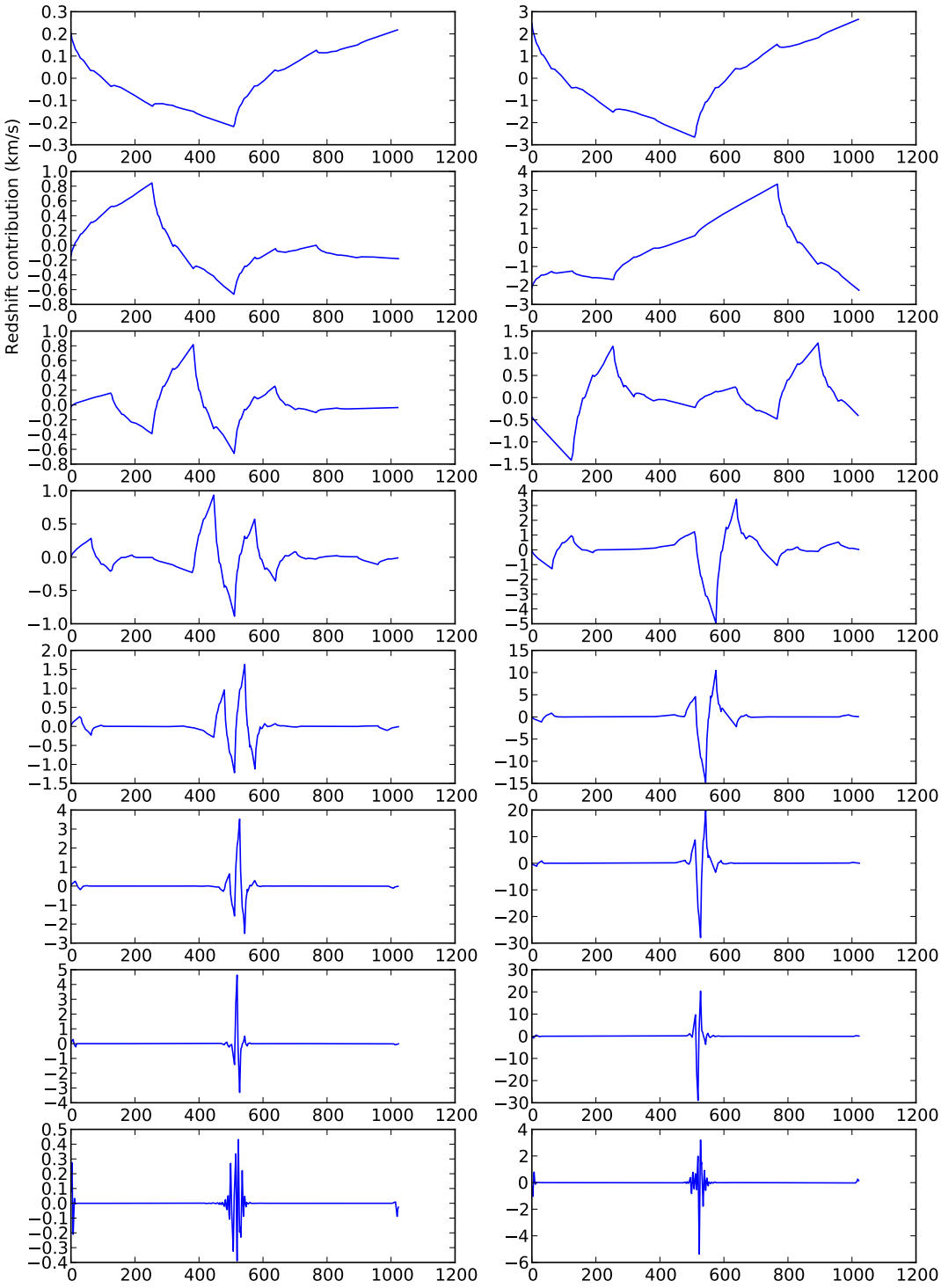

Figure 4: For the first 8 modes, we plot $F_n\left(z_{\rm Pert}\right) - F_n\left(z_{\rm Newt}\right)$ down the left, and $F_n\left(z_{\rm GR}\right) - F_n\left(z_{\rm Newt}\right)$ down the right. The relativistic signals come out at higher frequencies more than the extended-mass ones do.

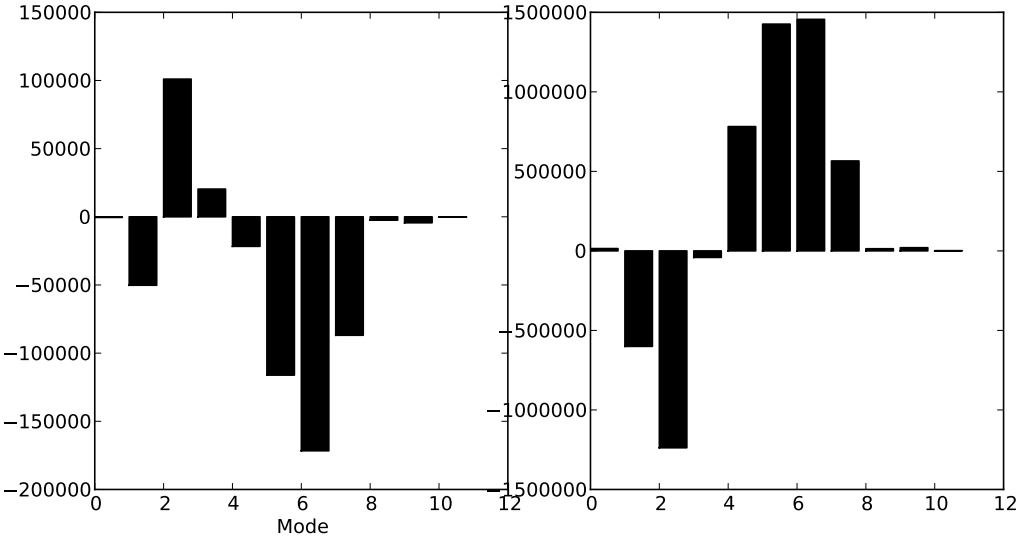

Figure 5: The left panel shows the difference $P\left[W\left(z_{\mathrm{Pert}}\right)\right] - P\left[W\left(z_{\mathrm{Newt}}\right)\right]$, and the right $P\left[W\left(z_{\mathrm{GR}}\right)\right] - \left[W\left(z_{\mathrm{Newt}}\right)\right]$. For this set of Keplerian elements, relativistic signals on the redshift have more power at high frequencies in comparison to the newtonian perturbations.

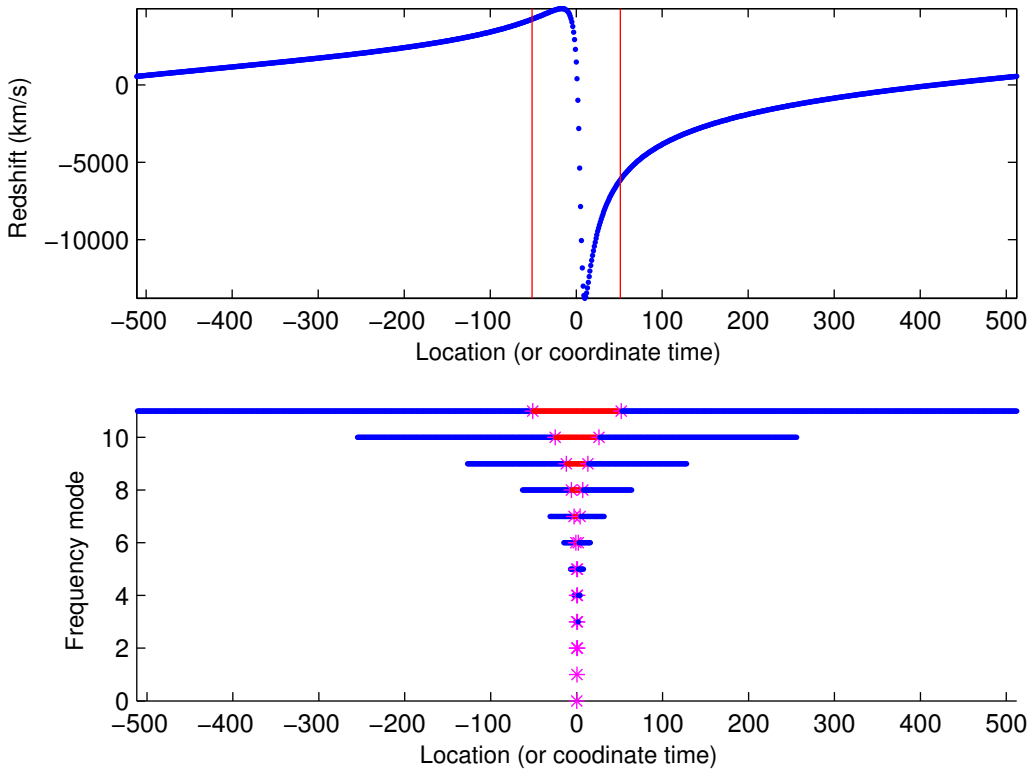

Figure 6: This schematic helps understand the structure of the wavelet transformation, and highlights its locality-preserving property. The upper panel shows a redshift curve with $a = 5000$ ($P \sim 1.2$ years), and e $= 0.9$. The epoch is such that pericenter occurs in the middle. The lower panel shows the structure of the wavelet transform. Each mark, regardless of colour, represents a coefficient. Their positions on the graph show what frequency they corresponds to, and what localization. The redshift curve has two arbitrarily chosen vertical red lines. Now we want to know which wavelet coefficients contain information between those red lines. By 'contain information', I mean that the inverse wavelet transform of these coefficients is non-zero over the region. Wavelet coefficients that are blue contain no information on what happens over this region. Magenta coefficients contain information on both what happens inside and outside the region (an overlap). Red coefficients contain information only on what happens within the region. Understanding the relationship between groups of coefficients and the extent to which they bear information on different parts of the redshift curve will be important in designing filters.